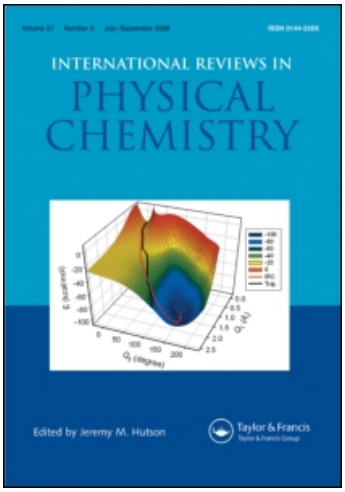

International Reviews in Physical Chemistry
Publication details, including instructions for authors and subscription information:
http://www.informaworld.com/smpp/title~content=t713724383

Quantum-chemical calculation of spectroscopic parameters for rotational spectroscopy

Cristina Puzzarini[a]; John F. Stanton[b]; Jürgen Gauss[c]
[a] Dipartimento di Chimica 'G. Ciamician', Università degli Studi di Bologna, I-40126 Bologna, Italy [b] Institute for Theoretical Chemistry, Department of Chemistry and Biochemistry, The University of Texas at Austin, Austin, Texas 78712, USA [c] Institut für Physikalische Chemie, Universität Mainz, D-55099 Mainz, Germany

Online publication date: 15 April 2010

To cite this Article Puzzarini, Cristina , Stanton, John F. and Gauss, Jürgen(2010) 'Quantum-chemical calculation of spectroscopic parameters for rotational spectroscopy', International Reviews in Physical Chemistry, 29: 2, 273 — 367
To link to this Article: DOI: 10.1080/01442351003643401
URL: http://dx.doi.org/10.1080/01442351003643401

International Reviews in Physical Chemistry
Vol. 29, No. 2, April–June 2010, 273–367

Taylor & Francis
Taylor & Francis Group

Quantum-chemical calculation of spectroscopic parameters for rotational spectroscopy

Cristina Puzzarini[a]*, John F. Stanton[b] and Jürgen Gauss[c]

[a]*Dipartimento di Chimica 'G. Ciamician', Università degli Studi di Bologna, Via Selmi 2, I-40126 Bologna, Italy;* [b]*Institute for Theoretical Chemistry, Department of Chemistry and Biochemistry, The University of Texas at Austin, Austin, Texas 78712, USA;* [c]*Institut für Physikalische Chemie, Universität Mainz, D-55099 Mainz, Germany*

(*Received 29 September 2009; final version received 13 January 2010*)

This review provides a computational chemist's perspective of rotational spectroscopy and discusses the theoretical background and application of state-of-the-art quantum-chemical methods for the accurate determination of the relevant spectroscopic parameters.

Keywords: rotational spectroscopy; quantum chemistry; coupled-cluster theory; analytic-derivative techniques; equilibrium structure; hyperfine interactions

Contents

*Corresponding author. Email: cristina.puzzarini@unibo.it

ISSN 0144–235X print/ISSN 1366–591X online

DOI: 10.1080/01442351003643401
http://www.informaworld.com

1. Introduction

Dating from the mid-twentieth century, the technique of rotational spectroscopy is a powerful tool for investigating the structure and dynamics of molecules [1–3]. Work in the millimeter and submillimeter wavelength range allows the study of small to medium-sized molecules, and has been a particularly useful technique for the detection of new chemical species (see, for example, [4–15]). Indeed, for gas-phase molecules, rotational spectroscopy remains the most accurate and reliable source for structural information [16]. High-resolution techniques such as Lamb-dip spectroscopy [17,18] allow the extraction of fine and hyperfine information (i.e., quadrupole coupling, spin–rotation and spin–spin interactions) and thus provide additional insight that extends into the realm of electronic structure [19].

In the field of astrochemistry [20–22], rotational spectroscopy is vital. Radioastronomical detection has been responsible for the detection of more than 140 chemical species in the interstellar medium [22–24], and is of course the reason why the list of known interstellar molecules includes exotic polar species such as cyclopropenylidene [25,26] but lacks more prosaic and non-polar molecules such as ethane, despite the probable existence of the latter in space. In the usual case, molecules found in space are first detected in the laboratory by rotational spectroscopy. The determination of precise rotational constants and centrifugal distortion parameters then enables the prediction of line positions in regions most accessible to radioastronomy (see, for example, Refs. [27–30]).

The detection, recording, and interpretation of experimental rotational spectra can be significantly facilitated by theoretical predictions (see, for example, Refs. [4,15,31]). Theoretical values for the relevant spectroscopic observables can be used to guide experimental investigations; in particular, accurate predictions of rotational constants permit laboratory spectroscopists to carry out searches in relatively narrow ranges of the frequency spectrum, thereby greatly facilitating the detection of unknown molecules. Once the spectrum is recorded, calculated spectroscopic parameters can also be useful for making assignments, especially in the more complicated spectra that are characteristic of radicals and/or molecules containing quadrupolar nuclei. Finally, theory is also important for extracting information from spectra. Computed vibrational corrections are vital for determining reliable equilibrium (bottom of the potential) structures [32], as these cannot be determined explicitly from the ground-state rotational constants that are usually measured.

The theoretical prediction of rotational spectra involves two tasks, namely (a) the determination of the required spectroscopic parameters, and (b) the simulation of the spectra based on the given set of spectroscopic parameters. The latter typically involves the diagonalization of an appropriate Hamiltonian. This step will not be reviewed in this work, and we refer the interested reader to the literature [33–35]. The focus of this review will be instead on the theoretical prediction of those parameters relevant for rotational spectroscopy. The accurate determination of these requires a quantum-mechanical treatment of the molecular system under consideration. The parameters of interest are the rotational constants that are related to the moments of inertia (and, hence, to the geometry of a molecule), first-order properties such as the dipole moment (which governs the intensities of rotational transitions) and electric-field gradients (for the quadrupole coupling), as well as higher-order properties such as the spin–rotation tensor required for the hyperfine interactions. All of these properties depend on the geometrical and electronic structure of the molecule under consideration and are thus accessible via quantum-chemical calculations. In addition, the vibrational contributions (especially those associated with the vibrational ground state of the molecule) are vital for accurate predictions. To lowest order, the theoretical prediction of ground-state vibrational corrections depends on the quadratic and cubic force field of the molecule and can again be determined in a straightforward manner from quantum-chemical calculations (see, for example, Refs. [36–38]).

In this review, we will provide a computational chemist's perspective of rotational spectroscopy and discuss how state-of-the-art quantum-chemical methods can best be used for the accurate determination of the essential spectroscopic parameters. In the next section (Section 2), we begin with a brief description of the theoretical background of

rotational spectroscopy which will be followed by a brief discussion of vibrational perturbation theory (Section 3). In Section 4, currently available quantum-chemical techniques are presented and their implementation for the calculation of the parameters of interest is discussed. Following that, the use of quantum-chemical calculations in the area of rotational spectroscopy is reviewed and discussed in Section 5; focus is on the accuracy that can be achieved in the quantum-chemical calculations via applications to specific examples.

2. Rotational spectroscopy

2.1. *Hamiltonian operator and energy expressions for rotational spectroscopy*

The Hamiltonian of a fixed rigid rotor is simply the kinetic-energy operator, which is most conveniently expressed in terms of the components of the angular momentum $\hat{\mathbf{J}}$ [1,2]. In a *molecule-fixed* coordinate system with the principal axes x, y, and z, this operator is

$$\hat{H}_{rot} = \frac{1}{2}\left(\frac{\hat{J}_x^2}{I_x} + \frac{\hat{J}_y^2}{I_y} + \frac{\hat{J}_z^2}{I_z}\right), \tag{1}$$

where $\hat{J}_x$, $\hat{J}_y$, and $\hat{J}_z$ are the components of $\hat{\mathbf{J}}$ and I_x, I_y, and I_z the principal moments of inertia.

The eigenvalues of the Hamiltonian given in Equation (1) are the quantized energies from which the transition frequencies are determined. With the rotational Hamiltonian given in terms of angular-momentum operators, one often makes use of a representation in terms of angular-momentum eigenfunctions in order to find the energy levels [1,2]. If the Hamiltonian commutes with the angular-momentum operators, it will be diagonal in such a representation. In all cases, however, the required matrix elements for the Hamiltonian are readily obtained from the known matrix elements of the angular-momentum operators.

It is useful at this point to recall the most important facts concerning angular-momentum operators. We start by describing the commutation relations of $\hat{\mathbf{J}}$ in the *space-fixed* system, where X, Y, and Z denote the corresponding axes. Then, it is easily shown that $\hat{J}^2$ ($=\hat{J}_X^2 + \hat{J}_Y^2 + \hat{J}_Z^2$) commutes with its components, for example,

$$\left[\hat{J}^2, \hat{J}_Z\right] = \hat{J}^2\hat{J}_Z - \hat{J}_Z\hat{J}^2 = 0. \tag{2}$$

However, the components of $\hat{\mathbf{J}}$ do not commute among themselves; instead they satisfy the commutation relations[1]

$$\begin{aligned}\left[\hat{J}_X, \hat{J}_Y\right] &= i\hat{J}_Z,\\ \left[\hat{J}_Y, \hat{J}_Z\right] &= i\hat{J}_X,\\ \left[\hat{J}_Z, \hat{J}_X\right] &= i\hat{J}_Y.\end{aligned} \tag{3}$$

Therefore, only $\hat{J}^2$ and one projection of $\hat{\mathbf{J}}$, typically chosen as the Z component, have common eigenfunctions, which are usually designated as $|J, M\rangle$. Starting from the

commutator rules given in Equation (3), the following eigenvalue equations for $\hat{J}^2$ and $\hat{J}_Z$ are obtained,

$$\hat{J}^2|J,M\rangle = J(J+1)|J,M\rangle$$
$$\hat{J}_Z|J,M\rangle = M|J,M\rangle. \tag{4}$$

Here, the quantum number J is a non-negative integer and M takes the values $M = J, J-1, J-2, \ldots, -J$. The non-vanishing matrix elements of $\hat{J}^2$ and $\hat{J}_Z$ in the J, M representation are thus

$$\langle J,M|\hat{J}^2|J,M\rangle = J(J+1)$$
$$\langle J,M|\hat{J}_Z|J,M\rangle = M. \tag{5}$$

In the next step, we apply what has been discussed so far to determine the eigenvalues of the rotational Hamiltonian. Let us consider as an example the symmetric-top rotor [1–3], which has two identical moments of inertia, with the third one being different. Using a *molecule-fixed* coordinate system with z as the symmetry axis, it is easily demonstrated that the component of angular momentum about this internal symmetry axis, $\hat{J}_z$, is a constant of motion and commutes with $\hat{J}^2$ which is also a constant of motion [1–3]. Thus, both $\hat{J}_z$ and $\hat{J}_Z$ commute with $\hat{J}^2$ and, as they also commute with each other [1,2], they have a common set of eigenfunctions, $|J,K,M\rangle$. The eigenvalues of $\hat{J}^2$ and $\hat{J}_Z$ are those previously given (see Equation (4)). In a similar way, the eigenvalues of $\hat{J}_z$ can be found from the commutation rules of the angular-momentum operators expressed in the *molecule-fixed* coordinate system [2]

$$\left[\hat{J}_\alpha, \hat{J}^2\right] = 0 \quad \text{for all } \alpha = x,y,z$$
$$\left[\hat{J}_\alpha, \hat{J}_\beta\right] = -i\hat{J}_\gamma \quad \text{for } \alpha,\beta,\gamma = x,y,z \text{ and cyclic permutations} \tag{6}$$

which differ from those for the space-fixed components only by sign [1–3]. For the symmetric top, the diagonal matrix elements are thus

$$\langle J,K,M|\hat{J}^2|J,K,M\rangle = J(J+1)$$
$$\langle J,K,M|\hat{J}_Z|J,K,M\rangle = M$$
$$\langle J,K,M|\hat{J}_z|J,K,M\rangle = K, \tag{7}$$

where, in analogy to M, K takes the values $K = J, J-1, J-2, \ldots, -J$.

The Hamiltonian for a symmetric top can be expressed in terms of $\hat{J}^2$ (with $I_x = I_y$) and $\hat{J}_z^2$

$$\hat{H}_{rot} = \frac{\hat{J}^2}{2I_x} + \left(\frac{1}{2I_z} - \frac{1}{2I_x}\right)\hat{J}_z^2. \tag{8}$$

Making use of the eigenvalues previously introduced, the following expression for the eigenvalues of the rotational Hamiltonian in Equation (8) is easily derived:

$$E_{J,K} = \langle J,K,M|\hat{H}_{rot}|J,K,M\rangle = \frac{1}{2}\left[\frac{J(J+1)}{I_x} + \left(\frac{1}{I_z} - \frac{1}{I_x}\right)K^2\right]. \tag{9}$$

Further notational simplifications of this expression are possible if one introduces the rotational constants[2]:

$$B^{\alpha} = \frac{1}{2I_{\alpha}}, \tag{10}$$

where α stands for x, y, or z. The x, y, and z axes are frequently denoted as a, b and c, but the order of the correspondence is not unambiguous and is a matter of choice. The particular choice (which can be accomplished in six different ways) defines a "representation" (I^r, II^r, III^r, I^l, II^l or III^l), which is explained, for example, in Ref. [39]. The a, b, c notation also leads (by convention) to the usual definition of the rotational constants A, B, and C with $A \geq B \geq C$. Therefore, Equation (9) can be rewritten in the case of a prolate (American football-like) top ($A > B = C$) as[3]

$$E_{J,K} = BJ(J+1) + (A-B)K^2, \tag{11}$$

and in the case of an oblate (pancake-like) top ($A = B > C$) as

$$E_{J,K} = BJ(J+1) + (C-B)K^2. \tag{12}$$

For a more detailed discussion of the classifications of molecules in terms of rotators as well as the corresponding energy and wavefunction expressions together with the selection rules, the reader is referred to more specialized literature on this topic (see, for instance, [1–3]). Here, we simply recall the energy expression for the linear (or diatomic) rotor as it might be useful in subsequent discussions.

For a linear rigid-rotor, the simple energy expression

$$E_J = BJ(J+1) \tag{13}$$

applies. Only one rotational constant is needed as $I_z = 0$ and $I_x = I_y \equiv I$. In contrast, the energy-level structure of asymmetric rotors (three unequal moments of inertia) is quite complicated and can in fact no longer be expressed in terms of a convenient equation.

In the discussion so far, we have focused on the rigid rotor. This has proved in many cases to be a useful approximation for the interpretation of rotational spectra. Nevertheless, a more detailed theoretical treatment needs to account for the non-rigidity of the molecules in the way that the nuclear positions are no longer fixed at their equilibrium positions. While the effect of molecular vibrations on the spectroscopic parameters is treated in Section 3, we discuss here the effect of the rotation itself on the energy levels. This effect is easily visualized in classical terms and known as centrifugal distortion.

The phenomenological Hamiltonian for a semi-rigid rotor with centrifugal distortion included can be written in the form [1–3]

$$\hat{H}_{rot} = \frac{1}{2}\sum_{\alpha,\beta} \mu^{e}_{\alpha\beta}\hat{J}_{\alpha}\hat{J}_{\beta} + \frac{1}{4}\sum_{\alpha,\beta,\gamma,\delta} \tau_{\alpha\beta\gamma\delta}\hat{J}_{\alpha}\hat{J}_{\beta}\hat{J}_{\gamma}\hat{J}_{\delta} + \sum_{\alpha,\beta,\gamma,\delta,\varepsilon,\eta} \tau_{\alpha\beta\gamma\delta\varepsilon\eta}\hat{J}_{\alpha}\hat{J}_{\beta}\hat{J}_{\gamma}\hat{J}_{\delta}\hat{J}_{\varepsilon}\hat{J}_{\eta} + \cdots, \tag{14}$$

where $\mu_{\alpha\beta}$ are elements of an effective inverse inertia tensor, $\hat{J}_{\alpha}$ is the α-th component of the total angular momentum, and the sums over α, β, γ, δ, ϵ, η run over the inertial axes. The first term on the right-hand side represents the usual rigid-rotor energy, while the others introduce contributions due to centrifugal distortion. The $\tau_{\alpha\beta\gamma\delta}$ and $\tau_{\alpha\beta\gamma\delta\epsilon\eta}$ are the

quartic and sextic centrifugal-distortion constants, respectively. The former are given by the expression

$$\tau_{\alpha\beta\gamma\delta} = -\frac{1}{2}\sum_r \mu^r_{\alpha\beta}(\omega_r)^{-1}\mu^r_{\gamma\delta}, \tag{15}$$

with ω_r as the r-th harmonic frequency and $\mu^r_{\alpha\beta}$ as the first derivative of $\mu_{\alpha\beta}$ with respect to the r-th normal coordinate. Higher-order terms, i.e., sextic, octic, ... terms, are also often considered in the analysis of experimental spectra, but quantum-chemical calculations usually neglect them.

A convenient way to treat the effect of centrifugal distortion on rotational spectra is perturbation theory. Setting up the rigid-rotor problem in the principal-axis system the Hamiltonian in Equation (14) can be expressed as

$$\hat{H}_{rot} = \hat{H}^0_{rot} + \hat{H}'_{dist}, \tag{16}$$

where $\hat{H}^0_{rot}$ is the Hamiltonian given in Equation (1) and $\hat{H}'_{dist}$ is the perturbation operator that corresponds to the second term on the right-hand side of Equation (14). A detailed discussion of the perturbative treatment of centrifugal-distortion effects is found in Ref. [40]. Here, we focus only on those issues that might be useful in the context of this review. As in the case of the rigid-rotor, we restrict our discussion to some representative cases.

For symmetric-top molecules $\hat{H}'_{dist}$ can be rewritten as

$$\hat{H}'_{dist} = -D_J\hat{J}^4 - D_{JK}\hat{J}^2\hat{J}_z^2 - D_K\hat{J}_z^4. \tag{17}$$

The D's are the quartic centrifugal-distortion constants of the symmetric top and can be written as combinations of the $\tau_{\alpha\beta\gamma\delta}$'s [1,40]. The corresponding energy correction is then

$$E'_{dist} = -[D_J J^2(J+1)^2 + D_{JK}J(J+1)K^2 + D_K K^4]. \tag{18}$$

In the case of a linear molecule, the expression of $\hat{H}'_{dist}$ is with

$$\hat{H}'_{dist} = -D\hat{J}^4, \tag{19}$$

simpler and gives rise to an energy correction of the form

$$E'_{dist} = -D_J J^2(J+1)^2. \tag{20}$$

The situation for asymmetric-top molecules is substantially more complicated. Inclusion of centrifugal-distortion effects is here usually accomplished by means of a so-called reduced Hamiltonian. We do not give details and instead refer the reader to Watson's original papers [40–43] as well as to the perhaps more accessible summary found in Ref. [1].

Rotational transitions are induced by the interaction of molecular electric-dipole components (fixed in the rotating body) with the electric components (fixed in space) of the radiation field. Without going into detail, the selection rules governing rotational transitions are [1,2]

$$\Delta J = 0, \pm 1, \quad \Delta M = 0, \pm 1. \tag{21}$$

Additional selection rules apply for symmetric-top rotors:

$$\Delta K = 0, \tag{22}$$

and asymmetric-top rotors:

$$\Delta K_{-1} = 0, \pm 1, \ \Delta K_{+1} = 0, \pm 1, \tag{23}$$

where K_{-1} and K_{+1} represent the quantum numbers of the limiting prolate and oblate symmetric-top rotors, respectively. The strength of rotational transitions are then proportional to the square of the corresponding dipole-moment components. The situation is more complicated in Fourier transform microwave spectroscopy, where the dependence goes roughly with the first instead of the second power of the moment [44]. Although the most fundamental selection rule for rotational spectroscopy is that the molecule should have a non-vanishing permanent dipole moment, we note that molecules without a permanent dipole moment can have perturbation-allowed rotational spectrum [39]. For spherical tops (three identical moments of inertia), for example, centrifugal-distortion effects can produce a small permanent dipole moment that allows the observation of the rotational spectrum [1,45] (see also, for instance, Refs. [46–48]). Analogously, "forbidden" (perturbation-allowed) $\Delta K = \pm 3, \ \pm 6, \ldots$ rotational transitions can be observed for symmetric-top rotors [1,45] (see also, for example, Refs. [49,50]).

With the selection rules for dipole absorption, the rotational frequencies for a linear rotor are [1]

$$\nu = 2B(J+1) - 4D(J+1)^3 + H(J+1)^3[(J+2)^3 - J^3] + \cdots. \tag{24}$$

In a similar manner, the ground-state rotational frequencies of a symmetric-top molecules [1] are

$$\begin{aligned}\nu = {} & 2B(J+1) - 4D_J(J+1)^3 - 2D_{JK}(J+1)K^2 + H_J(J+1)^3[(J+2)^3 - J^3] \\ & + 4H_{JK}(J+1)^3K^2 + 2H_{KJ}(J+1)K^4 + \cdots,\end{aligned} \tag{25}$$

where the D and H constants are the quartic (first-order) and sextic (second-order) centrifugal-distortion constants of the symmetric-top molecule, respectively. Expressions for D_J, D_{JK}, H_J, H_{JK}, and H_{KJ} are given in the literature [1].

2.2. *Fine and hyperfine structure in rotational spectra*

The fine and hyperfine structure in rotational spectra is due to interactions of the molecular electric and/or magnetic fields with the nuclear moments. The most important of these interactions is the one between the molecular electric-field gradient and the electric quadrupole moments of certain nuclei. As far as magnetic interactions are concerned, the end-over-end rotation of a molecule generates a weak magnetic field that interacts with the nuclear magnetic moments to produce a slight magnetic splitting or shift of the lines. In addition to these two interactions which are referred to as quadrupole and spin–rotation interactions, respectively, spin–spin interactions between different nuclear spins may arise.

The overall Hamiltonian can be written as a sum of different contributions

$$\hat{H} = \hat{H}_{rot} + \hat{H}_Q + \hat{H}_{SR} + \hat{H}_{SS}, \tag{26}$$

where $\hat{H}_{rot}$ accounts for the pure rotational part (see previous section) and is given either by Equation (1) or Equation (14) depending on the treatment of centrifugal distortion. The additional terms, i.e., $\hat{H}_Q$, $\hat{H}_{SR}$, and $\hat{H}_{SS}$ account for nuclear quadrupole-coupling, as well as spin–rotation and spin–spin interactions, respectively.

For nuclei with a quadrupole moment, i.e., those with nuclear spin quantum number $I_K \geq 1$, the main contribution to the (hyper)fine structure is due to interactions of the nuclear quadrupole moments with the electric-field gradients at the corresponding nuclei given by [51]:

$$\hat{H}_Q = \frac{1}{2}\sum_K \frac{eQ_K q_J^K}{I_K(2I_K-1)J(2J-1)}\left|3(\hat{\mathbf{I}}_K\cdot\hat{\mathbf{J}})^2 + \frac{3}{2}(\hat{\mathbf{I}}_K\cdot\hat{\mathbf{J}}) - \hat{\mathbf{I}}_K^2\hat{\mathbf{J}}^2\right]. \tag{27}$$

In Equation (27), the quadrupole moment for the K-th nucleus is denoted by eQ_K, while q_J^K is the expectation value of the space-fixed component V_{ZZ}^K of the electric-field gradient tensor at the same nucleus averaged over the rotational motion:

$$q_J^K = \frac{2}{(J+1)(2J+3)}[V_{aa}^K\langle\hat{J}_a^2\rangle + V_{bb}^K\langle\hat{J}_b^2\rangle + V_{cc}\langle\hat{J}_c^2\rangle]. \tag{28}$$

The elements of nuclear quadrupole-coupling tensors are usually reported as

$$\chi_{\alpha\beta}^K = eQ_K V_{\alpha\beta}^K, \tag{29}$$

where α, β refer to the inertial axes a, b, and/or c.

Instead of an elaborate exposition, we will provide a brief discussion of how nuclear quadrupole-coupling affects the rotational spectrum. Let us consider the case of a linear molecule. In this case, the molecular field-gradient tensor is symmetric about the bond axis. Therefore, due to symmetry and Laplace's equation (the electric-field gradient is a traceless property) we have

$$V_{xx} = V_{yy} = -\frac{1}{2}V_{zz}. \tag{30}$$

With the selection rules for hyperfine transitions in rotational absorption spectra

$$\Delta F = 0, \pm 1 \qquad \Delta I_K = 0, \tag{31}$$

where F is the quantum number arising from the coupling scheme $\mathbf{F} = \mathbf{J} + \mathbf{I}_K$, the rotational frequencies perturbed by quadrupole coupling are

$$\Delta E = E_{rot}(J+1) - E_{rot}(J) + E_Q(J+1, I_K, F') - E_Q(J, I_K, F), \tag{32}$$

where $F' = F$, $F \pm 1$ and

$$E_Q = -\chi\frac{\frac{3}{4}D(D+1) - I_K(I_K+1)J(J+1)}{2(2J-1)(2J+3)I_K(2I_K-1)}, \tag{33}$$

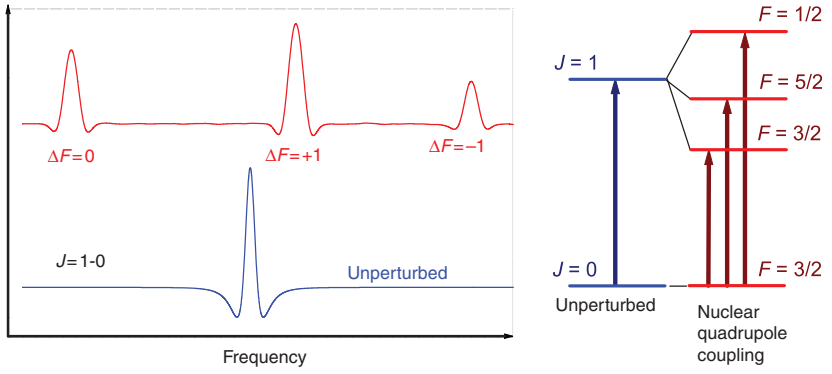

Figure 1. [Colour online]. Effect of nuclear quadrupole coupling on the $J=1\leftarrow 0$ rotational transition of a diatomic molecule with one quadrupolar nucleus ($I_K=5/2$, $\chi<0$). The spectrum at the bottom is the one without quadrupole coupling, while the one at the top illustrates the splittings due to the coupling.

with $D=F(F+1)-J(J+1)-I_K(I_K+1)$.[4] The overall effect therefore is that the transition is split into various hyperfine components, as illustrated in Figure 1 for the $J=1\leftarrow 0$ transition of a diatomic molecule with one quadrupolar nucleus (in this case χ is negative).

Concerning spin–rotation interactions, Flygare derived a formulation in terms of a second-rank tensor $\boldsymbol{C}$ [52]:

$$\hat{H}_{SR}=\sum_K \hat{\mathbf{I}}_K\cdot\boldsymbol{C}^K\cdot\hat{\mathbf{J}}, \tag{34}$$

where the sum over K runs over all nuclei of the molecule with non-vanishing spin.[5]

Let us consider again the case of a linear molecule in order to see how the unperturbed transition frequency ν_0 is affected by one interacting nucleus. Due to symmetry, the spin–rotation tensor can be characterized in this case by just one spin–rotation constant, C. The hyperfine energy levels are then given by

$$E_{SR}=\frac{C}{2}[F(F+1)-I_K(I_K+1)-J(J+1)]. \tag{35}$$

The selection rules are the same as for the quadrupole hyperfine structure (Equation (31)). Therefore, for a rotational transition $J\rightarrow J+1$ we obtain (all quantities in frequency units)

$$\nu_{F+1\leftarrow F}=\nu_0-C(J+1)+C(F+1), \tag{36}$$

$$\nu_{F\leftarrow F}=\nu_0-C(J+1), \tag{37}$$

$$\nu_{F-1\leftarrow F}=\nu_0-C(J+1)-CF. \tag{38}$$

An example is given in Figure 2, where the effect of the spin–rotation interaction is illustrated for the $J=2\leftarrow 1$ transition in the rotational spectrum of a diatomic molecule with one nuclear spin (in this case C is negative).

The direct (dipolar) spin–spin interaction between two nuclear magnetic moments $\hat{\mathbf{I}}_K$ and $\hat{\mathbf{I}}_L$ is described by the Hamiltonian

$$\hat{H}_{SS}^{KL}=\hat{\mathbf{I}}_K\cdot\boldsymbol{D}^{KL}\cdot\hat{\mathbf{I}}_L \tag{39}$$

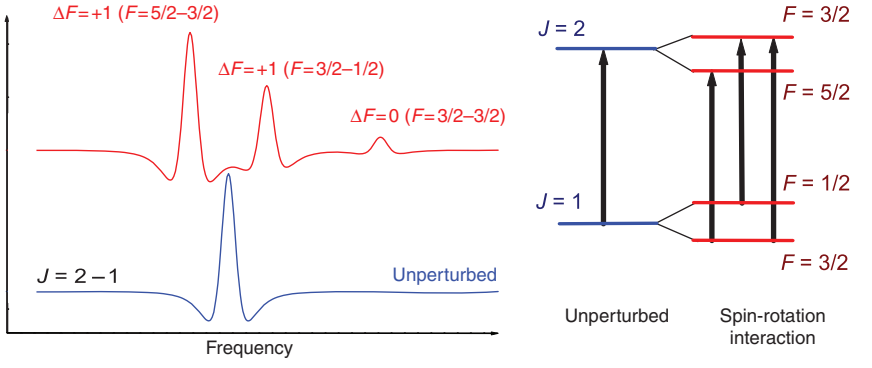

Figure 2. [Colour online]. Effect of spin–rotation interaction on the $J = 2 \leftarrow 1$ rotational transition of a diatomic molecule with one nuclear spin ($I_K = 1/2$, with $C < 0$). The spectrum at the bottom is the one without spin–rotation interaction, while the one at the top illustrates the splittings due to spin–rotation interaction.

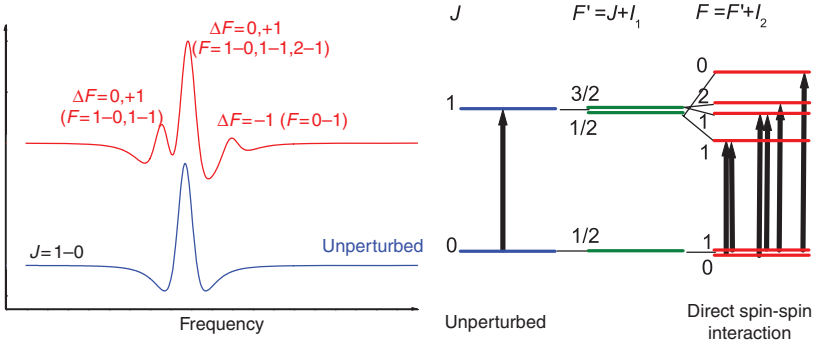

Figure 3. [Colour online]. Effect of spin–spin interaction on the $J = 1 \leftarrow 0$ rotational transition of a diatomic molecule with two nuclear spins (both I_K and I_L equal 1/2). The spectrum at the bottom is the one without spin–spin interaction, while the one at the top illustrates the splittings due to spin–spin interaction.

where the components of the dipolar spin–spin coupling tensor $\boldsymbol{D}^{KL}$ are given by [1,53,54]

$$\boldsymbol{D}_{ij}^{KL} = -\frac{1}{c^2}\gamma_K\gamma_L\frac{3(\boldsymbol{R}_{KL})_i(\boldsymbol{R}_{KL})_j - \delta_{ij}\boldsymbol{R}_{KL}^2}{R_{KL}^5}. \tag{40}$$

In Equation (40), $\boldsymbol{R}_{KL}$ denotes the vector from nucleus K to L, γ_K and γ_L are the gyromagnetic ratios for both nuclei. From Equation (40), it is clear that the dipolar-coupling tensor $\boldsymbol{D}^{KL}$ is completely determined by the molecular geometry and the magnetic properties of the nuclei. An example of the effect of the dipolar spin–spin interaction on the rotational spectrum is provided by Figure 3.

There are additional, so-called indirect contributions to the spin–spin coupling constant, which, while important in nuclear-magnetic resonance (NMR) spectroscopy, play no significant role in rotational spectroscopy (see, for example, Ref. [55]).

2.3. *Molecular parameters needed in rotational spectroscopy*

In the previous two sections, the Hamiltonian needed for the description and analysis of rotational spectra has been discussed in some detail. At this point, it should be emphasized that this Hamiltonian is an effective Hamiltonian. With this it is meant that the Hamiltonian solely deals with the rotational motion and for this purpose involves parameters that are specific for the molecule under consideration and unknown *a priori*. They enter the Hamiltonian since it is necessary to integrate over the electronic as well as vibrational degrees (see next section) of freedom. Nevertheless, the rotational Hamiltonian introduced in the previous sections is useful, as (a) it permits prediction of the rotational spectrum as soon as the required molecular (or spectroscopic) parameters are known (or specified) and, as (b) it allows one to extract the corresponding molecular parameters from experiment [1–3]. However, here we will go one step further and actually construct the rotational Hamiltonian on purely theoretical grounds. This is made possible by exploiting the corresponding expressions for the spectroscopic parameters (partially already given in the previous sections) and requires, as discussed in the following, knowledge of the molecular geometry, a treatment of the electronic structure, and consideration of vibrational effects. The latter are discussed in Section 3, while the quantum-chemical treatment of the electronic structure is the topic of Section 4. Here, we only summarize what *in principle* is needed for the evaluation of the spectroscopic parameters of a molecule.

Let us start with the apparently most important quantities in rotational spectroscopy, the rotational constants B^{α}. Ignoring vibrational corrections, the rotational constants, actually their equilibrium values, are given by the inverse of the principal moments of inertia I_{α} (see, Equation (10)). Those are obtained by diagonalizing the inertia tensor of the molecule which is given by

$$\mathbf{I} = \sum_{K} M_K (R_K^2 \mathbf{1} - \mathbf{R}_K \mathbf{R}_K^T). \tag{41}$$

The inertia tensor can be constructed using an arbitrary Cartesian coordinate system with its origin at the center of mass, and the sum in Equation (41) runs over all nuclei K in the molecule. Note that the masses M_K refer to atomic masses. One might consider the use of nuclear masses more appropriate, but the atomic masses are the preferred choice, as in this way it is possible to account at least partially for the electronic contribution to the inertia tensor. Of course, as discussed in Section 5.1, it is possible to explicitly consider the electronic contribution to the moment of inertia and, thus, the rotational constants via the corresponding rotational g tensor. Returning to Equation (41), we note that the nuclear coordinates $\mathbf{R}_K$ needed to calculate the inertia tensor $\mathbf{I}$ are those of the equilibrium configuration. They are obtained in quantum-chemical calculations within a geometry optimization of the molecule of interest.

Concerning centrifugal distortion, we note that Equation (15) provides the basis for a computational determination of the quartic centrifugal-distortion constants. Required here is the harmonic force field of the molecule, i.e., the harmonic frequencies, as well as the derivatives of the inverse inertia tensor with respect to the normal coordinates. The determination of the sextic centrifugal-distortion constants requires, as discussed in Ref. [56], the additional evaluation of the cubic force field.

The computational determination of the nuclear quadrupole couplings necessitates, as outlined in Section 2.2, the evaluation of the electric-field gradients at the corresponding nuclei. These are first-order properties and, thus, computed either as a simple expectation value of the following (one-electron) operator

$$\hat{V}^K = Z_K \frac{\mathbf{1}(\mathbf{r}-\mathbf{R}_K)^2 - 3(\mathbf{r}-\mathbf{R}_K)(\mathbf{r}-\mathbf{R}_K)^T}{|\mathbf{r}-\mathbf{R}_K|^5}, \tag{42}$$

with $\mathbf{R}_K$ and $\mathbf{r}$ denoting the position of the K-th nucleus and of the electron, respectively, or as first derivative of the energy with respect to the nuclear quadrupole moment [57]. The perturbing operator is identical to the one given in Equation (42). The nuclear spin–rotation tensors on the other hand are second-order properties and can be obtained using either analytic-derivative theory or linear-response theory [58]. This means more or less that the nuclear spin–rotation tensor is computed as a second derivative with respect to the nuclear spin and the rotational angular momentum as perturbations. The corresponding perturbed (one-electron) operators are [58]

$$\hat{h}^{(1)} = -(\mathbf{I}^{-1}\mathbf{J}) \cdot \hat{\mathbf{l}} \tag{43}$$

with the electronic angular momentum $\hat{\mathbf{l}}$,

$$\hat{h}^{(2)} = \frac{1}{c^2} \sum_K \gamma_K \frac{\mathbf{I}_K \cdot \hat{\mathbf{l}}_K}{|\mathbf{r}-\mathbf{R}_K|^3} \tag{44}$$

with γ_K as the gyromagnetic ratio of the K-th nucleus and $\hat{\mathbf{l}}_K$ as the electronic angular momentum defined with respect the nuclear position $\mathbf{R}_K$, as well as

$$\hat{h}^{(2)} = -\frac{1}{c^2} \sum_K \gamma_K \mathbf{I}_K \frac{(\mathbf{R}_K \cdot \mathbf{r})\mathbf{1} - \mathbf{R}_K \mathbf{r}^T}{|\mathbf{r}-\mathbf{R}_K|^3} \mathbf{I}^{-1}\mathbf{J}. \tag{45}$$

Note that the nuclear spin–rotation tensor also involves a nuclear contribution which is determined solely by the molecular geometry. The spin–spin interaction finally, as is obvious from the given Equation (40), does not involve an electronic contribution and can be easily computed from the geometry determined within a geometry optimization.

Table 1 summarizes what is actually needed for a theoretical determination of the spectroscopic parameters of interest for rotational spectroscopy.

2.4. *Frequency ranges and magnitude of spectroscopic parameters in rotational spectroscopy*

According to the region of the electromagnetic spectrum (see Figure 4), rotational transitions are typically detected in the range of 1 GHz to 3 THz [1–3,59], mostly depending on the rotational constant(s) (loosely speaking, the size) of the molecule investigated. The microwave region covers approximately the range 1–100 GHz and the millimeter-wave region 100–600 GHz. The latter overlaps the far-infrared region, which is, for the part of interest to rotational spectroscopy, also referred to as the submillimeter-wave region.[6]

Nowadays, the principal classification of rotational spectrometers is the following. Fourier-transform (FT) techniques can be applied up to roughly 40 GHz, while

Table 1. Computational requirements for the determination of the relevant parameters in rotational spectroscopy.

Parameter	Symbol(s)	Computational task(s)
Rotational constant	A, B, C	Molecular geometry, geometry optimization
Quartic centrifugal-distortion constants	$\tau_{\alpha\beta\gamma\delta}$, D_J, D_K, D_{JK}, ...	Harmonic force field, i.e., harmonic frequencies and normal coordinates
Sextic centrifugal-distortion constants	$\tau_{\alpha\beta\gamma\delta\epsilon\eta}$, H_J, H_K, H_{JK}, ...	In addition; cubic force field
Dipole moment	μ	First derivative of energy with respect to electric-field components
Nuclear quadrupole coupling	$\chi^K_{\alpha\beta}$, q^K, ...	Electric-field gradient as first derivative with respect to nuclear quadrupole moment
Nuclear spin–rotation tensor	C^K	Second derivative of energy with respect to angular momentum and nuclear spin
Spin–spin (dipolar) interaction	D^{KL}	Molecular geometry

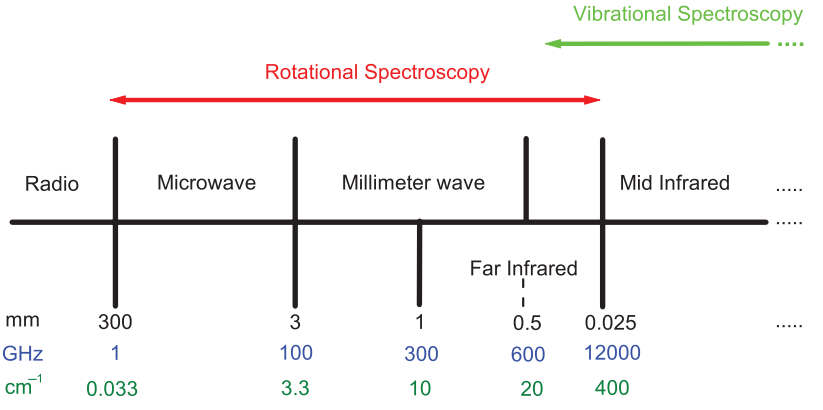

Figure 4. [Colour online]. Typical frequency ranges used for the detection of rotational spectra.

continuous-wave (CW) measurements are mostly used in the remainder of the frequency range. For the former, as Doppler and pressure-broadenings are largely reduced, the typical resolution is about 5–10 kHz [60,61]. For the latter, as the resolution strongly depends on different factors but mainly on the Doppler effect, in the best cases, the resolving power is 20–500 kHz [1,3,62,63]. But, there are special methods such as, for example, the Lamb-dip technique [17,18] that can be applied to improve the resolution. With the latter, a resolution of 15–20 kHz can be reached which turns out to be sufficient to observe in many cases the hyperfine structure in a rotational spectrum.

Concerning the magnitude of the various effects that govern a rotational spectrum, it should be borne in mind that the frequency of a rotational transition is mainly

determined by the rotational constant(s). Their values, usually given in GHz (in cm^{-1} when coming from rovibrational investigation), range from less than 1 GHz for large molecules up to ~1300 GHz for small molecules such as HD. Centrifugal-distortion effects, with the corresponding constants given in MHz and/or kHz, are small compared to rotational constants, ranging from less than 1 kHz up to ~1 GHz, but the effects can be substantial for high J values. Among the fine and hyperfine interactions, the nuclear quadrupole coupling is the most dominant. The coupling constants are typically of the order of hundreds of kHz up to several MHz (depending on the quadrupolar nucleus under consideration). The corresponding spin–rotation and spin–spin interactions are smaller and reported in kHz.

3. Vibrational effects

In order to compare theoretically calculated spectroscopic parameters to experiment, one must consider the effect of molecular vibrations. This is because the properties alluded to in the previous section depend upon the structure of the molecule and therefore must be averaged over the vibrational motion of the system under consideration. Theoretical considerations in this realm are discussed in the present section, where we will outline a perturbative treatment of vibrational effects and give the relevant expressions for computing vibrational corrections to rotational constants (Section 3.1) as well as other spectroscopic parameters (Section 3.2).

3.1. *Vibrational perturbation theory*

The starting point for our treatment of vibrational perturbation theory is the semi-rigid Hamiltonian due to Watson [64,65],

$$\hat{H} = \frac{1}{2}\sum_{\alpha,\beta}(\hat{J}_\alpha - \hat{\pi}_\alpha)\mu_{\alpha\beta}(\hat{J}_\beta - \hat{\pi}_\beta) + \frac{1}{2}\sum_r \omega_r \hat{p}_r^2 + V(\mathbf{q}) - \frac{1}{8}\sum_\alpha \mu_{\alpha\alpha}. \tag{46}$$

This operator is expressed in the representation of the dimensionless normal coordinates defined by

$$q_r = \omega_r^{1/2} Q_r, \tag{47}$$

with Q_r as the usual normal coordinates, defined via the eigenvectors of the mass-weighted Hessian, and ω_r as the associated harmonic wavenumbers. In Equation (46), $\hat{J}_\alpha$ is again the rotational angular-momentum operator about axis α, and $\hat{\pi}_\alpha$ represents the α-th component of vibrational angular momentum. The latter is defined by

$$\hat{\pi}_\alpha = \sum_{r,s} \zeta_{rs}^\alpha \left(\frac{\omega_s}{\omega_r}\right)^{1/2} q_r \hat{p}_s, \tag{48}$$

where the ζ_{rs}^α are elements of the antisymmetric Coriolis zeta matrix (for a definition, see Refs. [1–3]); the $\mu_{\alpha\beta}$ are those of an effective inverse inertia tensor, which will be addressed in the next paragraph. $V(\mathbf{q})$ is the potential in terms of the dimensionless normal coordinates, and the final term in Equation (46), sometimes called the Watson term

(denoted $\hat{U}$), is due to the use of a normal-coordinate representation and leads to a nearly constant shift in the spectrum that has negligible spectroscopic importance [66].

The spectrum of the Watson Hamiltonian gives the rovibrational energy-level structure of the molecule under consideration. The eigenvalues may be approached in a perturbation expansion in which the inverse inertia tensor and the potential in the Watson Hamiltonian are both expanded as Taylor series in the normal coordinates q_r.

$$\mu_{\alpha\beta} = \mu^e_{\alpha\beta} + \sum_r \mu^r_{\alpha\beta} q_r + \frac{1}{2}\sum_{r,s} \mu^{rs}_{\alpha\beta} q_r q_s + \cdots \tag{49}$$

$$V(\mathbf{q}) = \frac{1}{2}\sum_r \omega_r q_r^2 + \frac{1}{6}\sum_{r,s,t} \phi_{rst} q_r q_s q_t + \frac{1}{24}\sum_{r,s,t,u} \phi_{rstu} q_r q_s q_t q_u + \cdots. \tag{50}$$

The leading terms are here just the inverse principal moments of inertia

$$\mu^e_{\alpha\beta} = \frac{\delta_{\alpha\beta}}{I^e_\alpha} \tag{51}$$

with the latter determined for the equilibrium structure of the molecule and the harmonic potential. The corrections to the potential are then given by cubic, quartic, etc. terms where ϕ_{rst}, ϕ_{rstu}, etc. specify the corresponding force constants. It can further be shown [1] that the first and second derivatives of the effective inverse inertia tensor elements can be written solely in terms of the first derivatives of the inertia tensor itself

$$\mu^r_{\alpha\beta} = \left(\frac{\partial \mu_{\alpha\beta}}{\partial q_r}\right)_e = -\frac{a^{\alpha\beta}_r}{I^e_\alpha I^e_\beta} \tag{52}$$

$$\mu^{rs}_{\alpha\beta} \equiv \left(\frac{\partial^2 \mu_{\alpha\beta}}{\partial q_r \partial q_s}\right)_e = \frac{3}{4}\sum_\xi \frac{a^{\alpha\xi}_r a^{\xi\beta}_s + a^{\alpha\xi}_s a^{\xi\beta}_r}{I^e_\alpha I^e_\beta I^e_\xi}, \tag{53}$$

where

$$a^{\alpha\beta}_r = \left(\frac{\partial I_{\alpha\beta}}{\partial q_r}\right)_e. \tag{54}$$

A perturbation series can be developed by at least two methods: the contact transformation of Van Vleck [67,68], first applied to the vibrational problem by Nielsen [69], and Rayleigh–Schrödinger perturbation theory (RSPT). The former lends itself to expressions that are written as an expansion in $v_r + \frac{1}{2}$ (v_r is a vibrational quantum number), while RSPT is perhaps simpler to apply when one is interested in just a single vibrational state. Within the RSPT framework, the harmonic potential, the kinetic energy and the leading term of $\mu_{\alpha\beta}$ are zeroth-order quantities, which permit the partitioning of the Watson Hamiltonian into the rigid-rotor harmonic-oscillator Hamiltonian $\hat{H}^0$ and a perturbation

$$\hat{H} = \hat{H}^0 + \hat{H}' \tag{55}$$

$$\hat{H}^0 = \sum_\alpha B^\alpha \hat{J}^2_\alpha + \frac{1}{2}\sum_r \omega_r (\hat{p}_r^2 + q_r^2), \tag{56}$$

where the rotational constant B^{α}, Equation (10), is associated with the coefficient of the $\hat{J}_{\alpha}^{2}$ operator. Now, all of the terms in the perturbing Hamiltonian $\hat{H}'$ contain the position operator to some power. For example, the Coriolis operator (Equation (48)) is linear in q, the first and second derivatives of the effective inverse inertia tensor are linear and bilinear in q, and the higher-order potential terms have three, four, etc. q_r operators. These additional terms are then collected according to an overall order which is defined by the number of q_r operators present. The cubic and quartic potential are treated as first- and second-order contributions, respectively; the harmonic potential, which is quadratic in q_r, is a zeroth-order quantity. One then applies the usual formulas of perturbation theory, specifically

$$E_L = \langle i|\hat{H}'|i\rangle \tag{57}$$

$$E_Q = \sum_{k\neq i} \frac{\langle i|\hat{H}'|k\rangle\langle k|\hat{H}'|i\rangle}{E_i^{(0)} - E_k^{(0)}} \tag{58}$$

$$\vdots$$

The designation of these as linear (L) and quadratic (Q) follows a recent paper of Vázquez and Stanton that applies fourth-order RSPT to the Watson Hamiltonian [70]. Corrections to a given order (for example, second) for the specific vibrational state i, $|i\rangle = |v_1 v_2 \cdots v_r \cdots\rangle$, are then obtained by inserting the individual contributions to $\hat{H}'$ into Equations (57) and (58), and collecting terms that correspond to a fixed overall order.[7]

Note that the perturbational treatment is only applied to the vibrational wavefunction. The rotational part is ignored in this treatment, and the angular momentum $\hat{J}_{\alpha}$ is simply considered a parameter which is used to characterize the corresponding corrections later on. In the context of this review, the important terms are those that multiply $\hat{J}_{\alpha}^{2}$, as these are the effective rotational constants, and contain contributions beyond the rigid-rotator harmonic-oscillator approximation.

There are no first-order corrections to the simple rigid-rotor rotational constant defined by the moments of inertia of the equilibrium structure, as a consequence of the usual harmonic oscillator integral selection rules (specifically $\langle i|q_r^{2n+1}|i\rangle = 0$). In second order, there are three contributions. The first comes from the quadratic term in the expansion of the effective inverse inertia tensor,

$$B_{eff}^{\alpha} \Leftarrow \frac{1}{2}\left\langle i\left|\frac{1}{2}\sum_{r,s}\mu_{\alpha\alpha}^{rs}q_r q_s\right|i\right\rangle \tag{59}$$

(a linear term in the sense above), and two "quadratic terms". The first of these comes from the Coriolis operator

$$B_{eff}^{\alpha} \Leftarrow \frac{1}{I_{\alpha}^{2}}\sum_{k\neq i}\frac{\langle i|\hat{\pi}_{\alpha}|k\rangle\langle k|\hat{\pi}_{\alpha}|i\rangle}{E_i^{(0)} - E_k^{(0)}} \tag{60}$$

and the third term comes from the first-order correction to the inverse mass tensor together with the cubic anharmonicity

$$B_{eff}^{\alpha} \Leftarrow \frac{1}{2}\sum_{k\neq i}\frac{\langle i|\sum_r \mu_{\alpha\alpha}^{r}q_r|k\rangle\langle k|\frac{1}{6}\sum_{r,s,t}\phi_{rst}q_r q_s q_t|i\rangle}{E_i^{(0)} - E_k^{(0)}} + \text{hermitian conjugate.} \tag{61}$$

If the vibrational state i is taken to be the ground vibrational level, the rules for harmonic oscillator integrals [71] and the definitions given earlier in this section can easily be applied to show that the total second-order correction to the rotational constant B^α can be written as

$$B_e^{\alpha 2}\left[\sum_{\beta,r}\frac{3(a_r^{\alpha\beta})^2}{4I_\beta^e}-\frac{1}{2}\sum_{r,s}\frac{(\zeta_{rs}^\alpha)^2(\omega_r-\omega_s)^2}{\omega_r\omega_s(\omega_r+\omega_s)}+\frac{1}{2}\sum_{r,s}\frac{\phi_{rrs}a_s^{\alpha\alpha}}{\omega_s^{3/2}}\right]. \tag{62}$$

At this point, it is appropriate to comment that the usual contact-transformation method gives the second-order result [36]

$$B_i^\alpha = B_e^\alpha - \sum_r \alpha_r^\alpha\left(v_r+\frac{1}{2}\right) \tag{63}$$

with $\alpha = a, b, c$ and where the sum is taken over all fundamental vibrational modes r. The corresponding α_r^α constants[8] are given by

$$\alpha_r^\alpha = -2B_e^{\alpha 2}\left[\sum_{\beta}\frac{3(a_r^{\alpha\beta})^2}{4I_\beta^e}+\sum_{s}\frac{(\zeta_{rs}^\alpha)^2(3\omega_r^2+\omega_s^2)}{\omega_r(\omega_r^2-\omega_s^2)}+\frac{1}{2}\sum_{s}\frac{\phi_{rrs}a_s^{\alpha\alpha}}{\omega_s^{3/2}}\right]. \tag{64}$$

It is important to point out that the individual α_r^α constants might be subject to a resonance term in the Coriolis contribution, but that their sum (the corresponding correction to the ground-state rotational constants, seen in Equation (62)) is unaffected by possible resonances. This is, of course, as it must be, as the ground state is non-degenerate and its treatment by perturbation theory should therefore be free of potential singularities. This issue has caused a bit of confusion in the literature, as it is common to say that one has to "calculate the α's" to correct rotational constants. That problems affecting the calculation of the individual vibration–rotation interaction constants has anything whatsoever to do with calculating the difference between equilibrium and ground-state rotational constants is manifestly false; one only has to calculate their sum, which can be done quite directly via Equation (62). It was East *et al*. [72] who first derived the form of the Coriolis contribution in Equation (62), by explicitly summing the corresponding contribution in Equation (64) over the vibrational states. The more direct derivation of the rotational constant correction outlined here, to our knowledge, does not appear in the previous literature.

It is often assumed that the second-order correction to the rotational constants outlined in the preceding paragraph accounts nearly quantitatively for all differences between the ground-state constants B_0^α and the corresponding rigid-rotor constants B_e^α. The perturbation treatment can be extended to fourth order (the third-order contribution to the rotational constants again vanishes, as do all odd-order contributions), although this is a very tedious and somewhat complicated process. Vázquez and Stanton have recently presented partial analytical equations for the fourth-order correction and have implemented its full calculation in a numerical sum-over-states program [70]. For water, it turns out that the fourth-order contribution to the A rotational constant is quite sizable ($>10\%$ of the second-order contribution), a result that had been anticipated in a previous exhaustive theoretical study by Barletta *et al*. [73]. Apart from this work, not very much is known about the general magnitudes of the fourth-order corrections to rotational constants, although experimental values for the

so-called second-order vibration–rotation interaction constants γ_{rs}^{α} have been reported in the literature (see, for instance, Refs. [74–78]).

3.2. *Vibrational corrections to molecular properties*

Force-field evaluations in conjunction with vibrational perturbation theory allow the estimation of zero-point vibrational (ZPV) corrections to first- and second-order molecular properties. Quantum-chemical calculation of the properties of interest for this review – those affecting rotational spectra – will be discussed in the following section and the details of these calculations can be found there. Here, we focus only on how vibrational averaging of generic properties can be carried out within the framework of quantum chemistry together with perturbation theory.

The procedure presented here is based on an approach [79] which was described in detail in Ref. [80] and applied there for NMR shielding tensors. It consists of expanding the expectation value of the generic property X over the vibrational wavefunction in a Taylor series around the equilibrium geometry with respect to normal-coordinate displacements

$$\langle X\rangle = X_{eq} + \sum_r \left(\frac{\partial X}{\partial Q_r}\right)_{Q=0}\langle Q_r\rangle + \frac{1}{2}\sum_{r,s}\left(\frac{\partial^2 X}{\partial Q_r \partial Q_s}\right)_{Q=0}\langle Q_r Q_s\rangle + \cdots, \tag{65}$$

where the expansion is truncated after the quadratic term. The expectation values over Q_r and Q_rQ_s are evaluated using a perturbation theory treatment starting from the rigid-rotator harmonic-oscillator approximation [36]. The corresponding expressions are, in the lowest order,

$$\langle Q_r\rangle = -\frac{1}{4\omega_r^{3/2}}\sum_s \phi_{rss} \tag{66}$$

and

$$\langle Q_r Q_s\rangle = \delta_{rs}\frac{1}{2\omega_r}. \tag{67}$$

The approach described above has been employed to investigate vibrational effects on various electric and magnetic molecular properties, specifically NMR shielding, spin–spin and spin–rotation constants as well as nuclear quadrupole-coupling constants, dipole and quadrupole moments. Other approaches have been suggested in the literature [81,82], as well. Noteworthy in the present context are the perturbational approach by Ruud *et al.* [81,82] based on an expansion around an effective geometry instead of the equilibrium geometry [83] as well as non-perturbative schemes [84–86]. In their application, the latter have typically been restricted to small systems.

4. Quantum chemistry

To predict the molecular properties of relevance to rotational spectroscopy (as well as other spectroscopic techniques beyond the focus of this review), the electronic Schrödinger equation needs to be solved within the Born–Oppenheimer approximation [87]. While it is

a straightforward matter – at least in a non-relativistic framework – to write down the electronic Hamiltonian of a molecule, it is considerably more difficult to find its eigenvalues and eigenvectors. Nevertheless, it is the electronic problem that is most fundamental for theoretical treatments in many area of molecular physics and chemistry. The nuclear-position dependent eigenvalues of the electronic Hamiltonian define the potential-energy surfaces that are the central paradigm of descriptive chemical physics. It is these surfaces that must be considered in conventional models of reactivity and dynamics [88] as well as the treatment of vibrational [71] and electronic spectra [89]. Thus, solution to the electronic problem (or its approximation by some means) is a prerequisite for studying any sort of nuclear dynamics including the rotational problem that is the focus of this review. Solution of the electronic Schrödinger equation is the central problem in quantum chemistry [90–94], which is the principal subject of this section.[9]

4.1. *Overview*

As the electronic Schrödinger equation cannot be solved exactly (except for one-electron systems such as the hydrogen-like atoms or the H_2^+ ion), the objective of quantum chemistry is to find approximate solutions that compromise as little accuracy as possible without incurring excessive costs. The balance between required accuracy and cost is the reason why there are so many approaches available to computational chemists. A bewildering array of acronyms for quantum-chemical methods exist, but there are at the end only a handful of distinct approaches. First of all, it must be realized that the basic problem in all approaches for the approximate solution of the electronic Schrödinger equation consists in setting up a suitable ansatz for the electronic wavefunction. The latter actually is a many-electron function and needs to obey the antisymmetry imposed on many-fermion systems by the Pauli principle. The usual procedure is to deal first with the one-electron problem (construction of molecular orbitals – MOs) and then in a second step with the actual many-electron wavefunction (the electron-correlation problem), as illustrated in Figure 5. The usual starting point is the choice of a set of one-electron basis functions (often called atomic orbitals (AOs), as the most common choices are atomic-centered functions that have spherical symmetry properties [95], see also Section 4.3) and to construct the molecular orbitals from them. This step already involves an approximation, as in practice only finite (and thus incomplete) basis sets can be used. One usually refers to this as the basis-set (or linear combination of atomic orbitals – LCAO) approximation, and the associated error is termed the basis-set error. In the second step, the MOs are used to construct many-electron functions. The simplest form is the Slater determinant [90], but the actual choice for the wavefunction is, at least for the more accurate schemes discussed here, a linear combination of determinants. The step from a single Slater determinant to a linear combination enables one to introduce electron-correlation effects, which by definition cannot be treated using just one determinant, as the latter corresponds to a model of independent particles. As for the first step, this second step also introduces an error in quantum-chemical calculations, as a truncated expansion in terms of Slater determinants only allows for an approximate treatment of electron-correlation effects. Basis-set and electron-correlation errors are the

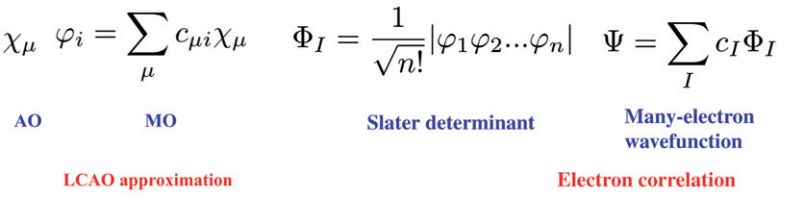

Figure 5. [Colour online]. "Construction kit" for many-electron wavefunctions typically used in quantum chemistry, thus illustrating the basis-set approximation and the electron-correlation problem.

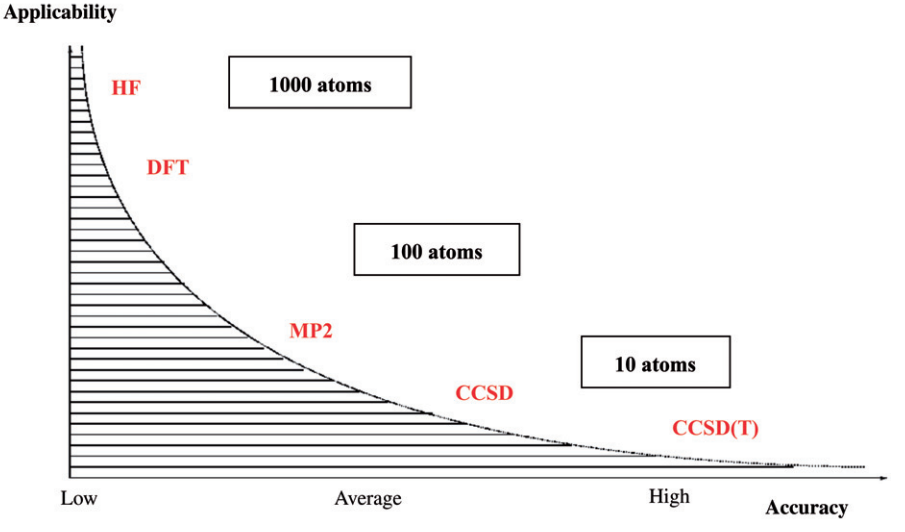

Figure 6. [Colour online]. Overview of quantum-chemical methods in terms of achievable accuracy and applicability.

main sources for errors in quantum-chemical calculations and are not independent; the actual electron-correlation energy strongly depends on the chosen basis set [95].

To summarize the discussion so far, a quantum-chemical calculation is typically characterized by the choice of both method and basis set. The various methods differ in the way the actual wavefunction is chosen and how the associated parameters are determined. Some of the more important schemes are compared in Figure 6 with respect to accuracy and applicability. From this, it can be seen that the Hartree–Fock self-consistent-field (HF-SCF, the wavefunction is given by a single Slater determinant and the molecular orbitals are determined via the variation principle [96]) and density-functional theory (DFT, based on the Hohenberg–Kohn theorems [97] with the electron density as the central quantity instead of the wavefunction, though the usual Kohn–Sham version [98] is equivalent to a single-determinant ansatz with an exchange-correlation functional depending on the density [99,100]) approaches offer limited accuracy but are quite broadly applicable due to both intrinsic simplicity and extensive algorithmic development in the past two decades [101]. Somewhat greater accuracy can be achieved with Møller–Plesset (MP)

perturbation theory (often also referred to as many-body perturbation theory) [102,103], i.e., with a perturbative treatment starting from the HF-SCF wavefunction as the zeroth-order solution and the sum of Fock operators as unperturbed Hamiltonian [104]. A nearly quantitative treatment of electron-correlation effects in many cases is finally provided by coupled-cluster (CC) techniques [105–110] which are characterized by an exponential ansatz for the wavefunction. However, the high accuracy can only be achieved at significant computational expense, thus rendering the CC schemes less applicable to larger molecules. To be more specific with respect to the applicability issue, we note that the computational cost of HF-SCF and DFT formally scales with $\mathcal{O}(N^4)$ (though efficient implementations permit an effectively linear scaling for sufficiently large molecules [111,112]). For the CC methods, on the other hand, the scaling is at least $\mathcal{O}(N^6)$ and can be higher. Here, N is a measure for the size of the system and often identified (imprecisely) with the number of basis functions. Among the approaches not listed in Figure 6 are those that are known as multi-reference schemes (multi-configurational SCF, multi-reference configuration-interaction, etc. [113–115]) and which, unlike the HF ansatz, directly start with several Slater determinants for the representation of the electronic wavefunction. The computational cost analysis of these methods is less straightforward, but they are in general, comparable in cost to CC methods for a similar level of accuracy.

In the area of rotational spectroscopy, the choice of an appropriate quantum-chemical method is more or less dictated by two considerations. First, rotational spectroscopy typically deals with small to medium-sized molecules. Second, it is also a technique that provides quite precise spectroscopic parameters. Since *useful* computational analysis of the spectra therefore requires quite accurate calculations and the size of the molecules does not present a serious obstacle to the use of computationally-intensive methods, it seems that CC methods are a natural choice for this area of application. Accordingly, we will focus on these methods in the following sections. However, in order to put the CC methods in the proper context, we will start with a brief recapitulation of HF as well as MP perturbation theory, before an extensive discussion of the currently available CC schemes is given.

4.2. *Quantum-chemical methods*

4.2.1. *Hartree–Fock theory*

In HF theory [96], the wavefunction for an n-electron atom or molecule is assumed to be given by a single Slater determinant

$$\Psi_{HF} = \frac{1}{\sqrt{n!}} |\varphi_1 \varphi_2 \cdots \varphi_n|. \tag{68}$$

The corresponding energy expectation value, the so-called HF energy, is then

$$E_{HF} = \sum_i h_{ii} + \frac{1}{2} \sum_{i,j} \langle ij \,||\, ij \rangle \tag{69}$$

with the one-electron integrals defined by

$$h_{pq} = \int d\tau_1 \; \varphi_p^*(1) h \varphi_q(1) \tag{70}$$

and the antisymmetrized two-electron integrals by

$$\langle pq||rs\rangle = \int d\tau_1 \int d\tau_2 \; \varphi_p^*(1)\varphi_q^*(2)\frac{1}{r_{12}}[\varphi_r(1)\varphi_s(2) - \varphi_s(1)\varphi_r(2)]. \tag{71}$$

The n spin orbitals φ_i that are used to set up the Slater determinant in Equation (68) are determined via the variation principle. This means that the HF orbitals are obtained as solution of the HF equations

$$F\varphi_i = \epsilon_i\varphi_i \quad i = 1, \ldots, n \tag{72}$$

with the ϵ_i as the orbital energies and the Fock operator defined by

$$F = h + \sum_j (J_j - K_j). \tag{73}$$

In Equations (69)–(73), h denotes the usual one-electron part of the Hamiltonian consisting of the kinetic energy as well as nuclear-electron potential [90]; J_j and K_j are the Coulomb and exchange operators defined via

$$\begin{aligned} J_j\varphi_i(1) &= \int d\tau_2\varphi_j^*(2)\frac{1}{r_{12}}\varphi_j(2)\varphi_i(1) \\ K_j\varphi_i(1) &= \int d\tau_2\varphi_j^*(2)\frac{1}{r_{12}}\varphi_i(2)\varphi_j(1), \end{aligned} \tag{74}$$

which account for the mean-field description of the two-electron interactions. The HF equations (in the basis-set representations they are known as the Roothaan–Hall equations, see Ref. [96]) can be solved using iterative schemes, typically of the self-consistent-field (SCF) type.

Spin symmetry is usually exploited for closed-shell systems. Two spin orbitals are then constructed from each spatial orbital ϕ_i, viz.

$$\phi_i \longrightarrow \phi_i\alpha \quad \text{and} \quad \phi_i\beta \tag{75}$$

with α and β the assigned spin functions. The corresponding Slater determinant in this restricted HF (RHF) ansatz is given by

$$\Phi_{RHF} = \frac{1}{\sqrt{n!}}|\phi_1\alpha \; \phi_1\beta \; \phi_2\alpha \cdots \phi_{n/2}\alpha \; \phi_{n/2}\beta| \tag{76}$$

and the corresponding RHF energy by

$$E_{RHF} = \sum_i 2h_{ii} + \sum_{i,j}(2\langle ij\,|ij\rangle - \langle ij\,|ji\rangle) \tag{77}$$

with the integrals now defined for the spatial orbitals

$$h_{pq} = \int d\mathbf{r}_1 \; \phi_p^*(1)h\phi_q(1) \tag{78}$$

and

$$\langle pq|rs\rangle = \int d\mathbf{r}_1 \int d\mathbf{r}_2 \; \phi_p^*(1)\phi_q^*(2)\frac{1}{r_{12}}[\phi_r(1)\phi_s(2)]. \tag{79}$$

The spatial orbitals are now determined by

$$F\phi_i = \epsilon_i \phi_i \quad i = 1, \ldots, n/2 \tag{80}$$

with the Fock operator for the RHF case defined by

$$F = h + \sum_{j}^{n/2} (2J_j - K_j) \tag{81}$$

and the Coulomb and exchange operators now defined for spatial instead of spin orbitals.

A corresponding treatment for open-shell systems requires, unlike for the closed-shell case, different spatial orbitals for the spin orbitals with α and β spin, namely ϕ_i^{α} and ϕ_i^{β}, and is referred to as unrestricted HF (UHF) [116]. The additional restriction to keep the spatial parts identical leads to the so-called restricted open-shell HF (ROHF) [96] approach.

4.2.2. *Møller–Plesset perturbation theory*

The simplest possibility to account for electron-correlation effects in quantum-chemical calculations is to apply perturbation theory starting from the HF wavefunction as zeroth-order approximation [102,103]. For this purpose, the Hamiltonian is divided in an unperturbed and perturbed part

$$H = H_0 + H'; \tag{82}$$

with the unperturbed part given as the corresponding sum of the Fock operators. This choice is usually referred to as the Møller–Plesset ansatz [104] and the corresponding perturbation treatment is known as Møller–Plesset (MP) perturbation theory, which can be viewed as a special case of the more general many-body perturbation theory (MBPT) [102]. It is straightforward to show that the HF wavefunction as well as all excited determinants Φ_i^a, Φ_{ij}^{ab}, ... obtained by replacing one, two, ... occupied by virtual orbitals are eigenfunctions of H_0. However, the HF energy is only recovered in first-order perturbation theory. The first contribution to the correlation energy is then obtained in second-order (MP2 or MBPT(2)) and given as

$$\Delta E(\mathrm{MP2}) = \frac{1}{4} \sum_{i,j} \sum_{a,b} \frac{|\langle ab||ij\rangle|^2}{\epsilon_i + \epsilon_j - \epsilon_a - \epsilon_b}. \tag{83}$$

In Equation (83), the sum runs over occupied (indices i, j) and virtual spin orbitals (indices a, b) and the expression involves the antisymmetrized two-electron integrals defined in Equation (71) as well as the (for perturbation theory characteristic) orbital-energy denominator. The computational cost of $\mathcal{O}(N^5)$ for MP2 stems from the integral transformation required to obtain the two-electron integrals in Equation (71) in the MO representation; the energy evaluation itself scales with N^4.

Higher orders of MP perturbation theory have also been formulated and implemented [117–120], but they are nowadays much less common. The reasons are that the perturbation expansion can be hampered by divergences [121] which render higher-order results unreliable and that at best MP perturbation theory provides rather slow convergence to the exact solution of the electron-correlation problem, i.e., the so-called

full-configuration interaction (FCI) limit [122]. Most important, there are more efficient treatments for the electron-correlation problem now available (see, for example, next section).

4.2.3. *Coupled-cluster theory*

CC theory [123,124] provides a treatment of electron correlation starting from a single Slater determinant (zeroth-order) reference function. The latter is most often (though not necessarily) obtained using Hartree–Fock (HF) theory and will be denoted in the following as $|0\rangle$. The reference determinant is composed of n occupied spin orbitals (indices $i, j, \ldots$). Solution of the HF-SCF equations (in a basis-set representation, i.e., the Roothaan–Hall equations) also yield unoccupied (virtual) spin orbitals (indices $a, b, \ldots$). By promoting electrons from the occupied to virtual orbitals, so-called singly, doubly, etc. excited determinants with respect to $|0\rangle$ are generated.

CC theory starts with the following ansatz for the wavefunction

$$|\Psi\rangle = \exp(T)|0\rangle \tag{84}$$

with the cluster operator T defined as

$$T \equiv T_1 + T_2 + T_3 + \cdots + T_N, \tag{85}$$

with

$$T_m \equiv \frac{1}{m!^2} \sum_{i,j,k,\cdots} \sum_{a,b,c,\cdots} t_{ijk\ldots}^{abc\cdots} a^+ i b^+ j \cdots. \tag{86}$$

The definition above makes use of the notation of second quantization [92], where p^+ and p denote creation and annihilation operators, respectively. The exponential of the T operator in Equation (84) is defined by the expansion

$$\exp(T) = 1 + T + \frac{1}{2!} T^2 + \frac{1}{3!} T^3 + \cdots. \tag{87}$$

The CC ansatz for the wavefunction so far involves no approximation; in fact, the ansatz in Equation (84) is equivalent to full configuration-interaction (FCI) [125]. The cluster expansion of the wavefunction is simply an alternative way to parameterize the wavefunction $|\Psi\rangle$ in the complete set of Slater determinants that can be constructed from the given spin orbitals.

The unknown parameters in the given ansatz for the wavefunction are the weighting factors t_i^a, $t_{ij}^{ab}, \ldots$ in the cluster operator. These quantities, typically termed amplitudes, need to be determined to obtain the actual wavefunction and energy of the system. While one could appeal to the variation principle, this approach is quite cumbersome in the present context and fraught with subtleties; it is thus not often used. The preferred approach is to use projection techniques. In the first step, we insert the ansatz for $|\Psi\rangle$ in Equation (84) into the electronic Schrödinger equation

$$H \exp(T)|0\rangle = E \exp(T)|0\rangle \tag{88}$$

and then multiply both sides of Equation (88) (from the left) by $\exp(-T)$ (this step is not necessary, but allows one to use nested commutator techniques or, alternatively, diagrammatic methods)

$$\exp(-T)H\exp(T)|0\rangle = E|0\rangle. \tag{89}$$

Left-projection onto the reference determinant $|0\rangle$ immediately gives an equation for the energy in terms of the unknown amplitudes, viz.

$$E = \langle 0|\exp(-T)H\exp(T)|0\rangle. \tag{90}$$

The amplitudes are then determined from the inhomogeneous nonlinear equations obtained by projecting Equation (89) from the left by the excited determinants Φ_p (which are orthogonal to $|0\rangle$),

$$0 = \langle \Phi_p|\exp(-T)H\exp(T)|0\rangle, \tag{91}$$

which, despite the notational simplicity, represent quite complicated equations that are best solved using sophisticated iterative subspace techniques (see, for example, Ref. [126]).

Nevertheless, with the theory given so far, the CC ansatz does not provide a practical scheme for solving the electronic Schrödinger equation, as the calculations would be at least as expensive as corresponding FCI calculations. To obtain a computationally feasible scheme, it is essential to introduce approximations that reduce the computational effort significantly without sacrificing too much in terms of accuracy. The first (and most obvious) choice is to restrict the excitations in the cluster operator as well as in the projection space to certain excitation classes. Since the HF determinant has non-zero Hamiltonian matrix elements only with double excitations, the most basic choice would be to enforce the restriction $T = T_2$, and to restrict the space of Φ_p to just double excitations, thereby giving a reasonably well-behaved system of equations. This is the so-called CC doubles (CCD) approach [127,128] and has a computational cost of the order of N^6. However, since the double excitations interact also with the single, triple, and quadruple excitations (and these, in turn, interact with higher levels of excitation in such a way that no sub-block of the Hamiltonian can be decoupled from the remainder of the matrix), CCD is subject to improvement and this is done by including other excitations in the T operator and the corresponding excited determinants into the projection space. Table 2 summarizes the most common CC models obtained in this way together with the corresponding computational scaling properties.

Table 2. Overview of CC models obtained by restricting the cluster operator T to certain excitation classes.

Approximation	Definition of T	Computational cost	Reference
CCD	$T = T_2$	N^6	[127,128]
CCSD	$T = T_1 + T_2$	N^6	[129]
CCSDT	$T = T_1 + T_2 + T_3$	N^8	[130,131]
CCSDTQ	$T = T_1 + T_2 + T_3 + T_4$	N^{10}	[132,133]
CCSDTQP	$T = T_1 + T_2 + T_3 + T_4 + T_5$	N^{12}	[134]
...			

Currently, the most common choice is the singles and doubles (CCSD) scheme [129] with single and double excitations included in T. The other schemes, i.e., in particular CC singles, doubles, triples (CCSDT) [130,131] and CC singles, doubles, triples, quadruples (CCSDTQ) [132–134] are also in use, but their computational costs ($\mathcal{O}(N^8)$ and $\mathcal{O}(N^{10})$, respectively) are daunting, even with modern computational resources.

Systematic investigations of the accuracy of CC calculations revealed the importance of triple excitations [135], as CCSD results do not provide the accuracy desired in many applications, and in fact can be sometimes even less satisfactory than those from MP2 theory. This led to considerable effort into how one might best include triple excitations in an economical manner (without performing a full and costly CCSDT calculation). In passing, we note that a similar challenge exists also with respect to the inclusion of quadruple and higher excitations.

Two options exist for including higher excitations at costs that are lower than those of the corresponding "full" CC method. The first is to approximate the equations for the triple excitation amplitudes such that the associated computational cost is reduced to the order of N^7 and, as it turns out, that the storage of the triple excitation amplitudes is no longer required. This idea has been used in the CCSDT-n (n = 1a, 1b, 2, and 3) schemes [130,136,137] as well as the CC3 approximation [138]. Perturbation theory arguments are used to decide which terms should be included and then all N^8 terms are skipped, irrespective of their importance from the viewpoint of perturbation theory. For quadruple excitations, a similar CCSDTQ-1 scheme [139] has been suggested that has a scaling of N^9 instead of N^{10} and also does not require storage of the (numerous) quadruple excitation amplitudes.

However, application of the CCSDT-n methods is still costly due to the iterative N^7 steps required to solve the amplitude equations. In this way, such calculations are an order of magnitude more expensive than CCSD and much less applicable. For this reason, non-iterative treatment of higher excitations based on perturbation theory attracted much interest [140–146], which ultimately led to the development of the well-known CCSD(T) method [141]. The basic idea is simply to augment a CCSD calculation with a perturbative estimate for triple excitations. To ensure high accuracy, however, it is essential to use converged amplitudes for the perturbative estimate and also to include higher-order contributions in terms of perturbation theory (a derivation of the CCSD(T) scheme somewhat more natural than its original rationale can be found in Ref. [147]). More recently, a similar approach has also been suggested for quadruple excitations and termed CCSDT(Q) [144–146]. Beside the high accuracy, CCSD(T) performs decidedly better than CCSDT-n methods and sometimes even outperforms full CCSDT. This is due to the fact that CCSD(T) tends to slightly overshoot the CCSDT energy, and therefore is often closer to the CCSDTQ energy (the quadruples contribution is usually negative) than it is to CCSDT. The attractive feature of CCSD(T) is that it involves only iterative N^6 and non-iterative N^7 steps and is therefore feasible even for medium-sized systems. Recent examples, especially those employing parallel implementations of the CCSD(T) scheme [148,149], attest to the current range of applicability of this method.

4.3. *Basis-set approximation*

The accuracy of quantum-chemical calculations is compromised not only by incomplete treatment of the electron-correlation problem but also by the use of finite basis sets for the

representation of the molecular orbitals. The usual choice of basis functions are contracted Gaussian functions of the form [95]

$$\chi_\mu(\mathbf{r}) = N(x - X_\mu)^n(y - Y_\mu)^l(z - Z_\mu)^m \sum_p d_p \exp(-\alpha_p(\mathbf{r} - \mathbf{R}_\mu)^2) \tag{92}$$

with exponents α_p, the contraction coefficients d_p, the normalization constant N, and the center of the basis function denoted by $\mathbf{R}_\mu$. The angular part of the basis function is here given in Cartesian from, i.e., via the polynomials $(x-X_\mu)^n$, $(y-Y_\mu)^l$, and $(z-Z_\mu)^m$ with the sum, $L \equiv (n+l+m)$, defining the "angular momentum" of the basis function (s functions are thus represented by $L=0$, p functions by $L=1$, d functions by $L=2$, etc.). Note, however, that most of the calculations actually use appropriate linear combinations of these Cartesian Gaussians, usually referred to as real solid-harmonic Gaussians, in order to allow a more mathematically consistent representation of the angular part [150]. As the centers of the basis functions usually coincide with the nuclear positions, it is clear that this choice of basis functions bears some resemblance with the actual atomic orbitals, as they are well-known from the hydrogen atom. However the chosen Gaussian functions, unlike the rather similar Slater functions [95], do not fulfill the cusp condition at the nuclear position. Nevertheless, their choice is advantageous, as the required one- and two-electron integrals over the basis functions, i.e., $\langle\chi_\mu|\chi_\nu\rangle$, $\langle\chi_\nu|h|\chi_\nu\rangle$, $\langle\chi_\mu\chi_\nu|1/r_{12}|\chi_\sigma\chi_\rho\rangle$, etc., can be efficiently and analytically calculated [151–154], while the same is not necessarily true for the otherwise better suited Slater functions. To compensate for the shortcomings of Gaussians, the common choices are most often fixed linear combinations of Gaussian functions, i.e., the so-called contracted Gaussian functions, and in this way an improved description is achieved. While contraction of a Gaussian basis set increases the cost of integral evaluation relative to an uncontracted basis, the number of MOs – which primarily governs the total amount of time required for the correlated calculation – is only dependent on the number of contracted functions and not on the contraction level.

Quantum-chemical calculations typically use predefined basis sets either available in the literature or in the basis-set library of the program package at hand. Those have been obtained by fitting Gaussian functions to the corresponding Slater functions (e.g., for example, the STO-nG sets by Pople and co-workers [155]), by energy optimizations (see, for example, the Dunning–Huzinaga [156–158] and the Karlsruhe basis sets [159–162]) or by some simple, though meaningful schemes, as in the case of the even-tempered basis sets [163,164]. Concerning the common choices (see Table 3), a minimal basis denotes a basis set which consists of one contracted function per AO for each atom, n-tuple zeta basis sets (e.g., double zeta (DZ), triple zeta (TZ), etc.) refer to sets which use n functions per AO, and split-valence (SV) sets are those with one basis function per inner-shell AO but multiple functions for each valence AO. Furthermore, use of polarization functions, i.e., functions with higher angular momentum, is compulsory for achieving reasonable accuracy. This means, for example, that a basis set for hydrogen contains p functions (note that d functions as well as functions with even higher angular momentum are possible and also used), and basis sets for carbon include d functions, etc. The use of polarization functions is often denoted by a "P", thus DZP refers to a double-zeta basis augmented by polarization functions, TZ2P to a triple-zeta basis augmented by two sets of polarization functions, etc. A rather exhaustive list of available basis sets can be found, for example, on the EMSL basis set exchange web page [165], from

Table 3. Characterization of some standard basis sets in terms of number and type of involved basis functions.

Basis set	Hydrogen	First-row elements	Second-row elements
Minimal basis (e.g., STO-3G)	1s	2s1p	3s2p
Double zeta (DZ)	2s	4s2p	6s4p
Triple zeta (TZ)	3s	6s3p	9s6p
...			
Double-zeta + polarization (DZP)	2s1p	4s2p1d	6s4p1d
Triple-zeta + polarization (TZP)	3s1p	6s3p1d	9s6p1d
...			
Split valence (SV)	2s	3s2p	4s3p
Split-valence + polarization (SVP)	2s1p	3s2p1d	4s3p1d
...			

which the corresponding sets can also be downloaded. Furthermore, there are several reviews which provide in-depth discussions concerning the "art" of choosing proper basis sets [166–168].

The error associated with the choice of a finite basis is usually termed basis-set error and is often of a magnitude similar to the correlation energy itself. Clearly, an obvious solution would be the use of sufficiently large basis sets, but it has been amply demonstrated that convergence of *correlated* calculations to the basis-set limit is quite slow. Obtaining converged results (with respect to basis set) is a challenging and in many cases impossible task [169,170]. Nevertheless, reliable results can be obtained by using some standard choices of basis sets in electron-correlated calculations.

A further important issue is that the use of only one basis set does not tell very much about the accuracy of a calculation. Thus, it is essential to perform calculations with different basis sets in order to monitor convergence, to estimate remaining errors, and to extrapolate the results to the basis-set limit. However, such a series of calculations are best performed with basis sets taken from a hierarchy of basis sets especially designed for such a task. The most popular choices in this regard are Dunning's correlation-consistent basis sets [171]. For frozen-core (fc) calculations (i.e., calculations in which only the valence electrons are correlated) the standard cc-pVXZ sets with X = D, T, Q, 5, and 6 [171–176] are recommended, while for all-electron calculations the corresponding core-valence sets [177–179], cc-p(w)CVXZ with X = D, T, Q, 5, and 6, are more appropriate. For properties, the choice of basis set depends on the characteristic of the property under consideration. For the calculation of electric properties, for example, it is important to add diffuse functions (which leads to the so-called aug-cc-pVXZ sets [174,180–182]), while properties that sample the electron density closer to the nucleus, such as the electric-field gradient, require the use of the core-valence sets [177–179]. Table 4 gives a summary of the size of the corresponding sets for first and second-row elements.

Based on calculations using Dunning's correlation-consistent basis sets, it is possible to estimate the basis-set limit using extrapolation techniques. For the HF energy, the following empirical formula [183]

$$E^{\infty}_{HF\text{-}SCF} = E^{X}_{HF\text{-}SCF} + a\exp(-bX) \tag{93}$$

Table 4. Size of the various correlation-consistent basis sets for hydrogen, first-row elements (B–Ne), and second-row elements (Al–Ar). Given are the number of contracted functions for each angular momentum and in parentheses the total number of basis functions per atom.

Basis	Hydrogen	First-row elements	Second-row elements
(a) cc-pVXZ sets, X = D, T, Q, 5, 6			
cc-pVDZ	2s1p (5)	3s2p1d (14)	4s3p1d (18)
cc-pVTZ	3s2p1d (14)	4s3p2d1f (30)	5s4p2d1f (34)
cc-pVQZ	4s3p2d1f (30)	5s4p3d2f1g (55)	6s5p3d2f1g (59)
cc-pV5Z	5s4p3d2f1g (55)	6s5p4d3f2g1h (91)	7s6p4d3f2g1h (95)
cc-pV6Z	6s5p4d3f2g1h (91)	7s6p5d4f3g2h1i (140)	8s7p5d4f3g2h1i (144)
(b) cc-pCVXZ, X = D, T, Q, 5, 6			
cc-pCVDZ	2s1p (5)	4s3p1d (18)	5s4p2d (27)
cc-pCVTZ	3s2p1d (14)	6s5p3d1f (43)	7s6p4d2f (59)
cc-pCVQZ	4s3p2d1f (30)	8s7p5d3f1g (84)	9s8p6d4f2g (109)
cc-pCV5Z	5s4p3d2f1g (55)	10s9p7d5f3g1h (145)	11s10p8d6f4g2h (181)
cc-pCV6Z	6s5p4d3f2g1h (91)	12s11p9d7f5g3h1i (230)	—
(c) aug-cc-pVXZ, X = D, T, Q, 5, 6			
aug-cc-pVDZ	3s2p (9)	4s3p2d (23)	5s4p2d (27)
aug-cc-pVTZ	4s3p2d (23)	5s4p3d2f (46)	6s5p3d2f (50)
aug-cc-pVQZ	5s4p3d2f (46)	6s5p4d3f2g (80)	7s6p4d3f2g (84)
aug-cc-pV5Z	6s5p4d3f2g (80)	7s6p5f4f3g2h(127)	8s7p5d4f3g2h (131)
aug-cc-pV6Z	7s6p5d4f3g2h (127)	8s7p6d5f4g3h2i (189)	—
(d) aug-cc-pCVXZ, X = D, T, Q, 5, 6			
aug-cc-pCVDZ	3s2p (9)	5s4p2d (27)	6s5p3d (36)
aug-cc-pCVTZ	4s3p2d (23)	7s6p4d2f (59)	8s7p5d3f (75)
aug-cc-pCVQZ	5s4p3d2f (46)	9s8p6d4f2g (109)	10s9p7d5f2g1h (134)
aug-cc-pCV5Z	6s5p4d3f2g (80)	11s10p8d6f4g2h (181)	12s11p9d7f5g2h1i (217)
aug-cc-pCV6Z	7s6p5d4f3g2h (127)	13s12p10d8f6g4h2i (279)	—

is used ubiquitously, and three calculations with different X are required to obtain the parameters a and b as well as the extrapolated energy $E^{\infty}_{HF\text{-}SCF}$. For the electron-correlation contribution, however, the most common extrapolation is that based on [169]

$$\Delta E^{\infty}_{corr} = \Delta E_{corr}(\mathrm{X}) - \frac{c}{X^3} \tag{94}$$

which, to some degree, is justified on the basis of the atomic partial-wave expansion and requires only two calculations to get the parameter c and the basis-set limit for the correlation energy ΔE^{∞}_{corr}. These admittedly empirical extrapolation schemes work quite well and are commonly used in high-accuracy quantum-chemical calculations [184–189]. There is also some evidence that these extrapolation schemes can be applied in property calculations [190,191]. In particular, it is there shown that a composite scheme in which the various contributions are evaluated separately at the highest possible level and then summed up, e.g.,

$$E_{tot} = E_{HF} + \Delta E_{CCSD(T)} + \Delta E_{CCSDT} + \Delta E_{CCSDTQ} + \Delta E_{core} + \cdots, \tag{95}$$

is suitable to account in an efficient manner for basis-set truncation as well as higher excitations and core-correlation effects.

There are clearly other useful basis sets available in the literature [159–162,193–199], but unfortunately most of them lack the embedding in a well defined hierarchy. Most promising in the future might be possibly the use of atomic natural orbital (ANO) sets by Almlöf and Taylor [195,196] for which it seems to be possible to construct similar well-defined sequences of sets.

In passing we also note that a promising strategy to overcome basis-set problems are the so-called explicitly correlated approaches (i.e., the R12 and F12 schemes [200–204]), but these methods are still experimental and not yet available for routine calculations.

4.4. *Molecular properties in terms of energy derivatives*

The key to the evaluation of many molecular properties are derivatives of the energy [205]. Let us start with the equilibrium geometry of a molecule which, within the Born–Oppenheimer approximation, is defined as a minimum on the corresponding potential energy surface. The necessary mathematical condition for this is

$$\frac{\mathrm{d}E}{\mathrm{d}X_\alpha} = 0 \tag{96}$$

i.e., that the gradient of the energy with respect to all nuclear coordinates X_α vanishes. Efficient search algorithms (schemes for geometry optimizations) [206] typically require in each step of the iterative procedure the evaluation of these gradients. The Newton–Raphson scheme also requires the second derivatives of the energy, i.e., the so-called Hessian matrix, while the most often used quasi-Newton algorithms [207] work with approximate Hessians that are initially estimated by some inexpensive means and then updated in each step based on the available energy and gradient information [206].

Moving further to harmonic, cubic, quartic,... force fields, we note that these quantities can be used to characterize the potential energy surface at a given point and that they are given via the corresponding second, third, fourth,... derivatives of the energy with respect to the nuclear coordinates,

$$\phi_{\alpha\beta} = \frac{d^2E}{\mathrm{d}X_\alpha \mathrm{d}X_\beta} \tag{97}$$

$$\phi_{\alpha\beta\gamma} = \frac{d^3E}{\mathrm{d}X_\alpha \mathrm{d}X_\beta \mathrm{d}X_\gamma} \tag{98}$$

...

The harmonic (or quadratic) force field $\phi_{\alpha\beta}$ is required for the determination of harmonic frequencies, while the cubic force field $\phi_{\alpha\beta\gamma}$ is needed in addition to account for vibrational effects on properties (see, for example, Section 3.2). Elements of the quartic force field $\phi_{\alpha\beta\gamma\delta}$ are needed to obtain anharmonic corrections to vibrational frequencies at the simplest level of approximation [36].

First-order properties generally can be obtained by computing first derivatives of the energy. The dipole moment, for example, is thus given as the (by convention negative) derivative of the energy with respect to the components of an external electric field:

$$\mu_\alpha = -\left(\frac{\mathrm{d}E}{d\epsilon_\alpha}\right)_{\epsilon=0}. \tag{99}$$

The derivative with respect to the electric-field gradient provides the quadrupole moment of a molecule and that with respect to a nuclear quadrupole moment leads to the electric-field gradient at the corresponding nucleus.

Higher-order properties are determined in an analogous manner via higher derivatives of the energies. The polarizability tensor is, for example, computed as the second derivative of the energy with respect to the electric field,

$$\alpha_{\alpha\beta} = -\left(\frac{d^2E}{d\epsilon_\alpha d\epsilon_\beta}\right)_{\epsilon=0}. \tag{100}$$

4.5. *Analytic derivatives of the energy*

The required derivatives of the energy with respect to the nuclear coordinates or external perturbation parameters such as, for example, the components of an electric field can be computed using either numerical or analytic techniques.

Within the numerical approach, the derivatives are computed using finite (and usually central) differences, and, for example, the first derivative of the energy with respect to x at the point x_0 can be obtained via

$$\left(\frac{\mathrm{d}E}{\mathrm{d}x}\right)_{x=x_0} \approx \frac{E(x_0+\Delta x) - E(x_0-\Delta x)}{2\Delta x} \tag{101}$$

with Δx as a small, but finite displacement. The computation of energy derivatives using such an approach is clearly of limited accuracy, considering the contamination due to higher derivatives for the right-hand side of Equation (101) in the case of too large values for Δx and the limited precision of actual computations in the case of too small values for Δx (although more sophisticated numerical differentiation formulas can be used at the price of additional energy calculations). The accuracy issue is not too severe in the case of first derivatives, but becomes a serious problem if second or higher derivatives are determined in this way from energies. The computational cost of the numerical differentiation approach is, for gradients, two times that of a simple energy calculation for each perturbation. Therefore, in a geometry optimization (with $3N_{atoms}$ coordinates) the total cost is about $6N_{atoms}$ that for a single energy calculation. It is clear that numerical schemes thus quickly become expensive and render the evaluation of gradients (as well as of higher derivatives) for larger molecules costly.

Within the analytic approach, one first derives an expression for the desired derivatives of the energy and then uses this for a direct evaluation of the energy derivatives [208]. The analytic approach has no accuracy problems and, as will be discussed, is also computationally advantageous with the cost for all gradients comparable to that of a single energy calculation. Furthermore, analytic differentiation facilitates the treatment of magnetic perturbations which would necessitate the use of complex wavefunction parameters in the case of finite-field calculations. Due to its close connection to response theory, it also can be used for frequency-dependent properties (see, for example, Ref. [209]). As a possible disadvantage, one might consider that additional theory and programming is required. However, this needs to be done only once. As soon as a computer code is available, this disadvantage becomes irrelevant. Table 5 summarizes the advantages and disadvantages of both numerical and analytic differentiation schemes.

From the discussion to this point, it is clear that the analytic approach to energy derivatives is the preferred way when they are available. The current standard in quantum chemistry thus is to compute, whenever possible, the needed energy derivatives using analytic techniques and to rely on finite-difference schemes only when analytic techniques are not available.

In the derivation of suitable expressions for the analytic evaluation of energy derivatives, some care is required to ensure computational efficiency. This means that the overall scaling of the computational cost with the size of the system should be the same as for the original determination of energy and wavefunction parameters (usually easy to fulfill) and that the scaling of the cost with the number of perturbations (e.g., the number of nuclear coordinates in the case of geometrical derivatives) should be as low as possible (the challenging part). Straightforward differentiation always leads to contributions involving the highest possible derivatives of the wavefunction parameters, e.g., the first derivative of the wavefunction is needed for the gradient, the second derivatives of the wavefunction for second derivatives, etc. This is clearly not desirable. The reason is simply that the determination of derivatives of the wavefunction parameters is as costly as the determination of the original unperturbed parameters. On the other hand, it is important to realize that the same argument does not apply for the derivatives of the one- and two-electron integrals. Though their evaluation (in particular for the higher derivatives)

Table 5. Comparison of the advantages and disadvantages of numerical and analytic approaches for the calculation of energy derivatives.

	Numerical	Analytic
Implementation	Easy	Difficult
Efficiency	Low	High
Precision	Low to moderate	High
Imaginary perturbations	Complex Ψ	Yes
Frequency dependence	No	Yes

energy: $E = E(x, c(x))$

external perturbation x

wavefunction parameters $c(x)$

variation principle: $\frac{\partial E}{\partial c} = 0$

energy gradient: $\frac{dE}{dx} = \frac{\partial E}{\partial x} + \frac{\partial E}{\partial c}\frac{dc}{dx} = \frac{\partial E}{\partial x}$

Figure 7. Energy gradients in variational methods.

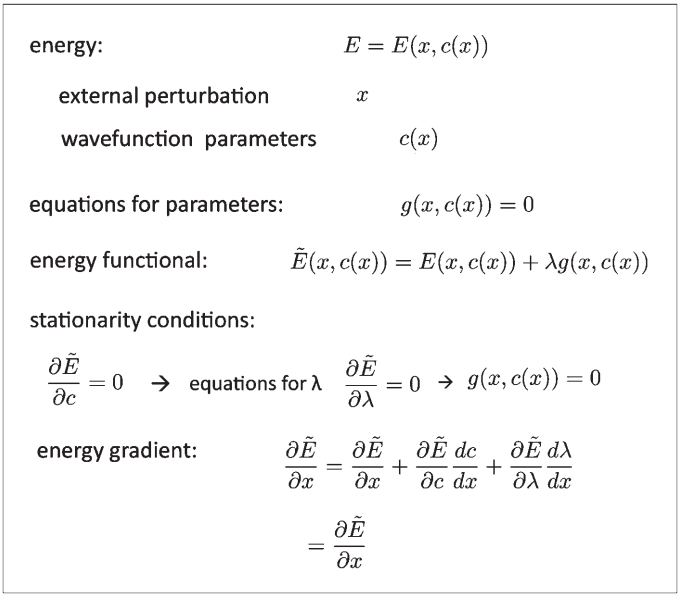

Figure 8. Energy gradients in non-variational methods.

might be technically challenging [210,211], the associated computational costs are not the bottleneck in a derivative calculation. As an example, consider the two-electron integral $\langle \chi_\mu \chi_\sigma \,|\, \chi_\nu \chi_\rho \rangle$ over the four basis functions χ_μ, χ_ν, χ_σ, and χ_ρ which are centered (and depend) on the corresponding positions $\mathbf{R}_\mu$, $\mathbf{R}_\nu$, $\mathbf{R}_\sigma$, and $\mathbf{R}_\rho$ that usually coincide with the nuclear positions. It is then clear that the corresponding derivatives with respect to the nuclear coordinates are only non-zero when they are taken with respect to one of the centers involved. That means that there are at most a total of twelve non-vanishing derivatives irrespective of the size of the system.

With respect to the derivatives of the wavefunction parameters, a lot of effort has been devoted to eliminate them as much as possible from the corresponding expression for the energy derivatives and to ensure in this way computational efficiency [212–218]. It is rather straightforward to demonstrate that the derivatives of parameters that are determined in a variational manner are not needed for the evaluation of the corresponding energy gradient (see Figure 7) and that, in a more general sense, a $(2n+1)$ rule [217,218] holds which states that the n-th derivatives of the wavefunction parameters suffice for the evaluation of the $(2n+1)$-th derivatives of the energy. The situation is somewhat more complicated with respect to parameters that are obtained in a non-variational manner, as it is, for example, the case for the CC amplitudes. Here, the appearance of the perturbed parameters in the gradient expression can be avoided via the method of undetermined multipliers (or Lagrange multipliers) with the equations for the determination of the non-variational parameters as a constraint (see Figure 8; a possible alternative would be the use of the interchange theorem of Dalgarno and Stewart [216]). In this way, an energy functional $\tilde{E}$ is introduced which can be made stationary with respect to both the wavefunction parameters and the Lagrange multipliers. Differentiation of $\tilde{E}$ then provides

the desired derivatives of E and is carried out using the $(2n+1)$ and $(2n+2)$ rules for the wavefunction parameters and the Lagrange multipliers, respectively [212,217,218]. The latter states that knowledge of the n-th derivatives of the Lagrange multipliers is adequate for the calculation of the $(2n+2)$-th derivative of E.

In HF theory, these concepts are applied in the following manner. The starting point is the suitably defined energy functional (for the RHF case)

$$\begin{aligned}\tilde{E}_{HF} &= E_{HF} - 2\sum_{i,j}\varepsilon_{ji}(\langle i|j\rangle - \delta_{ij}) \\ &= \sum_i 2h_{ii} + \sum_{i,j}(2\langle ij|ij\rangle - \langle ij|ji\rangle) - 2\sum_{i,j}\varepsilon_{ji}(\langle i|j\rangle - \delta_{ij})\end{aligned} \tag{102}$$

which is obtained by augmenting the RHF energy (see Equation (77)) by the orthonormality conditions multiplied with the Lagrange multipliers ϵ_{ij}. No further condition needs to be invoked for the HF orbitals (i.e., the MO coefficients), which are determined by minimization of Equation (102). For the first derivative, one then obtains using the $(2n+1)$ and $(2n+2)$ rules

$$\frac{dE_{HF}}{\mathrm{d}x} = \sum_i 2h_{ii}^x + \sum_{i,j}(2\langle ij|ij\rangle^x - \langle ij|ji\rangle^x) - \sum_{i,j}2\varepsilon_{ji}S_{ij}^x. \tag{103}$$

In Equation (103), the integral derivatives h_{pq}^x, S_{pq}^x, and $\langle pq|rs\rangle^x$ are defined such that they involve (in accordance with the $(2n+1)$ rule) only the AO integral-derivative contributions, i.e.,

$$h_{pq}^x = \sum_{\mu,\nu} c_{\mu p}^* \frac{\partial h_{\mu\nu}}{\partial x} c_{\nu q} \tag{104}$$

$$S_{pq}^x = \sum_{\mu,\nu} c_{\mu p}^* \frac{\partial S_{\mu\nu}}{\partial x} c_{\nu q} \tag{105}$$

and

$$\langle pq|rs\rangle^x = \sum_{\mu,\nu,\sigma,\rho} c_{\mu p}^* c_{\sigma q}^* \frac{\partial\langle\mu\sigma|\nu\rho\rangle}{\partial x} c_{\nu r} c_{\rho s}. \tag{106}$$

Equation (103) is usually recast in an AO formalism [208]

$$\frac{dE_{HF}}{\mathrm{d}x} = \sum_{\mu,\nu} D_{\mu\nu}\frac{\partial h_{\mu\nu}}{\partial x} + \frac{1}{2}\sum_{\mu,\nu,\sigma,\rho} D_{\mu\nu}D_{\sigma\rho}\left(\frac{\partial\langle\mu\sigma|\nu\rho\rangle}{\partial x} - \frac{1}{2}\frac{\partial\langle\mu\sigma|\rho\nu\rangle}{\partial x}\right) + \sum_{\mu,\nu} I_{\mu\nu}\frac{\partial S_{\mu\nu}}{\partial x}, \tag{107}$$

with the AO density and AO energy-weighted density matrices given by

$$D_{\mu\nu} = \sum_i 2c_{\mu i}^* c_{\nu i} \tag{108}$$

and

$$I_{\mu\nu} = -\sum_i 2c_{\mu i}^* \varepsilon_i c_{\nu i}. \tag{109}$$

A computationally efficient expression for the second derivatives of the HF energy is obtained by straightforward differentiation of Equation (107) with respect to a second perturbation y [219]

$$\frac{d^2E_{HF}}{\mathrm{d}x\,\mathrm{d}y} = \sum_{\mu,\nu} D_{\mu\nu}\frac{\partial^2 h_{\mu\nu}}{\partial x\partial y} + \frac{1}{2}\sum_{\mu,\nu,\sigma,\rho} D_{\mu\nu}D_{\sigma\rho}\left(\frac{\partial^2\langle\mu\sigma|\nu\rho\rangle}{\partial x\partial y} - \frac{1}{2}\frac{\partial^2\langle\mu\sigma|\rho\nu\rangle}{\partial x\partial y}\right) + \sum_{\mu,\nu} I_{\mu\nu}\frac{\partial^2 S_{\mu\nu}}{\partial x\partial y}$$
$$+ \sum_{\mu,\nu}\frac{\partial D_{\mu\nu}}{\partial y}\left\{\frac{\partial h_{\mu\nu}}{\partial x} + \sum_{\sigma,\rho} D_{\sigma\rho}\left(\frac{\partial\langle\mu\sigma|\nu\rho\rangle}{\partial x} - \frac{1}{2}\frac{\partial\langle\mu\sigma|\rho\nu\rangle}{\partial x}\right)\right\} + \sum_{\mu,\nu}\frac{\partial I_{\mu\nu}}{\partial y}\frac{\partial S_{\mu\nu}}{\partial x} \tag{110}$$

with the perturbed density matrices given by

$$\frac{\partial D_{\mu\nu}}{\partial x} = \sum_i 2\left\{\frac{\partial c^*_{\mu i}}{\partial x}c_{\nu i} + c^*_{\mu i}\frac{\partial c_{\nu i}}{\partial x}\right\} \tag{111}$$

and

$$\frac{\partial I_{\mu\nu}}{\partial x} = -\sum_i 2\left\{\frac{\partial c^*_{\mu i}}{\partial x}\varepsilon_i c_{\nu i} + c^*_{\mu i}\varepsilon_i\frac{\partial c_{\nu i}}{\partial x}\right\} - \sum_{i,j} 2c^*_{\mu j}\frac{\partial f_{ji}}{\partial x}c_{\nu i}. \tag{112}$$

The perturbed MO coefficients are usually expanded in terms of the unperturbed MO coefficients

$$\frac{\partial c_{\mu p}}{\partial x} = \sum_q U^x_{qp}c_{\mu q}. \tag{113}$$

The coefficients U^x_{pq} are determined either via the differentiated orthonormality condition and/or solution of the coupled-perturbed HF (CPHF) equations [219,220].

Within CC theory, the concepts of analytic-derivative evaluation are applied as follows. The energy functional is given by [205,221,222]

$$\tilde{E} = E + \sum_p \lambda_p\langle\Phi_p|\exp(-T)H\exp(T)|0\rangle$$
$$= \langle 0|\exp(-T)H\exp(T)|0\rangle + \sum_p \lambda_p\langle\Phi_p|\exp(-T)H\exp(T)|0\rangle \tag{114}$$

with the λ_p as the corresponding Lagrange multipliers and the CC amplitude equations as the constraint. It is convenient to introduce the following shorthand notation

$$\tilde{E} = \langle 0|(1+\Lambda)\exp(-T)H\exp(T)|0\rangle \tag{115}$$

where Λ is a de-excitation operator [223,224] defined analogously to the cluster operator of Equations (85),

$$\Lambda \equiv \Lambda_1 + \Lambda_2 + \Lambda_3 + \cdots, \tag{116}$$

with

$$\Lambda_m \equiv \frac{1}{m!^2}\sum_{i,j,k,\cdots}\sum_{a,b,c,\cdots}\lambda^{ijk\cdots}_{abc\ldots} i^+aj^+b\cdots. \tag{117}$$

In a second step, the energy functional is made stationary with respect to the wavefunction parameters as well as the Lagrange multipliers. In the case of CC theory, the corresponding stationary conditions are

$$\frac{d\tilde{E}}{dt_{ij\cdots}^{ab\cdots}} = 0 \longrightarrow \langle 0|(1+\Lambda)(\exp(-T)H\exp(T) - E)|\Phi_{ij\cdots}^{ab\cdots}\rangle, = 0, \tag{118}$$

i.e., the so-called Λ equations, and

$$\frac{d\tilde{E}}{d\lambda_{ab\cdots}^{ij\cdots}} = 0 \longrightarrow \text{CC amplitude equations, see Equation (91).} \tag{119}$$

Differentiation of the CC energy functional in Equation (115) then yields for the first derivatives

$$\frac{\mathrm{d}E}{\mathrm{d}x} = \langle 0|(1+\Lambda)\exp(-T)\frac{\mathrm{d}H}{\mathrm{d}x}\exp(T)|0\rangle \tag{120}$$

and for the second derivatives

$$\begin{aligned}\frac{d^2E}{\mathrm{d}x\,\mathrm{d}y} = {} & \langle 0|(1+\Lambda)\exp(-T)\frac{d^2H}{\mathrm{d}x\,\mathrm{d}y}\exp(T)|0\rangle \\ & + \langle 0|(1+\Lambda)\left[\exp(-T)\frac{\mathrm{d}H}{\mathrm{d}x}\exp(T), \frac{\mathrm{d}T}{\mathrm{d}y}\right]|0\rangle \\ & + \langle 0|(1+\Lambda)\left[\exp(-T)\frac{\mathrm{d}H}{\mathrm{d}y}\exp(T), \frac{\mathrm{d}T}{\mathrm{d}x}\right]|0\rangle \\ & + \langle 0|(1+\Lambda)\left[\left[\exp(-T)H\exp(T), \frac{\mathrm{d}T}{\mathrm{d}x}\right], \frac{\mathrm{d}T}{\mathrm{d}y}\right]|0\rangle.\end{aligned} \tag{121}$$

An alternative expression for the second derivatives can be also obtained by explicit differentiation of the gradient expression [225,226]

$$\begin{aligned}\frac{d^2E}{\mathrm{d}x\,\mathrm{d}y} = {} & \langle 0|(1+\Lambda)\exp(-T)\frac{d^2H}{\mathrm{d}x\,\mathrm{d}y}\exp(T)|0\rangle \\ & + \langle 0|\frac{d\Lambda}{\mathrm{d}y}\exp(-T)\frac{\mathrm{d}H}{\mathrm{d}x}\exp(T)|0\rangle \\ & + \langle 0|(1+\Lambda)\left[\exp(-T)\frac{\mathrm{d}H}{\mathrm{d}x}\exp(T), \frac{\mathrm{d}T}{\mathrm{d}y}\right]|0\rangle.\end{aligned} \tag{122}$$

Unlike the first expression, the latter involves both derivatives of the cluster and Λ amplitudes but only for the second perturbation y. The required perturbed amplitudes $\mathrm{d}T/\mathrm{d}x$ are determined by solving the perturbed amplitude equations

$$0 = \left\langle \Phi_p \middle| \exp(-T)\frac{\mathrm{d}H}{\mathrm{d}x}\exp(T) \middle| 0 \right\rangle + \left\langle \Phi_p \middle| \left[\exp(-T)H\exp(T), \frac{\mathrm{d}T}{\mathrm{d}x}\right] \middle| 0 \right\rangle \tag{123}$$

which are obtained by differentiating Equation (91) with respect to perturbation x. The perturbed Λ amplitudes appearing in Equation (122) are solutions of the

perturbed Λ equations

$$0 = \left\langle 0 \left| \frac{d\Lambda}{dy} (\exp(-T) H \exp(T) - E) \right| \Phi_p \right\rangle + \left\langle 0 \left| (1+\Lambda) \left(\exp(-T) \frac{dH}{dy} \exp(T) + \left[\exp(-T) H \exp(T), \frac{dT}{dy} \right] - \frac{dE}{dy} \right) \right| \Phi_p \right\rangle \quad (124)$$

obtained by differentiating the unperturbed Λ equations in Equation (118) with respect to the perturbation y. The cost for the solution of the perturbed amplitude and Λ equations are roughly the same as that for the solution of the corresponding unperturbed equations.

Whether the first or second expression for analytical second derivatives (Equation (121) or (122)) is computationally more advantageous depends on the actual perturbations. For properties that correspond to two different classes of perturbation, the second (asymmetric) approach is probably advantageous. This choice necessitates the solution of 2 N_y perturbed equations instead of N_x and N_y equations for the first (symmetric) approach. N_x and N_y are here the number of x and y perturbations. For example, and in the context of this review, the determination of the spin–rotation tensor requires solution of 6 perturbed amplitude equations instead of $3+3N_{atoms}$. The symmetric approach is preferred if x and y belong to the same class of perturbation, only N_x equations need to be solved instead of the $2N_x$ for the asymmetric approach. An example is the analytic evaluation of harmonic force fields, for which the symmetric approach requires the solution of $3N_{atoms}$ perturbed equations.

The discussion has so far focused on the CC amplitudes as wavefunction parameters and ignored the dependence of the molecular orbitals on the perturbation in the context of CC theory. The equations given at this point are valid for so-called orbital-unrelaxed property calculations [227,228] in which orbital-relaxation effects are treated via the single excitations in the cluster operator. This approach can be used for electric properties [227,228] and is the appropriate choice in CC response theory [229]. However, for the calculation of geometrical and magnetic properties with perturbation-dependent basis functions it is mandatory to include the dependence of the orbitals. This can be done [205] by augmenting the energy functional in Equation (115) by additional constraints. If the CC calculation is performed with the HF-SCF determinant as reference, the Brillouin condition

$$f_{ai} = 0 \quad (125)$$

(f_{ai} denoting the elements of the virtual-occupied block of the spin–orbital Fock matrix) and the orthonormality conditions for the orbitals

$$S_{pq} - \delta_{pq} = 0 \quad (126)$$

(with S_{pq} as the corresponding overlap integral)

$$S_{pq} = \langle \varphi_p | \varphi_q \rangle \quad (127)$$

lead to the following CC energy functional [205]

$$\tilde{E} = \langle 0 | (1+\Lambda) \exp(-T) H \exp(T) | 0 \rangle + \sum_a \sum_i Z_{ai} f_{ai} + \sum_{p,q} I_{pq} (S_{pq} - \delta_{pq}) \quad (128)$$

with Z_{ai} and I_{pq} as the additional Lagrange multipliers.

The corresponding gradient expression is then given by

$$\frac{\mathrm{d}E}{\mathrm{d}x} = \langle 0|(1+\Lambda)\exp(-T)H^x\exp(T)|0\rangle + \sum_a \sum_i Z_{ai} f_{ai}^{(x)} + \sum_{p,q} I_{pq} S_{pq}^x. \tag{129}$$

In the derivation of this expression, we have exploited the $(2n+1)$ and $(2n+2)$ rules which means that H^x is the perturbed Hamiltonian in second quantization constructed from the derivative integrals h_{pq}^x and $\langle pq\|rs\rangle^x$ which do not involve contributions due to the derivatives of the MO coefficients. In the same way, the derivative of the Fock matrix $f_{pq}^{(x)}$ is defined as

$$f_{pq}^{(x)} = h_{pq}^x + \sum_m \langle pm||qm\rangle^x \tag{130}$$

and in this way ignores derivative contributions of the MO coefficients. While the form of the Λ equations has been already given (see Equation (118)), the new Lagrange multipliers Z_{ai} and I_{pq} are obtained by making $\tilde{E}$ stationary with respect to orbital rotations. Parametrization of these rotations via

$$\varphi_p' = \sum_q \varphi_q U_{qp} \tag{131}$$

leads to the stationary conditions

$$\frac{\partial \tilde{E}}{\partial U_{ai}} + \frac{\partial \tilde{E}}{\partial U_{ia}} = 0 \longrightarrow Z_{ai} \tag{132}$$

which are the the so-called Z-vector equations [215] for the multipliers Z_{ai}, while the other stationary conditions

$$\begin{aligned} \frac{\partial \tilde{E}}{\partial U_{ij}} &= 0 \longrightarrow I_{ij} \\ \frac{\partial \tilde{E}}{\partial U_{ai}} - \frac{\partial \tilde{E}}{\partial U_{ia}} &= 0 \longrightarrow I_{ai}, I_{ia} \\ \frac{\partial \tilde{E}}{\partial U_{ab}} &= 0 \longrightarrow I_{ab} \end{aligned} \tag{133}$$

provide expressions for the quantity I_{pq} (for detailed expressions, see here Ref. [230]).

The usual procedure is to rewrite the gradient expression in a density-matrix representation

$$\frac{\mathrm{d}E}{\mathrm{d}x} = \sum_{p,q} D_{pq} f_{pq}^{(x)} + \sum_{p,q,r,s} \Gamma_{pqrs} \langle pq||rs\rangle^x + \sum_{p,q} I_{pq} S_{pq}^x \tag{134}$$

where the one-particle density matrix D_{pq} contains the one-electron part of the original first term (see Equation (128)) as well as the "Z-vector" contribution. D_{pq} is often referred to as a relaxed (or effective) density matrix in contrast to the reduced density matrix which just consists of the first term. The second term involves the two-particle density matrix Γ_{pqrs} and is due to the two-electron part of the first term of Equation (128). The Lagrange multipliers I_{pq} on the other hand can be interpreted as the elements of a generalized

energy-weighted density matrix; the magnitude of these multipliers is related to the (in)sensitivity of the energy with respect to orbital rotations.

For computational purposes, it is advantageous to recast Equation (134) in the AO representation

$$\frac{\mathrm{d}E}{\mathrm{d}x}=\sum_{\mu,\nu}D_{\mu\nu}\left\{\frac{\partial h_{\mu\nu}}{\partial x}+\sum_{\sigma,\rho}D^{SCF}_{\sigma\rho}\frac{\partial\langle\mu\sigma||\nu\rho\rangle}{\partial x}\right\}+\sum_{\mu,\nu,\sigma,\rho}\Gamma_{\mu\sigma\nu\rho}\frac{\partial\langle\mu\sigma||\nu\rho\rangle}{\partial x}+\sum_{\mu,\nu}I_{\mu\nu}\frac{\partial S_{\mu\nu}}{\partial x} \quad (135)$$

where the corresponding AO density matrices $D_{\mu\nu}$, $I_{\mu\nu}$, and $\Gamma_{\mu\nu\sigma\rho}$ are obtained by straightforward "back transformation" from the MO to the AO representation.

The same can be also done for the second derivatives. Within the symmetric approach one then obtains

$$\begin{aligned}\frac{d^2E}{\mathrm{d}x\mathrm{d}y}=&\sum_{\mu,\nu}D_{\mu\nu}\left\{\frac{\partial^2 h_{\mu\nu}}{\partial x\partial y}+\sum_{\sigma,\rho}D^{SCF}_{\sigma\rho}\frac{\partial^2\langle\mu\sigma||\nu\rho\rangle}{\partial x\partial y}\right\}+\sum_{\mu,\nu,\sigma,\rho}\Gamma_{\mu\sigma\nu\rho}\frac{\partial^2\langle\mu\sigma||\nu\rho\rangle}{\partial x\partial y}+\sum_{\mu,\nu}I_{\mu\nu}\frac{\partial^2 S_{\mu\nu}}{\partial x\partial y}\\
&+\sum_{\mu,\nu}\left(\frac{\partial D_{\mu\nu}}{\partial y}\right)^{[1,0]}\left\{\frac{\partial h_{\mu\nu}}{\partial x}+\sum_{\sigma,\rho}D^{SCF}_{\sigma\rho}\frac{\partial\langle\sigma||\nu\rho\rangle}{\partial x}\right\}+\sum_{\mu,\nu,\sigma,\rho}\left(\frac{\partial\Gamma_{\mu\sigma\nu\rho}}{\partial y}\right)^{[1,0]}\frac{\partial\langle\mu\sigma||\nu\rho\rangle}{\partial x}\\
&+\sum_{\mu,\nu}\left(\frac{\partial D_{\mu\nu}}{\partial x}\right)^{[1,0]}\left\{\frac{\partial h_{\mu\nu}}{\partial y}+\sum_{\sigma,\rho}D^{SCF}_{\sigma\rho}\frac{\partial\langle\sigma||\nu\rho\rangle}{\partial y}\right\}+\sum_{\mu,\nu,\sigma,\rho}\left(\frac{\partial\Gamma_{\mu\sigma\nu\rho}}{\partial x}\right)^{[1,0]}\frac{\partial\langle\mu\sigma||\nu\rho\rangle}{\partial y}\\
&+\sum_{\mu,\nu}\left(\frac{\partial^2 D_{\mu\nu}}{\partial x\partial y}\right)^{[1,0]}\left\{h_{\mu\nu}+\sum_{\sigma,\rho}D^{SCF}_{\sigma\rho}\langle\sigma||\nu\rho\rangle\right\}+\sum_{\mu,\nu,\sigma,\rho}\left(\frac{\partial^2\Gamma_{\mu\sigma\nu\rho}}{\partial x\partial y}\right)^{[1,0]}\langle\mu\sigma||\nu\rho\rangle\\
&+\sum_{\mu,\nu}D_{\mu\nu}\sum_{\sigma,\rho}\left(\frac{\partial D^{SCF}_{\sigma\rho}}{\partial x}\right)\frac{\partial\langle\mu\sigma||\nu\rho\rangle}{\partial y}+\sum_{\mu,\nu}D_{\mu\nu}\sum_{\sigma,\rho}\left(\frac{\partial D^{SCF}_{\sigma\rho}}{\partial y}\right)\frac{\partial\langle\mu\sigma||\nu\rho\rangle}{\partial x}\\
&+\sum_{\mu,\nu}\left(\frac{\partial D_{\mu\nu}}{\partial x}\right)^{[1,0]}\sum_{\sigma,\rho}\left(\frac{\partial D^{SCF}_{\sigma\rho}}{\partial y}\right)\langle\mu\sigma||\nu\rho\rangle+\sum_{\mu,\nu}\left(\frac{\partial D_{\mu\nu}}{\partial y}\right)^{[1,0]}\sum_{\sigma,\rho}\left(\frac{\partial D^{SCF}_{\sigma\rho}}{\partial x}\right)\langle\mu\sigma||\nu\rho\rangle\end{aligned} \quad (136)$$

where the index "[1, 0]" indicates that all derivatives of the density matrices are computed according to the $(2n+1)$ and $(2n+2)$ rules and thus exclude all second derivatives of the wavefunction parameters and all first and second derivatives of the Lagrange multipliers. For the asymmetric approach, the corresponding expression is [231]

$$\begin{aligned}\frac{d^2E}{\mathrm{d}x\mathrm{d}y}=&\sum_{\mu,\nu}D_{\mu\nu}\left\{\frac{\partial^2 h_{\mu\nu}}{\partial x\partial y}+\sum_{\sigma,\rho}D^{SCF}_{\sigma\rho}\frac{\partial^2\langle\mu\sigma||\nu\rho\rangle}{\partial x\partial y}\right\}+\sum_{\mu,\nu,\sigma,\rho}\Gamma_{\mu\sigma\nu\rho}\frac{\partial^2\langle\mu\sigma||\nu\rho\rangle}{\partial x\partial y}+\sum_{\mu,\nu}I_{\mu\nu}\frac{\partial^2 S_{\mu\nu}}{\partial x\partial y}\\
&+\sum_{\mu,\nu}\frac{\partial D_{\mu\nu}}{\partial y}\left\{\frac{\partial h_{\mu\nu}}{\partial x}+\sum_{\sigma,\rho}D^{SCF}_{\sigma\rho}\frac{\partial\langle\sigma||\nu\rho\rangle}{\partial x}\right\}+\sum_{\mu,\nu,\sigma,\rho}\frac{\partial\Gamma_{\mu\sigma\nu\rho}}{\partial y}\frac{\partial\langle\mu\sigma||\nu\rho\rangle}{\partial x}+\sum_{\mu,\nu}\frac{\partial I_{\mu\nu}}{\partial y}\frac{\partial S_{\mu\nu}}{\partial x}\\
&+\sum_{\mu,\nu}D_{\mu\nu}\sum_{\sigma,\rho}\frac{\partial D^{SCF}_{\sigma\rho}}{\partial y}\frac{\partial\langle\mu\sigma||\nu\rho\rangle}{\partial x}.\end{aligned} \quad (137)$$

Note that, unlike for the symmetric approach, in the asymmetric approach the full derivatives of the density matrices need to be evaluated.

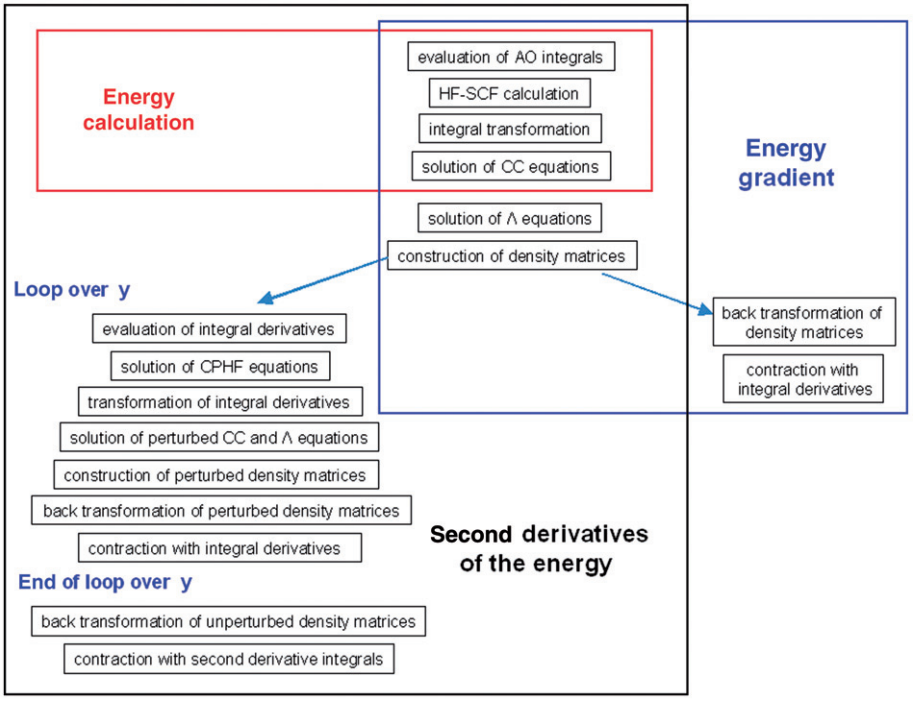

Figure 9. [Colour online]. Flowchart for CC energy, gradient, and second-derivative calculations.

A flowchart for the computation of analytic gradients and second derivatives is given in Figure 9. For a gradient calculation, the usual steps for a CC energy calculation are supplemented by the solution of the Λ equations, construction of the density matrices, their transformation into the AO basis and their subsequent contraction with the integral derivatives which are computed "on the fly". This means that they are computed and processed without storing them on disk. A CC second derivative calculation (using the asymmetric approach) requires, unlike a gradient calculation, a loop over the perturbation y. Within this loop, the perturbed amplitude and Λ equations need to be solved for the perturbation y and the perturbed density matrices are constructed. The latter are contracted after transformation into the AO basis with the corresponding derivative integrals. The final step after the loop over y is then the transformation of the unperturbed MO density matrices and their contraction with the second derivatives of the AO integrals. Note that a CC second derivative calculation necessitates the storage of the AO derivative integrals and their transformation into the MO basis. The advantage of the asymmetric approach, however, is that only derivatives with respect to one perturbation (i.e., y) need to be considered at each step. In this way the computational expenses are kept low, as only one additional set of integrals (as well as amplitudes and density matrices) need to be stored. A possible drawback is that contraction of the perturbed density matrices with the integral derivatives necessitates a recalculation of the latter for each perturbation y.

Analytic schemes for the evaluation of nuclear forces were first implemented at the HF-SCF level by Pulay in 1969 [208]. Analytic gradients for MP2 [219] as well as other

quantum-chemical schemes [232–235] were reported about a decade later, attesting to the difficulties of formulating and implementing such schemes. At the CC level, the first implementation of analytic gradients was reported by Scheiner *et al*. [236] in 1987. They presented analytic first derivatives for the closed-shell CCSD approach; corresponding open-shell implementations were carried out later in the Bartlett group [230,237,238]. The theory of CCSDT-n and CCSDT gradients was first worked out by Salter *et al*. [239], but the implementations were reported only later [240–242]. In 1988, Scuseria and Schaefer presented analytic gradients for CCSDT-1a [240], CCSDT-n (n = 2 and 3) gradients were presented in 2000 [241], and full CCSDT gradients only in 2001 [242]. Even more recently, using string-based algorithms for many-body techniques [134] analytic first derivatives for general CC approaches [243] have been implemented. Work on CCSD(T) gradients started in 1990 with an implementation of gradients for the (T) correction within the quadratic CI (QCI) context [244]. Using the same strategy, Scuseria reported shortly thereafter a first implementation for closed-shell CCSD(T) gradients [245]. The key to computational efficiency, i.e., the use of perturbed canonical orbitals in order to avoid recalculation of the triple amplitudes, was first suggested by Lee and Rendell in 1990 [246]. They reported an implementation for closed-shell CCSD(T) based on these ideas; corresponding generalizations to high-spin open-shell cases were subsequently worked out by Watts *et al*. [247,248].

Concerning the analytic evaluation of second derivatives with respect to nuclear coordinates, an implementation was first reported for HF-SCF wavefunctions [219] followed by corresponding implementations at the MCSCF and MP2 levels [249–255]. At the CC level, a first implementation was presented by Koch *et al*. [221] using the symmetric approach. However, to the best of our knowledge, this implementation was never used in any applications after the appearance of the original paper. The current availability of CC second derivatives is thus entirely due to the more recent implementations based on the asymmetric approach [231,256]. Analytic CCSD and CCSD(T) second derivatives for closed-shell cases were reported in 1997 [231], the corresponding implementations for UHF reference functions in 1998 [256]. The initial work was later extended to the CCSDT-n models [241] and finally in 2002 also to CCSDT [257]. Use of string-based techniques [134] has more recently enabled the implementation of analytic second-derivative techniques for general CC wavefunctions using both closed-shell and open-shell reference functions [258].

It should be noted that within CC theory analytic second-derivative techniques were first applied to compute nuclear magnetic shielding tensors [226,259,260] which in the present context is of relevance for the calculation of the nuclear spin–rotation tensor [58]. The reason was simply that the implementation for these properties was somewhat simpler even when using perturbation-dependent basis functions, as some terms in Equation (137) vanish. A lot of effort has also been devoted to the computation of first-, second- and third-order electrical response properties in the framework of CC response theory [209,229,261–263]. Simplifications result here from the neglect of orbital relaxation [229] as well as the fact that the electrical perturbation is a one-electron perturbation. The possible frequency dependence of the perturbation has also been considered in this context [209,261–263].

Analytic third derivatives of the energy with respect to nuclear coordinates have only been implemented at the HF-SCF level [264]. Nevertheless, the first steps toward an

implementation of general third derivatives has been undertaken that offers the possibility to compute CC hyperpolarizabilities [265–267] as well as to evaluate Raman intensities [268] which are related to the geometrical derivatives of the polarizability tensor.

As analytic schemes for higher derivatives are not yet available for correlated methods, one has to rely on numerical techniques. Focusing on cubic and quartic force constants, we note that numerical differentiation of analytically evaluated quadratic force constants seems to be a good choice. To estimate vibrational levels using second-order vibrational perturbation theory, the force fields are needed in the normal-coordinate representation. These are easily obtained by numerical differentiation of analytically evaluated second derivatives along the normal coordinates. This is especially convenient, as the calculation of anharmonic corrections to frequencies requires only the semi-diagonal elements of the quartic force-constant matrix. The corresponding formulas for the anharmonic force constants ϕ_{rst} and ϕ_{rrst} are thus given by [37,38,269]

$$\phi_{rst} = \frac{\phi_{st}^{+} - \phi_{st}^{-}}{2\Delta_r} \tag{138}$$

and

$$\phi_{rrst} = \frac{\phi_{st}^{+} + \phi_{st}^{-} - 2\phi_{st}}{\Delta_r^2} \tag{139}$$

with the ϕ_{st} as the quadratic force constant in normal-coordinate representation, ϕ^{+} and ϕ^{-} the corresponding force constants at the displaced geometries, and Δ_r as the displacement along the r-th normal coordinate.

Finally, we note that a number of codes are available for performing CC calculations. However, to our best knowledge the full set of tools for the efficient treatment of rotational spectra is currently only offered by the CFOUR program package [270].

5. Applications: interplay of theory and experiment

In this section, it is demonstrated how quantum-chemical calculations can be used to assist experimental investigations in the field of rotational spectroscopy. For this purpose, we first discuss the accuracy that can be obtained in high-level calculations of the various spectroscopic parameters (i.e., rotational constants, centrifugal-distortion constants, dipole moment, and hyperfine parameters). This discussion will be followed by a few representative examples that demonstrate the actual interplay of theory and experiment. No attempt is made here to review the literature in this field; the examples given are drawn primarily from our work.

5.1. *Rotational constants*

To guide investigations in rotational spectroscopy, an accurate estimate of the rotational constants is clearly fundamental and probably most important. As shown in Section 2, these play a fundamental role in the determination of the rotational energy levels of a molecule; therefore, their accurate theoretical prediction alone is often more than sufficient for identifying and assigning lines in a spectrum that belong to the carrier of interest.

The rotational constants in the vibrational ground state, usually denoted as B_0^α with α referring to the inertial axis, can be decomposed into an equilibrium contribution B_e^α, a vibrational correction ΔB_{vib}^α, and an (often ignored) electronic contribution ΔB_{el}^α:

$$B_0^\alpha = B_e^\alpha + \Delta B_{vib}^\alpha + \Delta B_{el}^\alpha. \tag{140}$$

As discussed before, the equilibrium rotational constants B_e are obtained in a straightforward manner from the equilibrium geometry of the molecule. The vibrational corrections are often approximated by second-order vibrational perturbation theory (see Section 3 and Equation (62)) and the electronic contributions, finally, are related to the rotational g tensor via the following relationship [19,191]

$$\Delta B_{el}^\alpha = \frac{m_e}{m_p}\, g^\alpha B_e^\alpha \tag{141}$$

with m_e and m_p as the mass of the electron and proton, respectively.

5.1.1. *Accuracy: statistical analysis*

Theoretical predictions are not particularly helpful without an estimate of the corresponding accuracy and uncertainty. Therefore, before presenting examples, we start with a thorough discussion of the accuracy that can be achieved in quantum-chemical calculations of rotational constants. The discussion is based on a recent statistical analysis of quantum-chemical results for the rotational constants [191] of 16 closed-shell molecules (HF, N_2, CO, F_2, HCN, HNC, CO_2, H_2O, NH_3, CH_4, HCCH, HOF, HNO, HNNH, CH_2CH_2, and H_2CO) for which a total of 97 isotopologues were considered.

Aiming at high accuracy, only CC results have been considered. To recover errors due to basis set and wavefunction truncation, the composite scheme described in details in Refs. [190,192] and mentioned in Section 4.3 has been employed. In a first step, frozen-core (fc) CCSD(T) calculations were performed in conjunction with correlation-consistent basis sets ranging from triple- up to hextuple-zeta quality [171,172,177]. The fc-CCSD(T) basis set limit was then estimated using extrapolation techniques (see Section 4 and Refs. [169,183]) as described in Ref. [190]. In a further step, corrections for core correlation (Δcore) as well as additional higher-order correlation effects covered through CCSDT and CCSDTQ calculations (ΔT and ΔQ, respectively) have been included. A final, best estimate for B_e^α is then taken to be

$$\text{fc-CCSD(T)/cc-pV}\infty\text{Z} + \Delta\text{core/cc-pCVQZ} + \Delta\text{T/cc-pVTZ} + \Delta\text{Q/cc-pVDZ}.$$

The core-correlation contribution Δcore is based on the difference of the all-electron and frozen-core CCSD(T)/cc-pCVQZ gradients, the ΔT correction is given as the corresponding difference between the frozen-core CCSDT/cc-pVTZ and CCSD(T)/cc-pVTZ gradients, while the ΔQ contribution is determined by means of the corresponding difference between frozen-core CCSDTQ/cc-pVDZ and CCSDT/cc-pVDZ gradients. The vibrational corrections ΔB_{vib}^α were computed with second-order perturbation theory at the CCSD(T)/cc-pCVQZ level of theory (with all electrons correlated). The electronic contribution, finally, requires the calculation of the rotational g tensor. The latter was computed at the fc-CCSD(T)/aug-cc-pVQZ level as described in Ref. [271].

Table 6. Statistical analysis of the relative errors (in %) in the computed rotational constants with respect to experimentally determined B_0 values.

Computational approach	$\bar{\Delta}$	$\bar{\Delta}_{abs}$	Δ_{std}	Δ_{max}
fc-CCSD(T)/cc-pVTZ	−0.188	0.816	1.051	4.087
fc-CCSD(T)/cc-pVQZ	0.254	0.531	0.790	2.628
fc-CCSD(T)/cc-pV5Z	0.335	0.486	0.691	2.527
fc-CCSD(T)/cc-pV6Z	0.356	0.489	0.668	2.492
fc-CCSD(T)/cc-pV∞Z	0.380	0.499	0.643	2.448
fc-CCSD(T)/cc-pV6Z + core	0.676	0.753	0.612	2.668
fc-CCSD(T)/cc-pV6Z + core + ΔT	0.706	0.782	0.604	2.674
fc-CCSD(T)/cc-pV6Z + core + ΔT + ΔQ	0.608	0.691	0.617	2.614
fc-CCSD(T)/cc-pV∞Z + core + ΔT + ΔQ	0.632	0.710	0.594	2.569
fc-CCSD(T)/cc-pV∞Z + core + ΔT + ΔQ + ΔB_{vib}	0.007	0.057	0.124	1.291
fc-CCSD(T)/cc-pV∞Z + core + ΔT + ΔQ + ΔB_{vib} + ΔB_{el}	−0.003	0.041	0.071	0.264

The data were analyzed employing the usual statistical measures, i.e., the mean error $\bar{\Delta}$, the mean absolute error $\bar{\Delta}_{abs}$, the maximum absolute error Δ_{max}, and the standard deviation Δ_{std}. Graphical representation of the results was based on normal distributions defined by

$$\rho(R) = N_c \exp\left[-\frac{1}{2}\left(\frac{R-\bar{\Delta}}{\Delta_{std}}\right)^2\right] \tag{142}$$

with N_c as a normalization constant.

Table 6 summarizes the results obtained from this statistical analysis and the corresponding pictorial representations of the results are given in Figure 10.

We note that for the best theoretical estimates the agreement with the corresponding experimental B_0 values is (on average) better than 0.1%. The corresponding mean absolute error is 0.04% and the standard deviation is 0.07%. This means that computational predictions for B_0 at this (admittedly very elaborate and computationally challenging) level of theory have an accuracy of generally better than 10 MHz (ca. 0.0003 cm^{-1}) for rotational constants of about 10 GHz (ca. 0.3 cm^{-1}) and of about 100 MHz (ca. 0.003 cm^{-1}) for those in the range of 100 GHz (ca. 3 cm^{-1}). Such accurate predictions clearly are useful in guiding experimental searches for lines and also useful for the analysis of experimental data.

The comparison of different computational approaches in Figure 10 underscores the importance of vibrational corrections for the high-accuracy prediction of rotational constants, as a narrow error distribution is only obtained when they are included. Significantly larger deviations between experiment and theory are observed for all computational results that do not consider vibrational corrections, and the corresponding error distributions are rather broad irrespective of the computational approach. In the absence of vibrational corrections, large basis sets, inclusion of core correlation, or consideration of higher excitations do not substantially improve the quality of the results. While vibrational contributions are essential for accurate theoretical predictions,

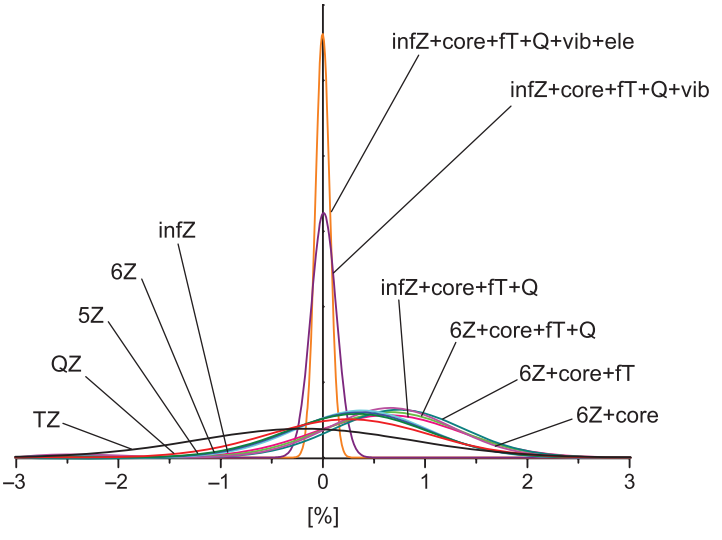

Figure 10. [Colour online]. Normal distribution $\rho(R)$ of the errors in the calculated rotational constants in comparison with experimental B_0 values [191].

Table 7. Comparison of the theoretical best estimates (for a definition, see text) and experimental values for the rotational constants A_0, B_0, C_0 (in MHz) of HF, N_2, and HOF.

	Experiment	Theory	Error
HF			
B_0	616565.219(13)[a]	616304.6	260.6 (0.042%)
N_2			
B_0	59646.48(11)[b]	59660.7	14.2 (0.024%)
HOF			
A_0	585631.508(72)[c]	585998.9	366.5 (0.06%)
B_0	26760.650(12)[c]	26818.0	57.4 (0.21%)
C_0	25509.886(12)[c]	25571.2	61.3 (0.24%)

[a]Ref. [272].
[a]Ref. [273].
[a]Ref. [274].

the electronic corrections to the rotational constants are typically one to two orders of magnitude smaller. Their consideration nevertheless leads to a minor improvement in most cases.

The good agreement between theory and experiment is also illustrated by the results given in Table 7, where we compare our best theoretical estimates for HF, N_2, and HOF with available experimental rotational constants [272–274]. For the hydrogen fluoride molecule, the vibrational corrections amount to 11811 MHz (1.92% of the total value) and the electronic contribution to 257 MHz (0.04%). With 616304.6 MHz as the best

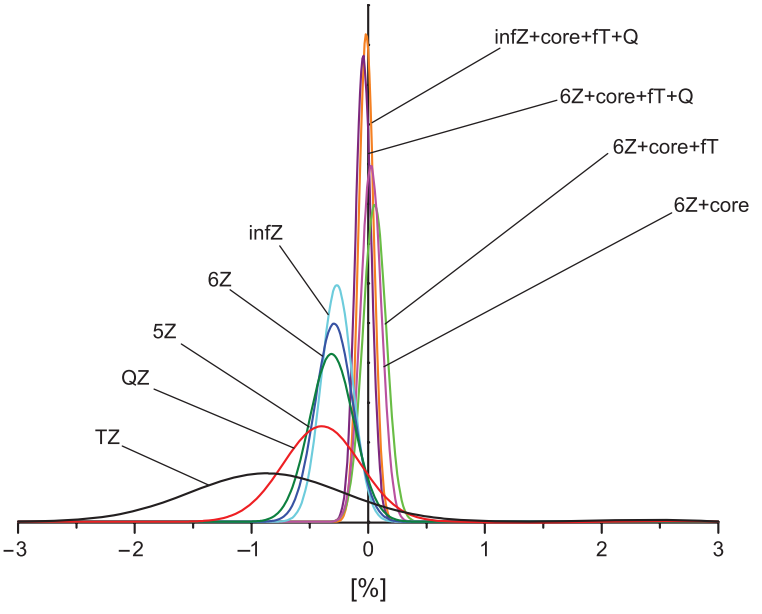

Figure 11. [Colour online]. Normal distribution $\rho(R)$ of the errors in the calculated rotational constants in comparison with B_e values derived from experimental B_0 values and computed vibrational corrections [191].

estimate for B_0 and 616565.219(13) MHz as the experimental value [272], the final error in the best theoretical prediction is 261 MHz (0.04%). It is clear that any further improvement in the theoretical predictions has to involve a more complete treatment of vibrational effects. The large magnitude of the vibrational corrections immediately poses the question of whether the perturbative approach to the vibrational problem is sufficient. The treatment of these effects using variational schemes (see, for example, Ref. [275] and references therein) might be a valid alternative or one might extend the perturbative treatment to higher-orders. The latter option necessitates the evaluation of the second-order vibration–rotation interaction constants γ_{rs}^{α}

$$B_0^{\alpha} = B_e^{\alpha} - \frac{1}{2}\sum_r \alpha_r^{\alpha} + \frac{1}{4}\sum_{r\leq s} \gamma_{rs}^{\alpha} \tag{143}$$

for which so far no routine computational treatment is available. Work along these lines is currently in progress [70].

Figure 11 provides a detailed comparison of the performance of the different computational schemes by comparing computed equilibrium rotational constants with corresponding values obtained from experiment by subtracting the vibrational corrections. First of all, it is obvious from the figure that improvements in the basis set lead to narrower error distributions. While for the cc-pVTZ basis a rather broad distribution is seen, the cc-pV6Z distribution is sharper, and only a marginal further improvement is observed for the results obtained via basis-set extrapolation. A further significant improvement is seen when core-correlation effects are included, thus confirming the

importance of these effects for accurate geometry predictions [192,276]. On the other hand, the consideration of a more rigorous treatment of triple excitations than CCSD(T) has only marginal effects. Inclusion of quadruple excitations at the CCSDTQ level, however, leads to a further gain in accuracy and results in a significantly sharper distribution function.

5.1.2. *Examples*

An excellent example where the prediction of rotational constants is vital is the recent detection of oxadisulfane (HSOH) via rotational spectroscopy [4]. A major key to the successful identification of HSOH among the products of the pyrolysis of $(t\text{-Bu})_2SO$ was the availability of accurate predictions of the spectroscopic parameters. Indeed, previous searches for HSOH without these predictions in hand were unsuccessful [4]. The theoretical prediction of the spectra was based on the equilibrium geometry obtained at the CCSD(T)/cc-pCVQZ level, i.e., with consideration of core correlation, and vibrational corrections to the rotational constants and centrifugal distortion constants computed from harmonic and anharmonic force fields obtained at the MP2/cc-pVTZ and CCSD(T)/cc-pVTZ levels of theory. In addition, the computed components of the dipole moment were used to predict the relative intensities of the rotational transitions. Figure 12 provides an example for a predicted spectrum (shown here is the $^rQ_1$ branch with a band center near 561 GHz) in comparison with the experimental spectrum [4]. The excellent agreement between theory and experiment attests to the fundamental role that quantum-chemical calculations can play in the detection of new molecules. The only noteworthy discrepancy between the observed and predicted spectrum in Figure 12 is the additional splitting due to the torsional motion seen in the experimental spectrum. This splitting has not been treated

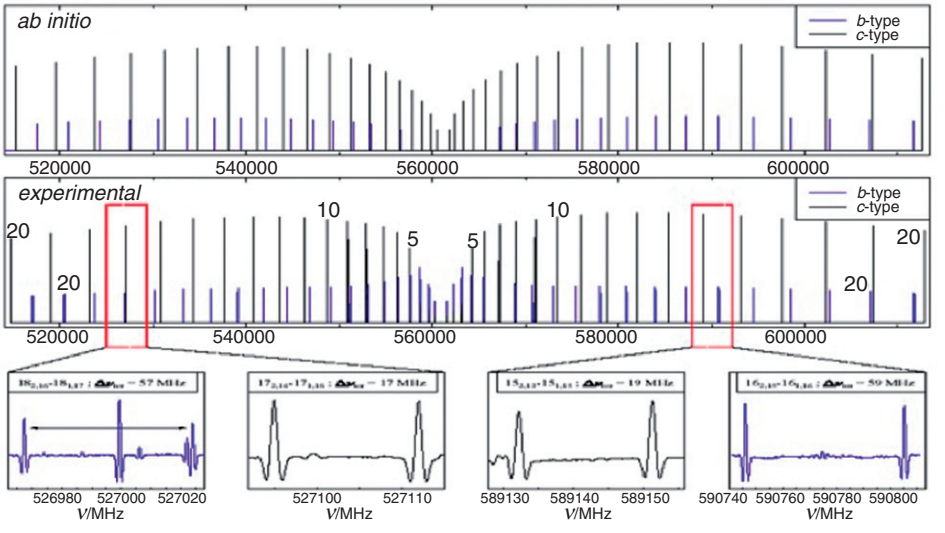

Figure 12. [Colour online]. Comparison of theoretically predicted and experimental rotational spectra of HSOH [4]. Shown is the $^rQ_1$ branch with a band center at 561 GHz.

in the theoretical prediction and this omission was of no relevance for the detection of HSOH. However, it should be noted that theoretical values for the corresponding torsional barriers have been calculated and given in Ref. [4]. The corresponding values of 2216 and 1579 cm^{-1} (for the *cis* and *trans* transition states) are in line with the measured splitting of about 20 MHz and 100 MHz observed in the experiment for the *b* and *c* type transitions, respectively. A more detailed theoretical treatment of the torsional motion together with theoretical values for the splittings have been given in Refs. [277–280]. In the initial investigation of HSOH, a total of about 600 lines were identified; among them about 120 could be attributed to $H^{34}SOH$, present in natural abundance [4]. For structural characterization of HSOH, however, it was essential to also determine the spectroscopic parameters of the corresponding deuterated species. As the synthesis of the deuterated precursor compounds was decided to be too involved, attempts were made to produce HSOH in discharges of mixtures of H_2S and H_2O. With the known spectra, it was rather straightforward to optimize the discharge conditions and then, again guided by quantum-chemical predictions, to carry out radio-frequency discharges of D_2S/D_2O and H_2O/D_2O in the presence of sulfur powder. In this way, the spectra of DSOD [281,282] and HSOD [283] could be detected, while, for unknown reasons, the DSOH isotopologue has not been observed. Table 8 summarizes the measured rotational constants for the HSOH isotopologues and compares them to corresponding theoretical predictions. The remaining discrepancies of less than 70 MHz for the *A* constant and about a few MHz for the *B* and *C* constants are surprisingly small. Nevertheless, the example of HSOH provides a convincing demonstration that accurate quantum-chemical calculations can

Table 8. Comparison of experimental and theoretical rotational constants (in MHz) for the known isotopologues of HSOH.

	Experiment	Theory
HSOH[a]		
A_0	202 069.05431(134)	202 135.8
B_0	15 281.956620(123)	15 278.9
C_0	14 840.216440(121)	14 840.4
$H^{34}SOH$[a]		
A_0	201 739.7641(129)	201 806.9
B_0	15 001.43940(38)	14 998.4
C_0	14 573.77816(39)	14 573.9
DSOD[b]		
A_0	106 850.4937(55)	106 908.5
B_0	13 865.38319(173)	13 864.6
C_0	13 173.54491(227)	13 176.4
HSOD[c]		
A_0	159 965.20(44)	159 973.5
B_0	14 132.204(40)	14 133.1
C_0	14 020.685(41)	14 023.5

[a]Ref. [4].
[b]Refs. [281,282].
[c]Ref. [283].

guide experiment and in particular help to restrict the searches to narrow frequency ranges. It is noteworthy in this context that, using a similar pyrolysis reaction (but starting from (*t*-Bu)-S(O)S-(*t*-Bu) and again based on quantum-chemical predictions of the rotational spectra, the *cis*- and *trans*-isomers of HSSOH could be detected using rotational spectroscopy [15,284].

There are many other examples in the literature (see for instance Refs. [9–11,31, 285–289]) where the spectroscopic investigations have been guided by theoretical predictions. We will not discuss them and instead refer the interested reader to the original work [9–11,31,285–289]. The context is more or less the same in all cases, namely, that first theoretical predictions of the rotational spectra and transitions help to define a suitable frequency range for the spectroscopic searches and second that the agreement between the theoretical and experimental parameters can be used to verify the assignment of the spectra. Clearly, the more accurate the predictions are the more useful are those for the spectroscopic searches and in this way it is obvious that high-level quantum-chemical calculations are essential for the interplay of theory and experiment in the area of rotational spectroscopy.

5.1.3. *Equilibrium structures*

The preferred choice for reporting structural information is to quote the equilibrium parameters that are defined via the corresponding minimum on the Born–Oppenheimer potential surface. In this way, vibrational effects are rigorously excluded and the reported structure is, at least to the extent the Born–Oppenheimer approximation is valid, independent of the isotopic species. The same is not true for other types of structural parameters often reported in the literature (for an overview and definition of these parameters, see, for example, Ref. [290]). Nevertheless, the use of those structures, e.g., of the r_0 and r_s structures in the case of rotational spectroscopy, is most often dictated by the fact that they are, unlike the r_e structure, obtained in a rather straightforward manner from the analysis of the rotational constants inferred from the experimental data.

While rotational spectroscopy is the method of choice for obtaining highly accurate structural information, it still is a formidable task to extract the desired information from the experimental data. The first problem is that there are as many rotational constants needed as there are independent structural parameters. For polyatomic molecules this usually necessitates the investigations of more than one isotopologue of the considered molecule. Furthermore, the number of isotopically substituted species increases with the size of the system, thus rendering structural determinations for larger molecules cumbersome or simply impossible using rotational spectroscopy. Clearly, for this reason rotational spectroscopy is the method of choice for small to medium-sized systems only. A second issue is that the derivation of an equilibrium structure requires the explicit consideration of vibrational effects. Though they can in principle be obtained from the analysis of ro-vibrational spectra, such an approach indeed is only practical in the case of diatomic and a few triatomic molecules. The main problem is that such a pure experimental approach to equilibrium structures requires the knowledge of all vibration–rotation interaction constants for all of the considered isotopic species. And usually, the complete set of these constants is not available, thus hampering the determination of the r_e structure. Furthermore, the experimental approach can be complicated by Coriolis resonances, which affect only the vibration–rotation constants, but not the overall

vibrational contribution [72]. A way out of this problem is the use of quantum-chemically computed vibrational corrections to the rotational constants. The combination of the experimentally determined ground-state rotational constants with these computed corrections then allows the determination of equilibrium rotational constants and consequently of an equilibrium structure. This combined experimental-theoretical approach to equilibrium geometries has turned out in recent years to be a powerful tool (see, for example, Refs. [10,32,72,269,289,291–322]) and the in this way obtained structures, due to the computational contribution, are usually referred to as ''empirical'', ''mixed experimental/theoretical'', or ''semi-experimental''.

The first example for an empirical structure has been reported more than thirty years ago in a study of methane, in which Pulay, Meyer, and Boggs [291] corrected the experimental rotational constants for CH_4 using computed corrections. The reported equilibrium C–H distance ($1.086_2 \pm 0.0005$ Å) turned out to be very accurate and has been more or less confirmed in a more recent redetermination of the CH distance [312] which suggested a value of $1.0859_5 \pm 0.0003$ Å). Efforts in the same direction have been subsequently made by many others, especially Allen [72,292,293], Botschwina [294–299], Gauss [10,269,283,289,300–311], Stanton [269,300–304,312–317], Puzzarini [289,308,311, 318–321], Demaison [322–329], Craig [330–333], Groner [330,332–335] and others.

5.1.3.1. *Procedure*. The empirical equilibrium structure is obtained by a least-squares fit of the molecular structural parameters to the equilibrium moments I_α^e (or alternatively the equilibrium rotational constants B_e^α) for a sufficiently large number of isotopologues of the considered molecule. The equilibrium values for I_α^e (more precisely B_e^α) are thereby obtained by correcting the experimental rotational constants (B_0^α) for vibrational effects according to Equation (62) with the sum of the vibration–rotation interaction constants determined via quantum-chemical calculations. The usual way for obtaining these corrections is second-order vibrational perturbation theory as described in Section 3, but clearly other, in particular non-perturbative approaches to these corrections are feasible. The moments of inertia are then obtained via Equation (10). However, there exist different opinions whether one should use the moments of inertia or the rotational constants in the least-squares fit to the structures. However, in out opinion, the choice of how one weights the various constants in the fit is more important. The use of moments of inertia with equal weights for all included values clearly is one of the possible recommended choices, while the use of rotational constants is often hampered by the large A constants. Those need to be either excluded from the fitting or considered with a rather low weight. Figure 13 illustrates the various steps involved in the determination of empirical equilibrium structures and also emphasizes that without the (computed) vibrational corrections it is only possible to determine the from a theoretical viewpoint and also in terms of accuracy less satisfying $r_0, r_s, \ldots$ structures.

5.1.3.2. *Examples*. A systematic investigation concerning the accuracy of this procedure to obtain empirical or semi-experimental equilibrium structures has been carried out by Pawłowski and coworkers [32]. They conclude that for molecules containing first-row elements the determined equilibrium bond distances typically have an accuracy of about 0.001 Å provided electron correlation is considered in the calculation of the

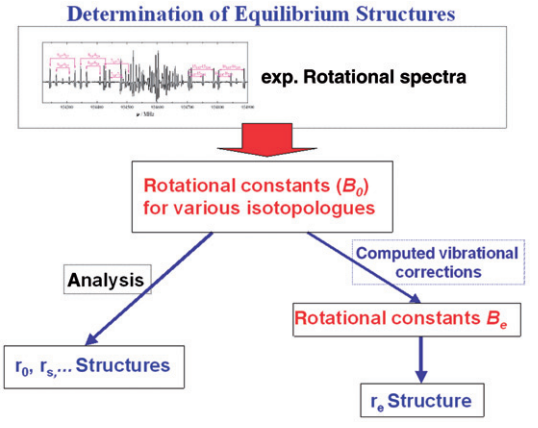

Figure 13. [Colour online]. Procedure for determining empirical equilibrium structures based on experimental rotational constants.

Table 9. Comparison of equilibrium bond distances (in Å) obtained from experimental rotational constants using experimental and computed vibrational corrections. The theoretical best estimates have been taken from Ref. [190].

	r_e(exp)	r_e(emp)	Theoretical best estimate
HF	0.91680(8)	0.9169	0.9171
CO	1.12832	1.1284	1.1284
N_2	1.09768(5)	1.0977	1.0975
H_2O	0.9572	0.9575	0.9578
NH_3	1.011(6)	1.0116	1.0109

vibrational corrections. In Table 9, we compare for a few molecules the empirical bond distances (vibrational corrections have been obtained at the CCSD(T)/cc-pVQZ level, for details, see Ref. [32]) with equilibrium distances obtained using experimentally determined vibration–rotation interaction constants for the estimation of the vibrational effects. The excellent agreement clearly attests to the power of the semi-experimental approach to equilibrium geometries.

In the following, we will give a few representative examples for the actual application of the semi-experimental approach. Let us first consider again oxadisulfane (HSOH). The spectroscopic investigation provided the rotational constants not only for the main isotopic species HSOH but also for $H^{34}SOH$ [4], DSOD [281,282], and HSOD [283]. The twelve available constants (A_0, B_0, and C_0) together with the computed vibrational corrections (available from the theoretical study for the prediction of the rotational spectra of HSOH) then enabled the determination of the equilibrium structure of this molecule, only shortly after its detection via rotational spectroscopy. The excellent agreement between the empirical structure obtained in this way and results from high-level calculations (CCSD(T)/cc-pCVQZ level) is documented in Figure 14.

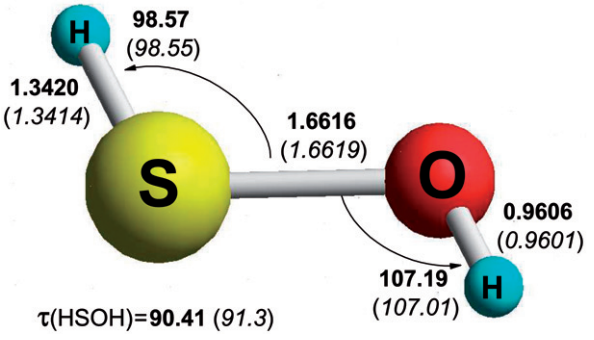

Figure 14. [Colour online]. Empirical equilibrium structure of HSOH [283]. Theoretical results as obtained at the CCSD(T)/cc-pCVQZ level are given in parentheses. Bond lengths are given in Å, angles in degrees.

The *trans* and *cis* isomers of 1-chloro-2-fluoroethylene (CHF=CHCl) provide another example for the joint experimental and theoretical determination of equilibrium structures [31,308]. In addition, this example demonstrates how quantum-chemical calculations are useful for verifying the proper assignment of the experimental spectra. Due to the fact that both isomers of CHF=CHCl have nine geometrical degrees of freedom, it is clear that the experimental investigation of the two main isotopic species (CHF=CH^{35}Cl and CHF=CH^{37}Cl) is not sufficient for the determination of the equilibrium structure and that deuterated and ^{13}C substituted species need to be investigated. No problems in this regard were encountered for the *cis* isomer and rotational constants for ten isotopologues could be determined [336,337]. However, for the *trans* isomer, some complications had to be overcome. After detection of the rotational spectra for the main isotopic species [338], it proved difficult to assign the corresponding spectra for the deuterated species. The usual procedure to improve the computed spectroscopic parameters via scaling based on the observed deviations between theory and experiment for the main isotopic species did not provide reliable estimates and, in particular, did not allow assignment of the corresponding spectra. Nevertheless, it was finally possible, albeit difficult, to assign the spectrum for CD^{35}Cl=CHF; however, the determined parameters showed rather large deviations with respect to the scaled values. Based on the values for CD^{35}Cl=CHF, it was then possible to assign the spectra for all other deuterated species. Unfortunately, it was then impossible to obtain a satisfactory fit for the equilibrium structure using the available set of experimental rotational constants. This was rather surprising, as theoretical considerations clearly indicated that the set of data should be sufficient for a determination of the equilibrium structure of *trans*-CHCl=CHF. A closer analysis revealed inconsistencies between the determined spectroscopic parameters for the main species and the others. This suggested, together with the difficulties in assigning the spectra for the deuterated species, that the reported data for the main species were not those for the vibrational ground state rather those for a vibrationally excited state. An experimental reinvestigation confirmed this conclusion [31] and provided the proper spectroscopic parameters for the two main isotopic species.

Using the available rotational constants together with the computed vibrational corrections obtained at either the MP2/cc-pVTZ or the CCSD(T)/cc-pVTZ level, it was

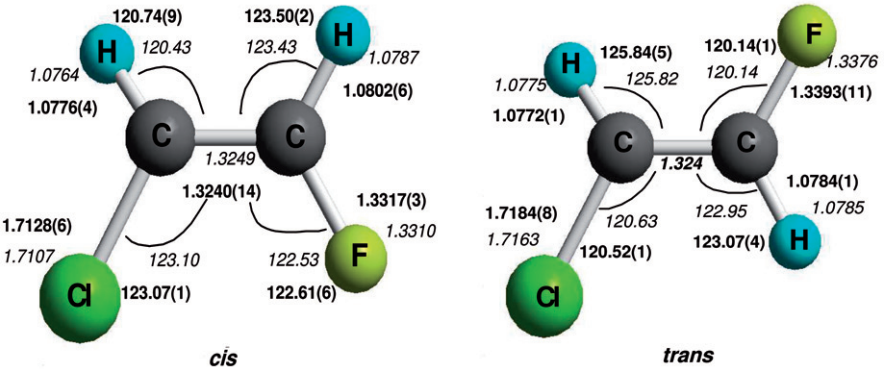

Figure 15. [Colour online]. Empirical equilibrium structure of *trans*- and *cis*-CHF=CHCl [283,308]. Theoretical results, given in italics, correspond to the best estimates given in Ref. [308] based on CCSD(T) calculations and the use of extrapolation techniques. Bond lengths are given in Å, angles in degrees.

possible to obtain an empirical equilibrium structure for both isomers of CHF=CHCl (see Figure 15). The geometrical parameters for both isomers are also given in Table 10 where they are compared to parameters for other substituted ethylenes. The comparison in Table 10 shows that in the *cis* form of CHCl=CHF the C–X distances (X = F and Cl) are considerably shorter (by about 0.005 to 0.007 Å) and that there are rather pronounced differences in the corresponding angles (up to 2.5°), thus reflecting the steric and electronic interactions in the halogenated ethylenes. It is also noteworthy that for both isomers a significantly shorter C–C distance than for unsubstituted ethylene (by about 0.010 Å) is found. The findings for CHCl=CHF are in good agreement with earlier results for 1,2-difluoroethylene [330] as well as for 1,2-dichloroethylene [331,339].

Concerning other examples reported in the literature, we would like to discuss only the following cases. The first deals with the two isomers of cyclic SiC_3 [7,303] for which it has been found essential to include the electronic contribution to the rotational constants (see Section 5.1) in order to reduce the inertial defect to an acceptable value. The latter is defined as [1,2]

$$\Delta = I_c - I_a - I_b \tag{144}$$

and vanishes for planar molecules provided the equilibrium inertial moments are used to evaluate Δ. The corresponding Δ values for the two isomers of SiC_3 are given in Table 11. It is clearly seen that, as expected, the use of the uncorrected rotational constants B_0 leads to a relatively large positive inertial defect. The latter is significantly, though not entirely, reduced by considering vibrational corrections to the rotational constants. However, unlike for many other cases, additional consideration of the electronic contributions to the rotational constants is required for both isomers of SiC_3 to reduce the inertial defect to an acceptable value. The (empirical) equilibrium structures of SiC_3 are depicted in Figure 16 together with the available theoretical values obtained at the CCSD(T)/cc-pCVQZ level [303]. The effect of including the electronic contribution is found here rather small. The largest correction of 0.0005 Å is seen for the transannular C–C bond of isomer I.

A larger effect on the equilibrium geometry due to the electronic contribution to the rotational constant is seen in the case of the diatomics BH and CH^+. Here, as documented

Table 10. Empirical equilibrium geometries of substituted ethylenes (distances in Å, angles in degrees).

	trans-1,2-difluoroethylene[a]	*cis*-1,2-difluoroethylene[a]	*trans*-1,2-dichloroethylene[b]	*cis*-1,2-dichloroethylene[b]
C–F	1.339(1)	1.334(1)		
C–Cl			1.7131(10)	1.7103(5)
C–H	1.078(1)	1.075(1)	1.0793(6)	1.0796(5)
C–C	1.324(1)	1.323(1)	1.3367(15)	1.3301(15)
∠ FCC	119.8(1)	122.3(1)		
∠ ClCC			121.32(5)	124.15(2)
∠ HCC	125.1(1)	122.5(1)	122.86(27)	120.85(5)
	vinylfluoride[b]	vinylchloride[c]	*trans*-1-chloro-2-fluoroethylene[b]	*cis*-1-chloro-2-fluoroethylene[b]
C–F	1.3430(4)		1.3383(12)	1.3317(3)
C–Cl		1.7263(2)	1.7187(9)	1.7128(6)
C–H	1.0790(1)	1.0783(1)	1.0784(1)	1.0802(6)
C–C	1.3209(4)	1.3262(3)	1.324^{fixed}	1.3240(14)
$C–H_t$[d]	1.0780(3)	1.0796(2)		1.0776(4)
$C–H_c$[d]	1.0785(1)	1.0796(1)	1.0772(1)	
∠ FCC	126.18(5)		120.15(2)	122.61(6)
∠ ClCC		122.75(1)	123.07(1)	123.07(1)
∠ HCC	121.69(1)	123.91(4)	125.80(6)	123.50(2)
∠ CCH_t	118.92(1)	119.28(2)		120.74(9)
∠ CCH_c	121.39(3)	121.77(2)	120.74(9)	

[a]Ref. [330].
[b]Ref. [31].
[c]Ref. [327].
[d]H_t means H in *trans* position with respect to X (X = F,Cl). H_c means H in *cis* position with respect to X (X = F,Cl). For 1-chloro-2-fluoroethylene H_t means H in *trans* position with respect to F (*cis* isomer) and H_c means H in *cis* position with respect to F (*trans* isomer).

Table 11. Inertial defects Δ (in amuÅ^2) as determined for the experimental (B_0) and the empirical equilibrium (B_e) rotational constants for the two isomers of cyclic SiC_3 [303].

	Isomer I	Isomer II
B_0	0.059	0.073
$B_e{}^a$	0.018	0.022
$B_e{}^b$	0.001	0.000

[a]Determined without consideration of the electronic contribution to the rotational constant.
[b]Determined with consideration of the electronic contribution to the rotational constant.

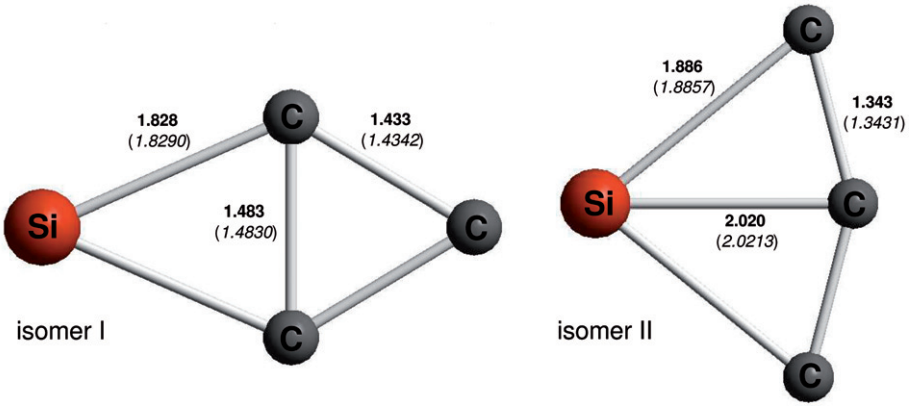

Figure 16. [Colour online]. Empirical equilibrium structure (in Å) of the two cyclic SiC_3 isomers [303] in comparison with theoretical results (in parentheses) obtained at the CCSD(T)/cc-pCVQZ level.

in Table 12, the inclusion of this contribution leads to changes in the bond distance of about 0.002 Å and thus is mandatory to reach agreement with results from high-level quantum-chemical calculations.

Furthermore, we would like to draw attention to the cases of CCH and FCCCCH, as these two examples nicely illustrate how a missing or non-rigorous treatment of vibrational corrections can lead to structural parameters (r_0 and/or r_s) that are not good approximations for the corresponding equilibrium values.

Let us start with the ethynyl radical. Its equilibrium structure has recently been determined via the mixed theoretical-experimental approach [307]. Comparison with the earlier determined r_s and r_0 structures [341] clearly reveals that the latter two provide a significantly too short C–H distance (see Figure 17) and thus are not good representatives for the true equilibrium geometry of this molecule. While this is not unexpected for the r_0 geometry, the failure of the substitution approach, which is often claimed to eliminate vibrational effects to a good approximation, is noteworthy and suggests that it should only be used with some care. The present findings are also supported by high-level quantum-chemical calculations [307,342] which confirm the reliability of the determined empirical equilibrium structure of the ethynyl radical. Another example in this context

Table 12. Equilibrium bond distance (in Å) of BH and CH^+ as determined from the experimental rotational constant with and without consideration of the electronic contribution to the rotational constant and from high-level quantum-chemical calculations performed at the fc-CCSD(T)/cc-pV∞Z + ΔT/cc-pVTZ + ΔQ/cc-pVDZ + Δ core/cc-pCVQZ level.

	BH	CH^+
Exp. (literature)	1.2324[a]	1.1309[a]
Emp. (without consideration of ΔB_{el})	1.2321	1.1309
Emp. (with consideration of ΔB_{el})	1.2299	1.1284
Theoretical best estimate	1.2302	1.1279

[a]Ref. [340].

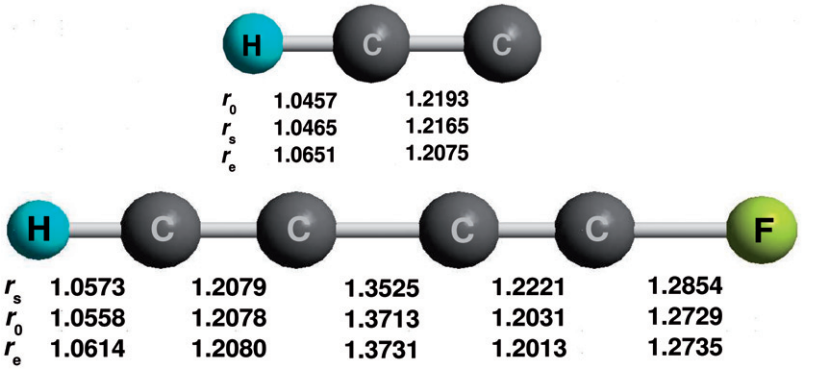

Figure 17. [Colour online]. Substitution (r_s), effective (r_0) and empirical equilibrium (r_e) structures (in Å) of ethynyl radical and monofluorodiacetylene.

is monofluorodiacetylene (see Figure 17). The substitution approach again yields in this case a too short C–H distance [297,343], but more severe is that the r_s structure is not able to properly describe the changes in the C–C distance due to substitution by fluorine with respect to diacetylene. A detailed account on the structural parameters in diacetylenes can be found, for example, in Ref. [309].

To conclude this section, we would like to recommend that structure determinations based on rotational spectroscopy should be – whenever possible – carried out using the mixed theoretical-experimental approach that has been described here. Only in this way is it possible to obtain reliable structural parameters with high accuracy and with a rigorous physical meaning. Furthermore, due to significant computational advances in the recent years, the calculation of the force fields required is usually not a major obstacle for obtaining such an equilibrium structure in the case of the small to medium-sized molecules typically studied. A final remark concerns molecules characterized by large-amplitude motion. In this case, some care is required when evaluating vibrational corrections, and a variational approach might be the preferred choice (see, for example, Refs. [344,345]).

5.1.4. *Rotational constants for vibrationally excited states*

As the investigation of molecules in vibrationally excited states by means of rotational spectroscopy has recently attracted some interest (see, for example, Refs. [76,77,287, 346–355]), it is important to guide corresponding investigations via quantum-chemical calculations. With the focus on the corresponding shift in the rotational constants, the relevant equations are

$$B^{\alpha}_{v_1,v_2,\ldots} = B^{\alpha}_{e} - \sum_r \alpha^{\alpha}_r \left(v_r + \frac{1}{2} \right) \tag{145}$$

or, when targeting at a state with a single vibrational level excited

$$B^{\alpha}_{v_r=1} = B^{\alpha}_{0} - \alpha^{\alpha}_r. \tag{146}$$

In other words, the prediction of the rotational constants $B^{\alpha}_{v_r=1}$ for such a vibrationally excited state requires the knowledge of the individual vibration–rotation interaction constants α^{α}_r. Expressions for computing these constants from available harmonic and cubic force fields have been given in Section 3 (see Equation (64)). One could now argue that these constants are already needed for the prediction of the B^{α}_0 values. However, there is one important difference. While for the determination of B^{α}_0 only the sum of all α^{α}_r is required, and in this way problems due to possible Coriolis resonances are avoided, this is no longer the case for the determination of $B^{\alpha}_{v_r=1}$, as the individual interaction constants are now needed. Consequently, the prediction of rotational constants for vibrationally excited states can be affected by Coriolis resonances and is therefore a fundamentally more difficult endeavor. In such cases, the use of special treatments beyond the perturbational approach discussed in Section 3 is warranted.

The computational requirements for the accurate determination of vibration–rotation interaction constants have been, for example, discussed in Ref. [32]. Table 13 demonstrates the accuracy that can be achieved in the prediction of these constants. A statistical analysis in Ref. [32] with respect to electron-correlation and basis-set treatment furthermore suggests that the corresponding calculations are best carried out at the MP2 or CC level using basis set of at least triple-zeta quality. The values obtained using MP2/cc-pVTZ or CCSD(T)/cc-pVTZ cannot be considered entirely converged, but the remaining errors are rather small. HF-SCF calculations turn out less useful in general, and the use of a double-zeta basis set cannot be recommended either.

5.1.4.1. *Examples*. As an example for the usefulness of theoretical predictions of the vibration–rotation interaction constants and the corresponding rotational constants for vibrationally excited states, we mention here the recent investigation of the $\nu_{11} = 1$ and $\nu_{14} = 1$ vibrationally excited states of methyldiacetylene (CH_3CCCCH) [346].

Quantum-chemical predictions were essential (see Table 14), as only in this way was it possible to distinguish in the crowded spectrum (see Figure 18) between transitions due to the various vibrationally excited states ($\nu_{11} = 1$, $\nu_{12} = 1$, $\nu_{13} = 1$, and $\nu_{14} = 1$ bending modes) and those for the ^{13}C containing species in natural abundance. Indeed, the transitions due to the vibrationally excited states turned out to be more intense than those of $CH_3C^{13}CCCH$ investigated in Ref. [320].

Table 13. Comparison of calculated and experimental α_r^b values (in MHz) for a few diatomic molecules. The last two columns report the absolute discrepancy $\delta\alpha_r^b(\text{abs}) = \alpha_r^b(\text{calc.}) - \alpha_r^b(\text{exp.})$ and relative discrepancy $\delta\alpha_r^b(\text{relat}) = \delta\alpha_r^b/\alpha_r^b(exp.)$ (in %) between the experimental and theoretical values. Computational results have been obtained at the CCSD(T)/cc-pVQZ level; for further details, see Ref. [32].

Molecule	B_0	α_r^b(calc.)	α_r^b(exp.)	$\delta\alpha_r^b$(abs)	$\delta\alpha_r^b$(relat)
H_2	1778788.6	90537.3	91796.4[a]	−1259.1	−1.4
F_2	26470.2	376.8	387.9[b]	−10.8	−2.9
N_2	59646.4	508.1	518.3[c]	−10.2	−2.0
HF	616343.3	23593.7	23923.4[a]	−329.8	−1.4
CO	57636.0	516.8	524.6[a]	−8.1	−1.5

[a]Ref. [340].
[b]Ref. [356].
[c]Ref. [357].

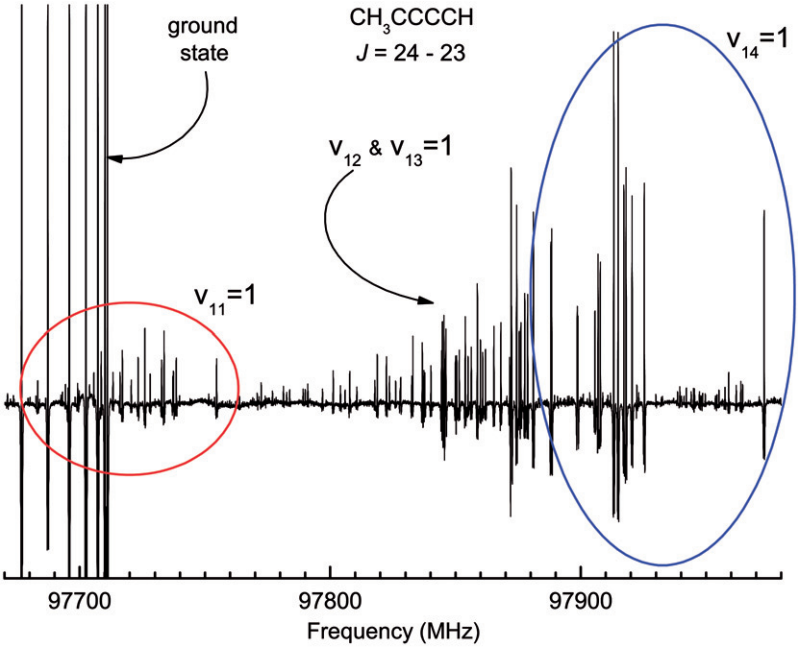

Figure 18. [Colour online]. A portion of the $J = 24 \leftarrow 23$ transition in the rotational spectrum of CH_3CCCCH is reported: the position of the four lowest and ground-state bands is made evident.

5.2. *Centrifugal-distortion constants*

For accurate line predictions, in particular when dealing with high J values, it is not sufficient just to provide the rotational constants; rather one must also compute the corresponding centrifugal-distortion constants. Figure 19 shows an example for the impact of centrifugal-distortion on rotational spectra and clearly underlines the need for the

Table 14. Comparison. of computed and experimental (given in parentheses) spectroscopic parameters for various vibrationally excited states of CH_3CCCCH. For further details, see Ref. [346].

	ν (cm^{-1})	A_v (MHz)[a]	α_v^a (MHz)[b]	B_v (MHz)[a]	α_v^b (MHz)[b]
$\nu_{14}=1$	154.4 (139)	158797.4	30.4	2039.8 (2040.14)	−4.1 (−4.40)
$\nu_{13}=1$	315.5 (320)	158825.5	2.3	2039.1	−3.4
$\nu_{12}=1$	431.3 (484)	158841.3	−13.5	2039.0	−3.3
$\nu_{11}=1$	591.0 (614)	158827.8	9.5	2036.5 (2036.33)	−0.8 (−0.59)
Ground state		158827.8		2035.7 (2035.74)	

[a]Obtained by combining equilibrium rotational constants from the best theoretical structure in Ref. [320] with vibrational corrections obtained at the MP2/cc-pVTZ level.
[b]MP2/cc-pVTZ calculations.

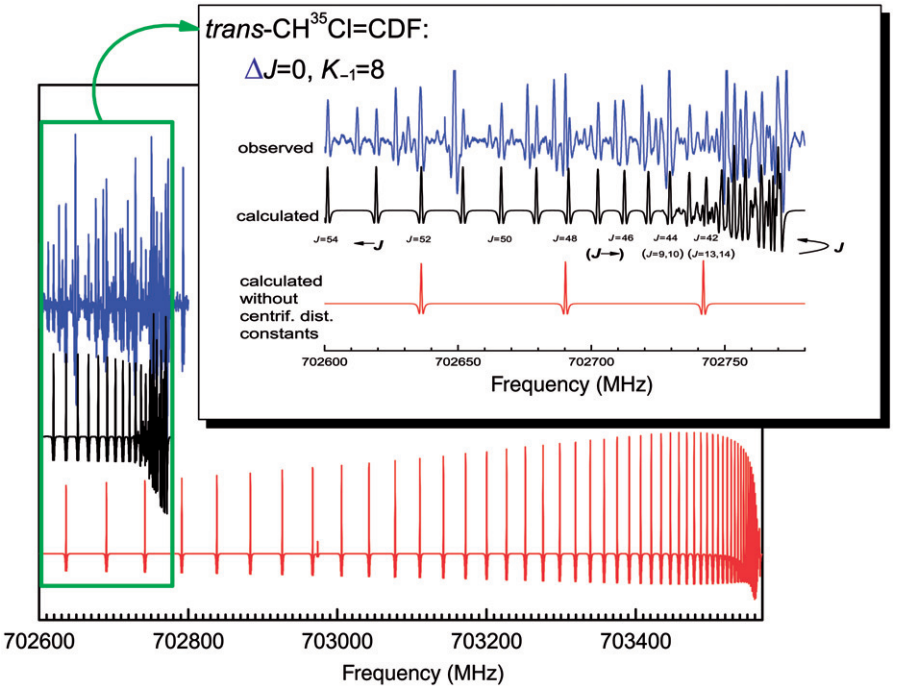

Figure 19. [Colour online]. Impact of centrifugal distortion on the rotational spectrum ($\Delta J=0$, $K_{-1}=8$, at ~703 GHz) of *trans*-$CH^{35}Cl$=CDF. Shown are the experimental (blue) and the with (black) and without (red) considering centrifugal distortion computed spectra [31].

knowledge of the centrifugal-distortion parameters for the reliable and accurate prediction of the corresponding transitions.

The relevant theory for centrifugal distortion has been outlined in Section 2 and can be found in greater detail in Refs. [1–3,45]. We only remind the reader that, for the theoretical determination of the quartic centrifugal-distortion constants, knowledge of the harmonic

Table 15. Experimental and calculated quartic centrifugal-distortion constants (in kHz) for various isotopologues of *trans*-1-chloro-2-fluoroethylene. The computational results have been obtained at the CCSD(T)/cc-pVTZ level and have been taken from Ref. [31].

	Experiment	Theory	Experiment	Theory
	$CH^{35}Cl{=}CHF$		$CH^{37}Cl{=}CHF$	
Δ_J	0.31904(10)	0.310	0.30524(12)	0.297
Δ_{JK}	−10.37041(64)	−10.909	−10.2591(10)	−10.787
Δ_K	759.992(65)	796.364	763.42(10)	800.168
δ_J	0.020720(74)	0.020	0.019397(20)	0.019
δ_K	2.2410(82)	2.083	2.158(12)	2.001
	$CD^{35}Cl{=}CHF$		$CD^{37}Cl{=}CHF$	
Δ_J	0.302[a]	0.302	0.289[a]	0.289
Δ_{JK}	−7.0651(32)	−7.502	−7.0122(61)	−7.470
Δ_K	502.694(56)	527.567	505.815(88)	530.700
δ_J	0.02474(61)	0.024	0.02410(92)	0.023
δ_K	2.086[c]	2.086	2.002[a]	2.002
	$CH^{35}Cl{=}CDF$		$CH^{37}Cl{=}CDF$	
Δ_J	0.309(31)	0.309	0.296[a]	0.296
Δ_{JK}	−5.3916(68)	−5.695	−5.3586(39)	−5.651
Δ_K	342.026(97)	351.130	343.05(10)	351.949
δ_J	0.0200(12)	0.023	0.02037(12)	0.021
δ_K	2.39(54)	2.239	2.15(29)	2.152
	$CD^{35}Cl{=}CDF$		$CD^{37}Cl{=}CDF$	
Δ_J	0.298(22)	0.300	0.288[c]	0.288
Δ_{JK}	−4.3563(14)	−4.639	−4.3449(12)	−4.628
Δ_K	241.080(22)	249.260	241.9643(93)	250.363
δ_J	0.02740(16)	0.027	0.02200(65)	0.025
δ_K	2.014[a]	2.014	1.936[a]	1.936

[a]Values kept fixed at the theoretical value in the analysis of the experimental spectra.

force field suffices, while the computation of sextic centrifugal-distortion constants in addition requires the cubic force field. For both type of centrifugal-distortion constants, computer programs are available (see, for example, Refs. [358–360]).

5.2.1. *Accuracy and examples*

To the best of our knowledge, no detailed investigation has been carried out concerning the accuracy of computed centrifugal-distortion constants with respect to electron-correlation and basis-set effects. Usually, these constants are evaluated at the same level as the corresponding force fields needed either for the prediction of the vibrational frequencies or the vibrational corrections to the rotational constants. It is assumed, and generally found, that the accuracy provided by these levels of theory (often MP2 or CCSD(T) with triple-zeta or quadruple-zeta quality basis sets) is sufficient.

As an example for the calculation of quartic centrifugal-distortion constants, we provide in Table 15 a comparison between theory and experiment for these constants

for the recently investigated *trans*-CHCl=CHF molecule [31]. The agreement is for all parameters within a few percent and, thus, it is obvious that corresponding theoretical predictions can be helpful in the analysis of experimental spectra. This is in particular the case when some of the constants cannot be determined solely on the basis of the experimental data. In those cases, it is recommended to set the corresponding constants to the theoretically predicted values and to keep them fixed during the fitting procedure (see, also Table 15).

5.3. *Dipole moments*

In rotational spectroscopy, quantum-chemical calculations of dipole moments are of interest mainly because the intensities of rotational transitions are determined by the corresponding components of the molecular dipole moment. Theoretical predictions are thus of importance for deciding whether a molecule is suitable for an investigation using rotational spectroscopy and for identifying observable transitions for the experimental investigation. For these tasks, reliable, though not necessarily highly accurate predictions of dipole moments are needed, as one is dealing here solely with the more qualitative aspects of rotational spectroscopy. Quantitative predictions, however, are relevant in connection with Stark measurements in the presence of external electric fields (see, for example, Chapter 7 of Ref. [2]). With this technique, it is possible to determine dipole-moment values by means of rotational spectroscopy, and quantum-chemical calculations are here useful for verifying experimental results.

5.3.1. *Accuracy and examples*

An extensive benchmark study concerning the quantum-chemical determination of dipole moments has been, for example, reported in Ref. [361]. Table 16 reproduces some of the results presented in that study. We note first of all that the use of basis sets augmented by diffuse functions, e.g., the use of the aug-cc-p(C)V*n*Z sets instead of the standard cc-p(C)V*n*Z sets within Dunning's hierarchy of correlation-consistent basis-sets (see Section 4.3), is strongly recommended [362,363]. This is a well-known recommendation and due to the fact that the dipole operator samples the outer valence region in a molecule. With the additional consideration of diffuse functions, the main requirement for an acceptable basis set is more or less met, and reasonable results are already obtained at MP2/aug-cc-pVTZ or CCSD(T)/aug-cc-pVTZ levels. HF-SCF calculations typically overestimate the magnitude of the dipole moment, while, on the other hand, electron-correlation effects beyond MP2 are often not substantial except in challenging cases such as, for example, CO or CH_2 (see Table 16). A rigorous comparison of computed dipole moments with experiment turns out difficult, as in many cases no accurate experimental values are available or the magnitude of vibrational effects is unknown. The latter can be non-negligible and amount, for example, for HF to 0.023 D ($>1\%$ of the total value). In the calculations, however, vibrational effects can be accounted for as described in Section 3.2 using perturbation theory.

An example of the utility of quantum-chemically calculated dipole moments is provided by the investigations of trisulfane (H_2S_3 [364,365]) and 1-oxatrisulfane (HSSOH [15,284]) by means of rotational spectroscopy. For both species, *cis* and *trans* forms exist

Table 16. Equilibrium dipole moments (in Debye) calculated for a set of small molecules at the HF, MP2, CCSD, and CCSD(T) levels using basis sets from the aug-cc-pV*n*Z hierarchy. For full computational details and experimental data, see Ref. [361].

				CCSD(T)			
	HF aug-cc-pVQZ	MP2 aug-cc-pVQZ	CCSD aug-cc-pVQZ	aug-cc-pVDZ	aug-cc-pVTZ	aug-cc-pVQZ	Exp.
CO	0.137	0.265	0.084	0.083	0.120	0.118	0.123(2)
NH_3	1.544	1.517	1.530	1.541	1.513	1.521	1.561(5)
HNO	1.877	1.708	1.718	1.674	1.683	1.694	—
CH_2	1.904	1.829	1.733	1.637	1.689	1.695	—
H_2O_2	1.863	1.764	1.782	1.747	1.742	1.750	2.2[a]
HF	1.884	1.811	1.813	1.799	1.797	1.800	1.803(2)
H_2O	1.936	1.864	1.870	1.859	1.845	1.853	1.8473(10)
HOF	2.024	1.875	1.901	1.914	1.883	1.888	—
CH_2O	2.703	2.395	2.440	2.397	2.385	2.392	2.3321(5)[a]
HCN	3.262	3.029	3.059	3.005	3.003	3.017	2.985188(3)[a]
HNC	2.956	3.271	3.104	3.072	3.107	3.110	3.05(1)[a]

[a]Not corrected for vibrational effects.

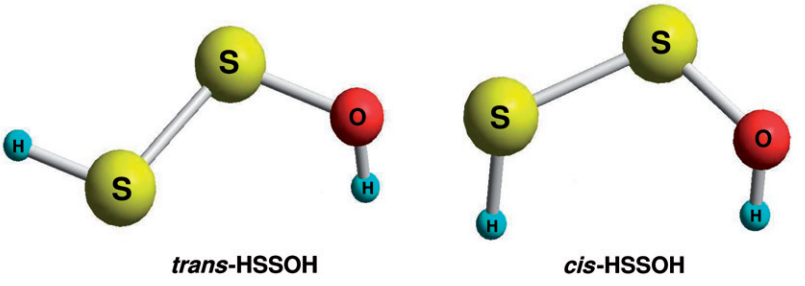

Figure 20. [Colour online]. Structures of *cis*- and *trans*-HSSOH as in predicted by means of CCSD(T)/cc-pCVQZ calculations. The computed geometrical parameters can be found in Ref. [15].

(see Figure 20 in the case of HSSOH) with the *trans* conformer being slightly more stable. Nevertheless, in accordance with quantum-chemical calculations, for both H_2S_3 (*cis*: $\mu_c = -1.5851$ D, and *trans*: $\mu_b = 0.5627$ D, $\mu_c = -0.5559$ D; CCSD(T)/cc-pCVQZ calculations) and HSSOH (*cis* form: $\mu_a = 0.187$ D, $\mu_b = 0.538$ D, $\mu_c = 2.179$ D; *trans* form: $\mu_a = 0.195$ D, $\mu_b = 0.539$ D, $\mu_c = 0.550$ D; CCSD(T)/cc-pCVQZ calculations [15]), the *cis* form has been first detected via rotational spectroscopy due to its stronger lines in the spectrum. In the case of HSSOH, it was furthermore possible, based on the measured relative intensities and the calculated dipole moments, to provide an estimate for the relative abundance of both forms. The ratio found for *trans* versus *cis* is 2.2 and in apparent agreement with the quantum-chemical prediction that the *trans* form is the more stable one (by about 2 kJ/mol). This interpretation, however, should be taken with some care, as the ratio in the reaction mixture is not in thermodynamic equilibrium and other factors might affect the *trans–cis* ratio as well.

As an example for the determination of dipole moments via Stark measurements, we cite a recent study of CH_2BrF [366]. The effect of the applied electric field on the rotational transition is illustrated in Figure 21. We note that the analysis of the corresponding spectra is further complicated by hyperfine interactions (see next section). Nevertheless, the determined experimental dipole-moment components are in good agreement with theoretical predictions. Table 17 provides a comparison and demonstrates the importance of basis-set extrapolation, proper inclusion of core-correlation effects, and vibrational corrections to yield satisfactory agreement. Despite the bromine, in the present case, relativistic effects are not important, as is consistent with the results of a benchmark study concerning relativistic effects on electrical properties [367].

5.4. *Nuclear quadrupole coupling*

In molecules with quadrupolar nuclei the nuclear quadrupole coupling is the main mechanism responsible for additional splittings in the rotational spectrum. The analysis of this fine structure is significantly facilitated by quantum-chemical calculations, which can provide, as discussed in Section 2.3, the electric-field gradient at the corresponding nuclei. We will present here examples for such calculations, but also point out that quadrupole-coupling constants from rotational spectroscopy when combined with results for

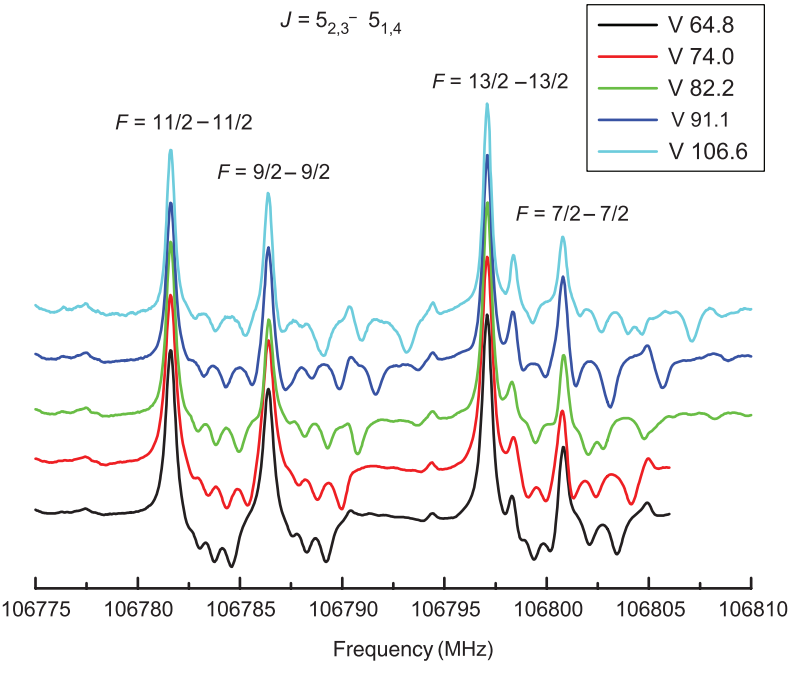

Figure 21. [Colour online]. Stark spectra of the $F=9/2$ and $F=11/2$ hyperfine components of the $J=5_{2,3} \leftarrow 5_{1,4}$ rotational transition for CH_2FBr recorded with different voltage applied (64.8 V, 74.0 V, 82.2 V, 91.1 V, and 106.6 V) to the electrodes ($d=0.28945(7)$ cm).

Table 17. Quantum-chemically calculated and experimental dipole-moment components (in Debye) of $CH_2{}^{79}BrF$ [366].

	μ_a	μ_b	μ_{tot}
CCSD(T)/aug-cc-pVTZ	−0.322	−1.678	−1.709
CCSD(T)/aug-cc-pVQZ	−0.341	−1.696	−1.730
CCSD(T)/aug-cc-pV5Z	−0.346	−1.700	−1.735
CBS	−0.350	−1.702	−1.738
CBS+CV[a]	−0.355	−1.710	−1.746
CBS+CV+ZPV[b]	−0.339	−1.701	−1.734
Experiment[c]	0.3466(11)	1.704(26)	1.739(26)

[a]Values extrapolated to the complete basis-set limit (CBS) plus core-correlation corrections (CV).
[b]Zero-point vibrational corrections (ZPV) added to the CBS+CV values.
[c]Absolute value. Reported uncertainties are 3 times the standard deviation of the fit.

electric-field gradients from quantum-chemical calculations can be used for the determination of nuclear quadrupole moments [368–370].

5.4.1. *Accuracy*

As the electric-field gradient operator, as given in Equation (42), exhibits a cubic dependence on $1/|\mathbf{r}-\mathbf{R}_K|$, it is strongly affected by the electronic structure in the

Table 18. Basis-set convergence and electron-correlation effects in the quantum-chemical calculation of electric-field gradients (in a.u.) for the BH molecule [362].

		HF-SCF	MP2	CCSD	CCSD(T)	FCI
H	cc-pVDZ	0.22215	0.22632			
	cc-pVTZ	0.16090	0.16016	0.16094	0.16096	0.16099
	cc-pVQZ	0.15717	0.15482	0.15539	0.15541	0.15545
	cc-pV5Z	0.15765	0.15482	0.15551	0.15552	0.15557
	cc-pCVDZ	0.19568	0.19660	0.19752	0.19753	0.19753
	cc-pCVTZ	0.16059	0.15952	0.16019	0.16019	0.16021
	cc-pCVQZ	0.15727	0.15480	0.15540	0.15540	0.15545
	cc-pCV5Z	0.15736	0.15449	0.15518	0.15519	0.15524
B	cc-pVDZ	0.42638	0.42263			
	cc-pVTZ	−0.73563	−0.72930	−0.68887	−0.68427	−0.68274
	cc-pVQZ	−0.74253	−0.73939	−0.69937	−0.69460	−0.69316
	cc-pV5Z	−0.74006	−0.73846	−0.69842	−0.69364	−0.69222
	cc-pCVDZ	−0.69794	−0.67862	−0.63437	−0.63077	−0.62933
	cc-pCVTZ	−0.69318	−0.68946	−0.65121	−0.64724	−0.64587
	cc-pCVQZ	−0.71045	−0.70899	−0.67037	−0.66595	−0.66457
	cc-pCV5Z	−0.70739	−0.70729	−0.66891	−0.66445	−0.66310

inner-valence and core region at the corresponding nucleus. Accordingly, additional tight basis functions are needed for the accurate prediction of electric-field gradients and nuclear quadrupole-coupling constants [362,371,372]. Adequate choices are provided by the core-polarized sets within Dunning's hierarchy of correlation-consistent basis sets. A benchmark study with the focus on both the basis-set convergence and electron-correlation treatment has been, for example, carried out by Halkier *et al.* in Ref. [362]. Table 18 summarizes their results together with a few additional calculations.[10] The electric-field gradient at the boron nucleus, $q(B)$, clearly demonstrates the importance of steep functions in the used basis set. The values obtained with the cc-pV*n*Z series of basis sets do not converge to the proper limit and, thus, can be dismissed as unreliable. On the other hand, straightforward convergence to the correct limit is seen when using the cc-pCV*n*Z sets. A corresponding effect is not seen for the electric-field gradient at the hydrogen nucleus which is in line with the fact that the electric-field gradient is a local property and only reflects the quality of the wavefunction at the nucleus considered. Concerning the principal number n of the basis sets, we note that double- and triple-zeta sets do not seem to be sufficient. Reliable calculations should be carried out with basis sets of quadruple-zeta quality or better. Electron-correlation effects are also pronounced for the electric-field gradients of BH. The deviations of the HF-SCF results from the FCI limit are quite large (i.e., about 7% for B). MP2 is in the present case (as also known from other benchmark calculations using BH [373]) not able to recover the large correlation contribution; CC calculations are hence mandatory. While CCSD already provides results in close agreement with the FCI values ($<1\%$ deviation), the agreement of the CCSD(T) results with FCI is excellent. Core-correlation effects on the other side are less important, as, for example, the all-electron CCSD(T)/cc-pCVQZ value of −0.676 a.u. differs only marginally (less than 2%) from the corresponding frozen-core CCSD(T) results given in Table 18.

Table 19. Comparison of spin-free Dirac-HF (DHF) with second-order direct perturbation theory (DPT2) and second-order Douglas–Kroll (DK2) results for the electric-field gradients (in a.u.) at the heavier nucleus in HX (X = F, Cl, Br, I, At). DK2 results, geometries, and basis sets were taken from Ref. [376], all other results from Ref. [367].

Molecule	q_{zz}^{nrl}	Δq_{zz}^{DHF}	Δq_{zz}^{DPT2}	Δq_{zz}^{DK2}	$\Delta^{DPT2/nrl}$ (%)	$\Delta^{DPT2/DHF}$ (%)
HF	2.8704	0.0101	0.0101	0.0097	0.4	0.0
HCl	3.6095	0.0502	0.0496	0.0492	1.4	1.2
HBr	7.0704	0.5351	0.5057	0.5294	7.2	5.5
HI	9.7311	1.9788	1.7167	1.9693	17.6	13.2
HAt	15.4088	11.4328	7.4555	11.5577	48.4	34.8

There is another important issue in the quantum-chemical calculation of electric-field gradients. In particular, for heavier nuclei, relativistic effects can be important (see, for example, Refs. [57,367,374–384]). Table 19 shows the increasing importance of relativistic effects when going to heavier elements. While relativistic effects are negligible for the halogen electric-field gradient of HF, they amount for HCl to about 1%, for HBr to about 7%, for HI to about 18%, and for HAt to about 48%. This means that already for second- and third-row elements, relativity is for this property of relevance, and the quantum-chemical treatment should include those effects. While for the heavier elements, four-component calculations [385] (such as Dirac-HF or corresponding electron-correlation treatments starting from the Dirac-HF ansatz) are mandatory, for lighter elements either perturbative schemes (e.g., second-order direct perturbation theory (DPT2) [386]) or quasi-relativistic approaches based on the Douglas–Kroll–Hess transformation [387] are sufficient. Vibrational corrections for electric-field gradients can be computed as explained in Section 3.2. They are in most cases not very pronounced, but clearly should be considered when aiming at high accuracy.

5.4.2. *Examples*

In the following, a few examples are given to demonstrate the use of quantum-chemical calculations of nuclear quadrupole-coupling constants for the detection and in particular the analysis of rotational spectra.[11]

Figure 22 compares a portion of the observed spectrum of *trans*-$CH^{35}Cl{=}CHF$ with those based on theoretical predictions. The first theoretical spectrum has been obtained without consideration of the chlorine quadrupole coupling, whereas the second spectrum has been simulated with this coupling properly taken into account. It is evident from the comparison depicted in Figure 22 that the inclusion of nuclear quadrupole coupling is essential for a reliable prediction of the actual rotational transitions and especially for their analysis. The first spectrum, i.e., the one which ignores nuclear quadrupole coupling, is clearly insufficient for this purpose as the characteristic features are not well reproduced and a systematic shift is apparent (see figure caption). The good agreement obtained between experiment and theory for *trans*-$CH^{35}Cl{=}CHF$ is seen in Table 20, where the computed values for the chlorine quadrupole-coupling tensor elements are compared with those determined from the experimental spectrum. The calculations have been here carried out at the CCSD(T) level using a weighted core-polarized valence triple-zeta

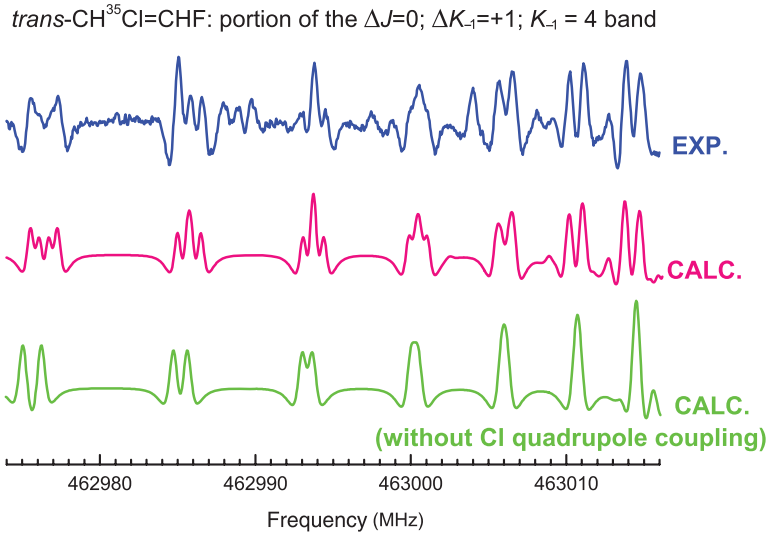

Figure 22. [Colour online]. Rotational spectrum of *trans*-$CH^{35}Cl$=CHF. Upper trace: observed spectrum of a portion of the $K_{-1}=4$ (~463 GHz) band. Lower traces: calculated spectrum with (pink) and without (green) chlorine quadrupole coupling. For the latter a frequency shift (approximately, +2 GHz) has been applied in order to compare the same transitions.

Table 20. Comparison of experimental and theoretical (CCSD(T)/cc-wCVTZ) ground-state chlorine quadrupole-coupling constants of *trans*-$CH^{35}Cl$=CHF [31].

	Theory	Experiment
χ_{aa}	−63.13	−63.586(58)
χ_{bb}	27.52	27.53(27)
χ_{cc}	35.61	36.05(27)
χ_{ab}	−33.34	

(cc-pwCVTZ) basis. Vibrational effects have not been included, but they seem (in the case of CHCl=CHF) less important. Their neglect might provide the reason for remaining deviations between theory and experiment, although other factors such as higher-order correlation effects and basis-set convergence might also play a role. Nevertheless, the agreement in the present case is more than sufficient to guide the experimental investigations and to support the analysis of the recorded spectrum via meaningful input values for the chlorine quadrupole-coupling tensor.

The second example deals with the bromine quadrupole-coupling in CH_2FBr. The focus here is on the role of relativistic effects as well as on the proper choice for the required bromine quadrupole moment. Concerning the latter, the large scatter in the literature values [389–396] is seen in Table 21. Indeed, excellent agreement between the calculated (non-relativistic) and experimental bromine quadrupole-coupling constants is

Table 21. Available values for the nuclear quadrupole moment of ^{79}Br (in mbarn) in the literature.

Authors	Year	Nuclear quadrupole moment	Reference
Lederer, Shirley	1978	293	[389]
Taqqu	1978	331(4)	[390]
Kellö, Sadlej	1990	304.5	[391]
Kellö, Sadlej	1996	298.9	[392]
Hass, Petrilli	2000	305(5); 308.7	[393]
Van Lenthe, Baerends	2000	300(10)	[394]
Bieron *et al.*	2001	313(3)	[395]
Yakobi *et al.*	2007	302(5)	[396]

Table 22. Non-relativistic (nrl)[a] and relativistic (rel)[b] values of quadrupole-coupling constants of $CH_2{}^{79}BrF$ for the different choices of bromine quadrupole moment (331(4) mbarn from Ref. [390], 313(3) mbarn from Ref. [395], and 307.5(10) mbarn from Ref. [397]) compared to experiment. All values include vibrational corrections. Uncertainties due to errors in quadrupole moment are given in parentheses.

		eQ from Ref. [390]		eQ from Ref. [395]		eQ from Ref. [397]	
	Experiment	nrl	rl	nrl	rl	nrl	rel
χ_{aa}	443.431(8)	446.5(5.4)	474.0(5.4)	422.2(4.0)	449.7(4.0)	414.8(1.3)	442.3(1.3)
χ_{bb}	−144.933(21)	−145.3(1.8)	−154.4(1.8)	−137.6(1.3)	−146.2(1.3)	−135.16(44)	−144.22(44)
χ_{cc}	−298.498(21)	−300.9(3.6)	−319.3(3.6)	−284.6(2.7)	−303.0(2.7)	−279.66(91)	−298.07(91)
$\lvert\chi_{ab}\rvert$	278.56(19)	282.1(3.4)	299.6(3.4)	266.9(2.5)	284.4(2.5)	262.27(84)	279.75(84)

[a]Non-relativistic values have been obtained at the CCSD(T)/cc-pCVQZ level; vibrational corrections have been determined at the MP2/cc-pCVTZ level.
[b]Relativistic corrections have been obtained using DPT2 at the CCSD(T) level using an uncontracted cc-pVQZ basis.

obtained in the case of CH_2FBr [289] if one takes the value of 331 mbarn from Ref. [390] which is also given on the webpage www.webelements.com (see Table 22). This agreement, however, is not in line with the importance of relativistic effects for third-row elements; the corresponding corrections should amount to about 7–8% in the case of bromine (see, for example, Table 19 and also Refs. [367,384]). In this respect, the use of the bromine quadrupole moment reported by Bieroń *et al.* [395] or Yakobi *et al.* [396] is more satisfying. Using, for example, the value of 313 mbarn given by Bieroń *et al.*, the expected disagreement (about 5%) between the experimentally determined quadrupole-coupling constants and the computed non-relativistic values is noted. Relativistic corrections as obtained at the DPT2 level [367,384] then restore the good agreement with experiment, now for the proper reason. The remaining deviations are in the range of 1.5–2.5%. Vibrational effects on the other hand are found to be one order of magnitude smaller than relativistic effects, but they have been included in the values given in Table 22. The persisting small discrepancy of 1.4–2.1% between the computed quadrupole-coupling

constants obtained using the quadrupole moment from Ref. [395] and the corresponding experimental values can be taken as an indication that the actual value for the bromine quadrupole moment is somewhat smaller (e.g., in the range of 306 to 309 mbarn) than the one given in Ref. [395]. This conclusion certainly is consistent with the lower value of 302(5) mbarn obtained by Yakobi *et al.* [396] and also confirmed by a recent redetermination of the bromine quadrupole moment (307.5(10) mbarn) [397]. Using this most recent value in the case of CH_2FBr, our final values for the elements of the bromine quadrupole-coupling tensor deviate by less than 0.4% from the corresponding experimental numbers. At this point, it should be also noted that if one uses these more recent values for the ^{79}Br and ^{81}Br quadrupole moments, good agreement between the (relativistic) quantum-chemical calculations of the quadrupole coupling constants is obtained not only for the two main isotopologues $CH_2F^{79}Br$ and $CH_2F^{81}Br$, but also for the corresponding deuterated species. For further details, we refer the reader here to Ref. [384] where a full account on the hyperfine structure in the rotational spectra of the various isotopologues of CH_2FBr can be found.

5.4.3. *Determination of nuclear quadrupole moments*

By inverting Equation (29),

$$eQ_K = \frac{\chi_{\alpha\beta}}{V^K_{\alpha\beta}}, \tag{147}$$

it is possible to use experimental nuclear quadrupole-coupling constants $\chi_{\alpha\beta}$ to determine values for the nuclear quadrupole moment eQ_K of the corresponding nucleus. Actually, this procedure, based either on atomic or molecular quadrupole-coupling constants, is the major source for this type of nuclear data [368–370]. As additional information, this conversion requires an accurate computed value for electric-field gradients. In the case of atomic systems, whose treatment is beyond the scope of this review, they are preferably obtained via large-scale numerical MCSCF calculations (see, for example, Ref. [395]). In the case of molecular systems, large basis-set CCSD(T) calculations are often used, and the challenge is to ensure the proper basis-set convergence as well as the adequate treatment of electron correlation. The reliable computation of electric-field gradients furthermore necessitates the inclusion of zero-point vibrational effects [392,395,398] and the consideration of relativistic effects [380,392,393,398]. The latter are particularly important for heavier nuclei (see, for example, Refs. [57,367,374–384]). In Table 23, we give one example which illustrates the sketched procedure in the case of ^{79}Br [395]. The experimental quadrupole-coupling constant of HBr used here is 532.3048 MHz [399].

The calculated value for the electric-field gradient from non-relativistic large basis-set CCSD(T) calculations is 6.768 a.u. [367]. Relativistic effects treated at the DPT2 level amount to 0.476 a.u. [367], while vibrational corrections contribute 0.090 a.u. [395]. The total value for the ^{79}Br electric field gradient is then 7.333 a.u. which corresponds to a value of 308.9 mbarn for the ^{79}Br nuclear quadrupole moment, which is in good agreement with values (313 mbarn [395], 302.5 mbarn [396], 307.5 mbarn [397]) derived from the quadrupole-coupling constant measured for the bromine atom.

Table 23. Determination of the nuclear quadrupole moment (in mbarn) of ^{79}Br based on the experimental nuclear quadrupole-coupling constant (in MHz) for H^{79}Br and computed bromine electric-field gradients (in a.u.).

	Value	Total value	Nuclear quadrupole moment eQ_K
Experimental nuclear quadrupole coupling ($v=0$) [399]	532.3048		
CCSD(T)/cc-pCV5Z (uncontracted) [367]	6.7678	6.7678	334.7
+ relativistic correction (DPT2) [367]	0.4759	7.2437	312.7
+ vibrational correction [395]	0.0900	7.3337	308.9

5.5. *Spin–rotation interactions*

After nuclear quadrupole coupling, spin–rotation interactions are the next major source for the hyperfine structure seen in rotational spectra and the focus of many recent experimental investigations (see, for example, Refs. [384,400–423]). There is also an interest in spin–rotation interactions beyond rotational spectroscopy, as the nuclear spin–rotation constants are closely related to the corresponding nuclear magnetic shielding constants [19] (see Section 5.5.3) and in this way essential for establishing absolute NMR scales [55,85,424–426].

As explained in Section 2.3, the nuclear spin–rotation tensor consists of an electronic and a nuclear part. While the latter is completely determined by the molecular geometry, the electronic contribution corresponds to a second-order property and in this way can be computed as a second derivative of the electronic energy with respect to the rotational angular momentum and the appropriate nuclear spin as perturbations [58]. This is efficiently done using analytic second-derivative techniques (see Ref. [38]). Initial calculations [427] carried out in a conventional manner using standard basis functions suffered from a slow basis-set convergence. Nowadays, the corresponding calculations are performed using perturbation-dependent basis functions [58]. In analogy to NMR chemical-shift calculations in which magnetic-field dependent basis functions, the so-called gauge-including atomic orbitals (GIAOs) or London orbitals, are used [428–431], the basis-set convergence in the calculation of nuclear spin–rotation tensors can be significantly accelerated when the following **J**-dependent basis functions are used [58]

$$\chi_\mu(\mathbf{r},\mathbf{J}) = \exp(i(\mathbf{I}^{-1}\cdot\mathbf{J})\times\mathbf{R}_\mu\cdot\mathbf{r})\ \chi_\mu(\mathbf{r}). \tag{148}$$

In Equation (148), $\chi_\mu(\mathbf{r})$ denotes the usual basis functions with center $\mathbf{R}_\mu$, e.g., the Gaussians discussed in Section 4.3. One can refer to the basis functions given in Equation (148) either as *J*-including atomic orbitals (JIAOs) or rotational London orbitals.

The improved basis-set convergence when using these type of basis functions has been amply documented in Ref. [58]. In addition, it should be noted that the use of JIAOs renders any discussion concerning the choice of origin for the electronic angular momentum in the perturbed operator (see Equation (43)) unnecessary.

5.5.1. *Accuracy*

The computational requirements for the reliable calculation of spin–rotation tensors are documented by the results given in Table 24 for the hydrogen of $H_2{}^{16}O$ [407]. Clearly, electron-correlation effects are important (about 3%) and the CCSD(T) approach appears to be the method of choice for the corresponding calculations. More interesting is the issue of basis-set convergence. While a significant speed-up is already obtained by using perturbation-dependent basis functions, it should be noted that still the basis-set requirements are rather demanding. In the case of $H_2{}^{16}O$, it is seen that basis sets of at least quadruple-zeta quality are required to obtain converged values. The changes when going from triple to quadruple-zeta are still in the range of a few percent, while a further increase in size only causes marginal changes. More important are in some cases the consideration of additional diffuse functions [58,432], though this is not the case for $H_2{}^{16}O$, and the inclusion of vibrational effects. In our example, the latter contribute about 0.5–1.5 kHz, and in this way need to be considered for accurate predictions. The best theoretical estimates for the individual tensor elements agree quite well with the

Table 24. Electron-correlation effects, basis-set convergence, and vibrational corrections for the hydrogen spin–rotation tensor of $H_2{}^{16}O$ (kHz). For further details, see Ref. [407].

	C_{aa}	C_{bb}	C_{cc}	C_{ab}	C_{ba}
HF-SCF/cc-pCVTZ	−35.35	−32.07	−34.00	±46.84	±20.99
HF-SCF/cc-pCVQZ	−34.68	−31.62	−33.62	±46.22	±20.93
HF-SCF/cc-pCV5Z	−34.55	−31.38	−33.48	±46.01	±21.01
HF-SCF/cc-pCV6Z	−34.51	−31.33	−33.44	±45.99	±21.01
HF-SCF/aug-cc-pCVTZ	−35.38	−32.16	−34.21	±47.11	±21.60
HF-SCF/aug-cc-pCVQZ	−34.78	−31.58	−33.68	±46.29	±21.18
HF-SCF/aug-cc-pCV5Z	−34.60	−31.40	−33.51	±46.07	±21.06
HF-SCF/aug-cc-pCV6Z	−34.53	−31.33	−33.44	±45.98	±21.01
MP2/cc-pCVTZ	−36.64	−32.63	−34.68	±48.63	±20.46
MP2/cc-pCVQZ	−35.74	−31.94	−34.04	±47.59	±20.19
MP2/cc-pCV5Z	−35.59	−31.56	−33.82	±47.22	±20.24
MP2/cc-pCV6Z	−35.56	−31.47	−33.75	±47.18	±20.23
MP2/aug-cc-pCVTZ	−36.82	−32.64	−34.89	±48.90	±21.10
MP2/aug-cc-pCVQZ	−35.95	−31.82	−34.10	±47.67	±20.48
MP2/aug-cc-pCV5Z	−35.69	−31.55	−33.85	±47.29	±20.29
MP2/aug-cc-pCV6Z	−35.58	−31.45	−33.75	±47.14	±20.22
CCSD(T)/cc-pCVTZ	−36.82	−32.98	−35.00	±49.79	±21.33
CCSD(T)/cc-pCVQZ	−35.87	−32.24	−34.33	±48.59	±21.10
CCSD(T)/cc-pCV5Z	−35.70	−31.88	−34.11	±48.20	±21.04
CCSD(T)/cc-pCV6Z	−35.67	−31.79	−34.05	±48.15	±21.02
CCSD(T)/aug-cc-pCVTZ	−36.96	−32.98	−35.20	±49.95	±21.90
CCSD(T)/aug-cc-pCVQZ	−36.05	−32.13	−34.39	±48.64	±21.27
CCSD(T)/aug-cc-pCV5Z	−35.79	−31.87	−34.15	±48.27	±21.09
CCSD(T)/aug-cc-pCV6Z	−35.69	−31.77	−34.05	±48.13	±21.01
Vibrational corrections[a]	1.19	0.62	1.54	±1.18	±0.12
Best theoretical estimate	−34.50	−31.15	−32.51	±49.31	±21.13
Experiment	−35.05(25)	−31.02(12)	−32.99(9)		

[a]Vibrational corrections computed at the CCSD(T)/aug-pCV5Z level using second-order vibrational perturbation theory.

corresponding experimental values [407] and in this way give an indication of what kind of accuracy can be achieved in theoretical predictions of spin–rotation constants.

5.5.2. *Examples*

As for the other spectroscopic parameters, the examples in this section have been chosen to demonstrate the importance of quantum-chemical calculations for the experimental investigation of spin–rotation interactions. We show how quantum-chemical computations can be used to verify or challenge experimental data, emphasize the role of calculated hyperfine parameters in the analysis of experimental spectra, and point out that nowadays quantum-chemical calculations are often used to guide experimental investigations.

Let us start with an example for the last case, i.e., the guidance of the experiment. In an effort to investigate spin–rotation interactions in silicon-containing compounds, silyl fluoride (SiH_3F) was chosen in Ref. [408] as a possibly interesting target molecule for Lamb-dip measurements. The reasons were simply that SiH_3F has a sufficiently large dipole moment ($\mu_0 = 1.2$ D, vibrationally averaged value at the CCSD(T)/cc-pCVTZ level) and that it is easily produced in a DC discharge reaction using phenyl silane ($C_6H_5SiH_3$) and tetrafluoromethane (CF_4) [408]. High-level quantum-chemical calculations together with simulations of the spectra based on the computed parameters have then been used to determine which spin–rotation constants (fluorine and/or hydrogen in the case of the main isotopologue and $^{30}SiH_3F$ as well as silicon, fluorine, and/or hydrogen in the case of $^{29}SiH_3F$) are determinable and which rotational transitions are most promising for this purpose. Table 25 summarizes the computed spin–rotation tensors, while Figure 23 provides examples for the simulated spectra (together with the recorded ones) of $^{28}SiH_3F$ and $^{29}SiH_3F$. In the case of the main isotopologue, the calculations indicate that only the fluorine spin–rotation interaction is sizable and the simulations reveal that, using the resolution provided by the Lamb-dip technique, the corresponding splittings are detectable only for larger K values. This expectation is confirmed by the actual measurements and Figure 23 shows the splitting due to the fluorine spin–rotation interaction for the $J = 15 \leftarrow 14$, $K = 13$, transition. In the case of $^{29}SiH_3F$, both the silicon and fluorine spin–rotation interactions are of comparable magnitude though of opposite sign. The simulations based on the computed parameters then suggest that these two interactions lead to a hyperfine structure that is hardly resolvable and that only a rather broad signal should be seen that cannot be analyzed further. The hydrogen spin–rotation interactions are again significantly smaller (see Table 25) but in this case, due to an additional broadening of the signal, hamper the analysis further. Again, the predictions are confirmed by the experimental investigations, and the $J = 15 \leftarrow 14$, $K = 13$, transition is shown in Figure 23. The reliability of the theoretical predictions is not only seen by the good agreement between the simulated and experimental spectra but also by the favorable comparison in the value for the fluorine spin–rotation interaction constants for $^{28}SiH_3F$. The theoretical value of 45.35 kHz agrees well with the experimentally derived one of 45.74(35) kHz. In the case of $^{30}SiH_3F$, an analysis of the hyperfine structure was hampered in Ref. [408] only by the fact that the corresponding spectra were recorded in natural abundance with low resolution. Though the original goal to determine the silicon spin–rotation interactions could not be achieved in the investigation of the rotational spectrum of silyl fluoride reported in Ref. [408], this example clearly shows how theory can be used

Table 25. Calculated spin–rotation tensors (in kHz) of SiH_3F, $^{29}SiH_3F$, and $^{30}SiH_3F$. Calculations of the equilibrium values have been carried out at the CCSD(T)/aug-cc-pCVQZ level; vibrational corrections have been determined at the CCSD(T)/cc-pCVTZ level. For further details, see Ref. [408].

	$^{28}SiH_3F$			$^{29}SiH_3F$			$^{30}SiH_3F$		
Constant	Equilibrium	Vibrational corrections	Total	Equilibrium	Vibrational corrections	Total	Equilibrium	Vibrational corrections	Total
$C_{xx}(F) = C_{yy}(F)$	2.44	0.28	2.72	2.42	0.28	2.70	2.40	0.28	2.68
$C_{zz}(F)$	44.16	1.19	45.35	44.16	1.19	45.35	44.16	1.19	45.35
$C_{xx}(Si) = C_{yy}(Si)$				−9.09	0.14	−8.95			
$C_{zz}(Si)$				−42.45	0.51	−41.94			
$C_{xx}(H)$	0.67	−0.02	0.65	0.67	−0.02	0.64	0.65	−0.02	0.63
$C_{yy}(H)$	−1.27	0.06	−1.21	−1.27	0.06	−1.19	−1.24	0.06	−1.18
$C_{zz}(H)$	−7.07	0.39	−6.68	−7.07	0.39	−6.68	−7.07	0.39	−6.68
$C_{xz}(H)$	0.62	−0.02	0.60	0.62	−0.02	0.59	0.61	−0.02	0.59
$C_{zx}(H)$	3.20	−0.19	3.01	3.20	−0.19	3.01	3.20	−0.19	3.01

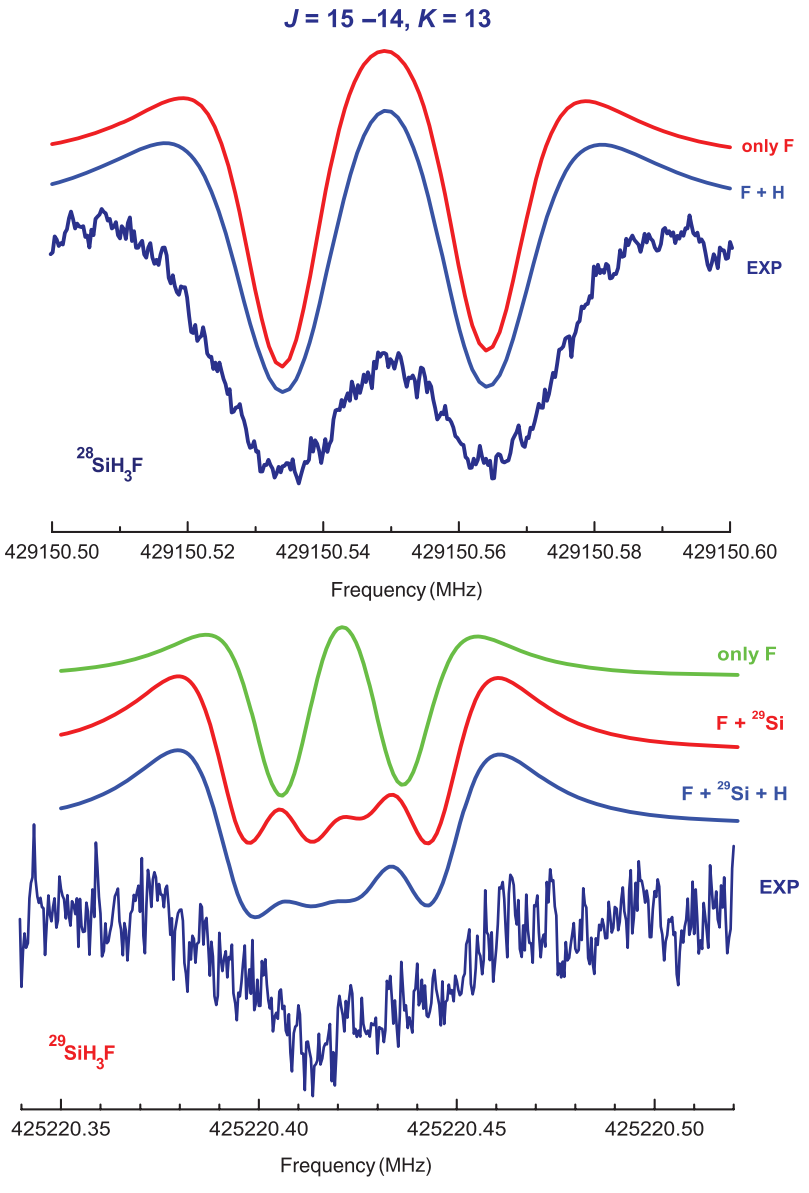

Figure 23. [Colour online]. The $J = 15 \leftarrow 14$, $K = 13$, transition in the rotational spectrum of silyl fluoride: comparison of experimental (P = 0.4 mtorr, mod. depth = 16 kHz for $^{28}SiH_3F$; P = 1.2 mtorr, mod. depth = 40 kHz for $^{29}SiH_3F$ – recorded in natural abundance) and calculated spectra (mod. depth = 15 kHz).

to guide the investigations and in particular predict which parameters are determinable and which are not.

In the second example, quantum-chemical calculations are used to verify/challenge the experimental values [400,402] for the halogen spin–rotation constants of the two carbenes

Table 26. Comparison of experimental and computed spin–rotation tensors (in kHz) for CF_2 and CCl_2 [433].

	C_{aa}	C_{bb}	C_{ab}	C_{ba}	C_{cc}
CF_2					
Best theoretical estimate[a]	380.86	33.14	±122.87	±16.76	13.83
Experiment (2000) [b]	783.(19)	108.(6)			−24.(6)
Experiment (revised, 2005)[c]	379.(11)	31.(4)			11.(4)
CCl_2					
Best theoretical estimate[a]	56.83	2.69	±20.46	±0.73	1.25
Experiment[d]	58.2(9)	2.8(2)			1.4(3)

[a]Ref. [433].
[b]Ref. [400].
[c]Ref. [401].
[d]Ref. [402].

CF_2 and CCl_2. For this purpose, high-level CCSD(T) calculations have been carried out using various sequences of correlation-consistent basis sets (for details, see Ref. [433]). Theoretical best estimates have been provided via extrapolation to the complete basis-set limit and consideration of corrections for core correlation and zero-point vibrational effects. The comparison with the experimental results taken from Refs. [400,402] revealed good agreement in the case of CCl_2 and a severe disagreement in the case of CF_2 (see Table 26). The good agreement seen in the case of CCl_2 as well as the high theoretical levels used in the calculations were strong arguments for the reliability of the computed values for CF_2 so that the only possible conclusion had been that the experimental values for CF_2 were erroneous. This suggestion was confirmed by a reanalysis of the experimental data [401] which revealed a misassignment of the hyperfine components of the $J_{K_a,Kc} = 9_{1,8} - 8_{2,7}$ transition. As seen in Table 26, the analysis based on the revised assignment led to quite different spin–rotation parameters that, unlike the original values, are in good agreement with the computational predictions. The essential point is that the verification of the assignment has been only possible via comparison of the final hyperfine parameters with the corresponding computed values; otherwise, both assignments lead to a satisfactory interpretation of the experimental results. Furthermore, and unlike for many other parameters, it is not easy to guess the proper values for the spin–rotation constants and in this way to dismiss one of the assignments as unreliable. It is clear that quantum-chemical calculations are essential to verify the "correctness" of the analysis of the experimental data and to provide reliable input values for the analysis of the experimental hyperfine structure.

The third example demonstrates how quantum-chemical calculations can support the analysis of experimental spectra. It deals with the hyperfine structure of the rotational spectrum of $H^{13}CN$ which has been measured using the Lamb-dip technique [404]. From the line profile analysis, it turns out that it is necessary to include all hyperfine interactions, i.e., the nitrogen quadrupole coupling, the spin–rotation interactions due to nitrogen, carbon, and hydrogen as well as the direct spin–spin interaction between hydrogen and carbon, to obtain satisfactory agreement between experiment and theory. However, the hydrogen spin–rotation constant, C(H), is found to be not experimentally determinable, and thus needs to be fixed to the computed value of −4.22 kHz. To be more specific, in this

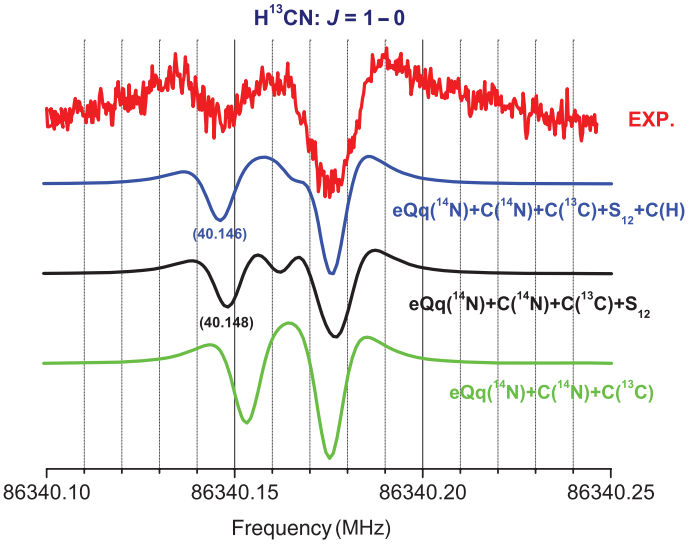

Figure 24. [Colour online]. A portion of the $J = 1 \leftarrow 0$ transition (the $\Delta F_N = 2 \leftarrow 1$ components) in the rotational spectrum of $H^{13}CN$ is shown. In addition to the experimental spectrum (in red), the contributions of each hyperfine parameter to the hyperfine pattern are also depicted (from the bottom to the top): (i) only $eQq(^{14}N) + C(^{14}N) + C(^{13}C)$ (in green); (ii) $eQq(^{14}N) + C(^{14}N) + C(^{13}C) + S_{12}$ (in black); (iii) $eQq(^{14}N) + C(^{14}N) + C(^{13}C) + S_{12} + C(H)$ (in blue) [404].

case neglect of the hydrogen spin–rotation constant affects the appearance of the spectrum (as seen in Figure 24), as the position of the left peak is only correctly reproduced once the hydrogen spin–rotation constant is included. In addition, the fit in this case yields a reliable value for the hydrogen-carbon spin–spin coupling constant only when $C(H)$ is considered. The values are 23.0(37) kHz and 30.4(35) kHz with and without inclusion of $C(H)$, respectively, in comparison with a computed value of 22.9 kHz. Unlike the spin–spin coupling, all other hyperfine parameters are unaffected by the neglect of the hydrogen spin–rotation interactions. This example demonstrates the importance of including all (or as many as possible) hyperfine interactions in the analysis of the spectra. Additionally, it shows that it is clearly preferable to fix those parameters that cannot be determined to the corresponding computed values instead of neglecting them entirely.

5.5.3. *Absolute NMR scales*

As already mentioned, the nuclear spin–rotation constants determined via rotational spectroscopy can be used to set up so-called experimental absolute NMR scales [55,85,409,424–426]. The theoretical basis for this is the following relationship

$$\sigma^K_{para} = -\frac{m_p}{3m_e g_K}\mathbf{I}^{-1}\mathbf{C}^K_{el} \tag{149}$$

between the electronic part of spin–rotation constant $\mathbf{C}^K_{el}$ and the paramagnetic part of the shielding for a given nucleus [52]. The analysis is then completed by augmenting the

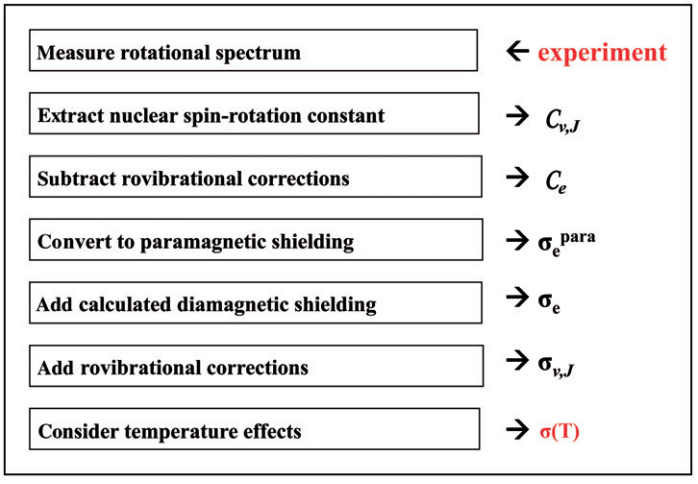

Figure 25. [Colour online]. Procedure for determining nuclear magnetic shielding constants $\sigma(T)$ and absolute NMR scales from experimentally derived nuclear spin–rotation constants.

Table 27. Determination of the absolute ^{17}O NMR scale based on experimental spin–rotation constants from Ref. [414] and [434]. For further details, see Refs. [85,425,435].

Contribution	Old scale (1984,1996)	New scale (2002)
$C(^{17}O)$ (kHz)	−30.4(12)[a]	−31.61(4)[b]
ΔC_{vib} (kHz)	−0.1	−0.1
σ_{para} (ppm)	−483.7(172)	−501.8(6)
σ_{dia} (ppm)	445.1	445.1
σ_{eq} (ppm)	−38.7(172)	−56.7(6)
$\Delta\sigma_{vib}$ (ppm)	−5.73	−5.73
$\Delta\sigma_{T=300\,K}$ (ppm)	−0.35	−0.35
$\sigma_{T=300\,K}$ (ppm)	−44.8(172)	−62.7(6)

[a]Ref. [434].
[b]Ref. [414].

paramagnetic shielding with a computed value for the diamagnetic part. The latter task is not difficult, as computation of the corresponding expectation value is rather straightforward and does not require special considerations with respect to the electron-correlation treatment and choice of basis set. The whole procedure is depicted in Figure 25 and involves also the adequate treatment of vibrational effects as well as temperature corrections. Note that these corrections are preferably obtained using computations, and thus the only experimental contribution to the absolute shieldings is actually the spin–rotation constants determined from the rotational spectrum.

As an example for the determination of an absolute shielding scale, we present in Table 27 the analysis in the case of oxygen based on experimental spin–rotation constant

for $C^{17}O$. The analysis based on the old value, which was determined in 1981 in a radioastronomical study [434], yields a value of −44.8 ppm for the oxygen shielding of CO. Based on the error estimate for the spin–rotation constant, the uncertainty for this shielding value is ±17.2 ppm. Quantum-chemical calculations [85] indicated, in line with the large error bar, that this value cannot be considered accurate and that a reinvestigation is warranted. The current best theoretical estimate for the oxygen shielding of CO amounts to −58.9 ppm and thus deviates by about 14 ppm from the experimental shielding reported in Ref. [435]. However, a new analysis was only possible after laboratory measurements of the rotational spectrum of $C^{17}O$ using the Lamb-dip technique were reported in 2002 [414]. The corresponding spin–rotation constant, which differed by 1.2 kHz from that in Ref. [434] (see Table 27), was then used [425] to improve the oxygen shielding scale and to achieve consistency between theory and experiment. In Table 27, we report the corrections as obtained in Refs. [85,409] within large-basis set CCSD(T) calculations. It should be pointed out that vibrational corrections are not negligible and contribute about −5.7 ppm to the final value. On the other hand, temperature corrections are an order of magnitude smaller. The new value of −62.7 ppm for σ(O) of CO is in good, though still not perfect, agreement with theory (−58.9 ppm). A somewhat better agreement, however, is achieved when using the oxygen spin–rotation constants of $H_2{}^{17}O$ as a basis for the ^{17}O NMR scale (for details, see [409]). The corresponding analysis yields then, thereby using the experimental shift of CO with respect to water, a value of −60.0(3) for σ(O) of CO which agrees within roughly 1 ppm with the corresponding theoretical estimate.

5.6. *Spin–spin couplings*

Dipolar spin–spin couplings often need to be considered for the proper analysis of the hyperfine structure of rotational spectra (see, for example, the case of $H^{13}CN$ in Section 5.5.2). Furthermore, spin–spin couplings offer an alternative route to geometric information [436]. This aspect can be also exploited in solid-state NMR spectroscopy which allows the determination of dipolar couplings (for an example, see Ref. [437]).

5.6.1. *Accuracy*

In principle, the determination of the dipolar coupling constants only requires knowledge of the molecular geometry (see Equation (40)). Quantum-chemical investigations, however, are necessary to provide the vibrational corrections which are given via

$$\boldsymbol{D}_{ij}^{KL} = -\frac{1}{c^2}\gamma_K\gamma_L\left\langle \frac{3(\boldsymbol{R}_{KL})_i(\boldsymbol{R}_{KL})_j - \delta_{ij}\boldsymbol{R}_{KL}^2}{R_{KL}^5}\right\rangle_{vib}. \tag{150}$$

The expectation value is taken here with respect to the vibrational wavefunction and most conveniently evaluated using the perturbative techniques discussed in Section 3.2 [436]. This means that the determination of vibrationally corrected dipolar couplings necessitates the computation of the quadratic (harmonic) and cubic (anharmonic) force fields and in this way is rather costly. These calculations, however, are necessary in order to obtain the spectroscopic parameters discussed earlier in this review. Thus, the computation of vibrationally averaged dipolar couplings is a rather trivial byproduct of the other calculations.

Table 28. Comparison of experimental and computed dipolar coupling constants (in kHz) for HF, HCl, and HCN. Reported are the coupling constants $D = -1/2D_{zz}$. The equilibrium and vibrationally averaged values have been obtained at the CCSD(T)/cc-pwCVQZ level. For further details, see Ref. [436].

Molecule	Equilibrium	Vibrationally averaged	Experiment
HF			
HF	147.219	144.191	143.375(25)[a]
DF	22.599	22.262	22.170(45)[a]
HCl			
$H^{35}Cl$	5.706	5.613	5.585[b]
$H^{37}Cl$	4.750	4.672	4.4(4)[c]
$D^{35}Cl$	0.876	0.866	0.86[d]
$D^{37}Cl$	0.729	0.721	0.72[d]
HCN			
$H^{13}CN$ (H–C)	24.977	22.931	23.0(37)[e]

[a]Ref. [272].
[b]Ref. [438].
[c]Ref. [411].
[d]Ref. [412].
[e]Ref. [404].

The importance of vibrational corrections for the accurate prediction of dipolar spin–spin couplings is seen in Table 28.

The agreement between theory and experiment is consistently improved when vibrational effects are accounted for with the latter amounting to up to a couple of kHz, i.e., a few percent. Another aspect which should be mentioned here is that rotational spectroscopy actually provides an effective spin–spin coupling constant, D_{eff}^{KL}, which also includes the (traceless) anisotropic part ΔJ^{KL} of the indirect spin–spin coupling

$$D_{eff}^{KL} = D^{KL} + \Delta J^{KL}/3. \tag{151}$$

There exists no experimental possibility to distinguish between these two contributions, and only quantum-chemical calculations provide a means to separate them. Techniques for the calculation of indirect spin–spin couplings have been developed [439–442] and can be also used for the present task, i.e., the evaluation of ΔJ^{KL}. Nevertheless, it is usually assumed that the indirect part of the spin–spin coupling is significantly smaller than the dipolar one and thus can be neglected, though there is some evidence that this is not always the case [443].

5.6.2. *Examples*

A case for which the dipolar spin–spin couplings have been investigated in some detail is phosphine, PH_3 [417]. Figure 26 demonstrates the importance of spin–spin interactions for the interpretation of the hyperfine structure of the corresponding rotational spectrum. In this figure, the $J = 1_0 \leftarrow 0_0$ rotational transition is shown as recorded using the

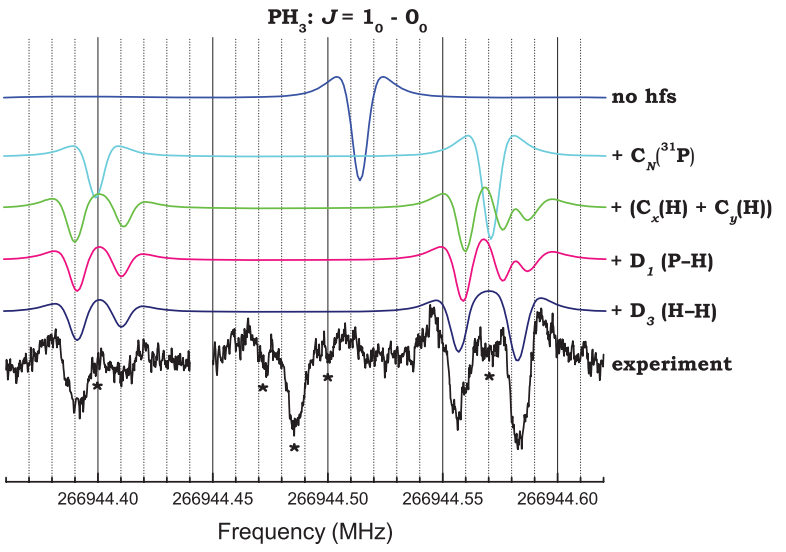

Figure 26. [Colour online]. The $J = 1_0 \leftarrow 0_0$ transition in the rotational spectrum of PH_3. In addition to the experimental spectrum, the contributions of each hyperfine parameter to the hyperfine pattern are also depicted. Starting from the top (unperturbed transition: "no hfs" spectrum) the effect of the inclusion of each relevant hyperfine constant is shown: (1) only $C_N(^{31}P)$, (2) $C_N(^{31}P) + (C_x(H) + C_y(H))$, (3) $C_N(^{31}P) + (C_x(H) + C_y(H)) + D_1(P\text{-}H)$, (4) $C_N(^{31}P) + (C_x(H) + C_y(H)) + D_1(P\text{-}H) + D_3(H\text{-}H)$ [417].

Table 29. Equilibrium structure of NH_3 from experimental dipolar coupling constants of $^{14}NH_3$ and computed vibrational corrections. Distances in Å and angles in degrees [436].

	r_e [DC]	Experiment[a]	CCSD(T)/cc-pwCVQZ
N-H	1.0121(11)	1.0114(6)	1.0111
∠HNH	107.05(9)	107.17(18)	106.38

[a]Ref. [32]: empirical equilibrium structure.

Lamb-dip technique and compared with simulated spectra that consider various subsets of the hyperfine interactions. It is clearly seen how the dipolar couplings change the appearance of the spectrum. Accordingly, they need to be considered in the analysis. The *a priori* knowledge of the spin–spin coupling constants (theoretical predictions at the CCSD(T)/cc-pwCVQZ level, for the exact definition of the D_1 and D_3 constants, see Ref. [417]) turned out to be essential for the analysis of the spectra which provide the first set of dipolar spin–spin couplings for PH_3. The corresponding experimental values (2.03(41) kHz for D_{zz}(P-H) and 16.9(13) kHz for D_{zz}(H-H)) are in good agreement with the computational results (vibrationally corrected data: 2.13 kHz and 16.90 kHz, respectively).

Table 29 documents how analysis of experimental dipolar coupling constants can provide geometrical information and in some cases even the equilibrium geometry [436].

The case shown is ammonia, NH_3, for which the experimental couplings have been given in Ref. [444]. These values can be corrected for vibrational effects, determined quantum-chemical calculations [436], to obtain equilibrium values for the dipolar coupling constants that can be then inverted by using Equation (40) in order to get the corresponding bond distances. The corresponding distances are given in Table 29 and compared with those derived from rotational constants, and satisfactory agreement is noted. Though the accuracy of the determined parameters is somewhat lower than that of the parameters determined in the traditional way via the rotational constants, we consider the determination of structures via dipolar coupling constants a viable alternative. The main advantages are first that the issues associated with isotopic species are avoided and second that the analysis of dipolar couplings allows the determination of partial structures. The use of computed vibrational corrections further enables the determination of empirical r_e geometries similar to the case of rotational constants. The only drawback is that dipolar couplings often have not been determined or are only known with limited accuracy. In this way, it will be certain that the traditional way based on rotational constants will remain the standard choice for accurate structure determination and that the use of dipolar couplings will remain the exception and only be applied in special cases.

6. Summary

An overview of state-of-the-art quantum-chemical techniques for evaluation of the parameters needed in the area of rotational spectroscopy has been given. A lengthy discussion of the theoretical background of the advocated quantum-chemical schemes has been supplemented by examples which on one hand document the accuracy which can be achieved in quantum-chemical computations of these parameters and on the other hand describe the interplay of theory and experiment in the field of rotational spectroscopy. It is the belief of the authors that this interplay represents a powerful synergism in chemical and physical research and significantly enhances the available possibilities. It is hoped that the examples given here convince the reader to take part in this interplay and to exploit the many possibilities that quantum-chemical calculations offer in the area of rotational spectroscopy. In this way, the review is intended to bridge the gap between two quite different scientific communities, namely quantum chemistry (theory) and rotational spectroscopy (experiment) and to serve the purpose of enriching interactions between the two fields.

Acknowledgements

The authors acknowledge fruitful collaborations as well as discussions with the following colleagues: A.A. Auer (Düsseldorf, Germany), A. Baldacci (Venezia, Italy), O. Baum (Köln, Germany), C. Berger (Mainz, Germany), M. Behnke (Köln, Germany), G. Cazzoli (Bologna, Italy), S. Coriani (Trieste, Italy), T.F. Giesen (Köln, Germany), J. Hahn (Köln, Germany), A. Halkier (Århus, Denmark), M.E. Harding (Mainz, Germany, and Austin, USA), M. Heckert (Mainz, Germany), T. Helgaker (Oslo, Norway), P. Jørgensen (Århus, Denmark), M. Kállay (Budapest, Hungary), W. Klopper (Karlsruhe, Germany), M. Koerber (Köln, Germany), M. McCarthy (Harvard, USA), T. Metzroth (Mainz, Germany), H.S.P. Müller (Köln, Germany), J. Olsen (Århus, Denmark), A. Rizzo (Pisa, Italy), K. Ruud (Tromsø, Norway), S. Schlemmer (Köln, Germany), S. Stopkowicz

(Mainz, Germany), D. Sundholm (Helsinki, Finland), P.G. Szalay (Budapest, Hungary), F. Temps (Kiel, Germany), S. Thorwirth (Köln, Germany), J. Vázquez (Austin, USA), G. Winnewisser (Köln, Germany). This work has been supported in Bologna by RFO funds (University of Bologna), in Austin by the United States National Science Foundation (Grant CHE0710146), the US Department of Energy, Basic Energy Sciences (Contract FG02-07ER15884), and the Robert A. Welch Foundation (Grant F-1283), as well as in Mainz by the Deutsche Forschungsgemeinschaft (DFG GA 370/5-1) and the Fonds der Chemischen Industrie.

Notes

1. Note that we use here and in the following atomic units, i.e., $\hbar = 1$, $m_e = 1$, $e = 1$, and $1/4\pi\epsilon_0 = 1$.
2. Rotational constants are here given in atomic units (see note 1). The conversion factors to the commonly used units in rotational spectroscopy are: 219474.7 in the case of cm^{-1} and 6.579874×10^9 in the case of MHz.
3. The following expressions are valid if the rotational and, later on in the text, centrifugal distortion constants are given in energy units. If they are in frequency units, an additional factor of $1/h$ is required and Equation (11) reads $E_{J,K}/h = BJ(J+1) + (A-B)K^2$.
4. Note that this function D, which is usually labeled as C in spectroscopy textbooks [1,2], has been so designated in order to avoid any confusion with the spin–rotation constants discussed here, as well.
5. In the present review, a sign convention for spin–rotation constants opposite to that originally used by Flygare [52] has been adopted; i.e., the convention that leads to negative spin–rotation constants for hydrogen has been adopted.
6. In the working wavelength region of rotational spectroscopy, the methods of generation and detection of the radiation render it more convenient to use frequency instead of wavenumber for the characterization.
7. In the perturbation treatment, the operator $\hat{U}$ has historically been ignored, apart from the leading term, which gives a constant contribution of $-\frac{1}{4}\sum_\alpha B_e^\alpha$ to the zero-point energy of polyatomic molecules. This is justified empirically, as the effects of $\hat{U}$ result in contributions to energy level splittings that are barely detectable spectroscopically.
8. Note that α as a regular symbol stands for the vibration–rotation interaction constant, while the α used as a superscript refers to inertial axes a, b or c.
9. In the present section, to simplify notations and to be consistent with what is the standard in quantum chemistry, no hats are used to denote operators.
10. Note that the FCI results have been recalculated with orbital-relaxation effects included.
11. It should be noted that such predictions are equally useful in the field of solid-state nuclear-magnetic resonance spectroscopy. For an example, see Ref. [388].

References

[1] W. Gordy and R. L. Cook, in *Microwave Molecular Spectra* , 3rd ed, edited by A. Weissberger (John Wiley, New York, 1984).
[2] H. W. Kroto, *Molecular Rotation Spectra* (John Wiley, London, 1975).
[3] C. H. Townes and A. L. Schawlov, *Microwave Spectroscopy* (McGraw-Hill, New York, 1955).
[4] G. Winnewisser, F. Lewen, S. Thorwirth, M. Behnke, J. Hahn, J. Gauss, and E. Herbst, Chem. Eur. J. **9**, 5501 (2003).
[5] L. Sari, M. C. McCarthy, H. F. Schaefer III, and P. Thaddeus, J. Am. Chem. Soc. **125**, 11409 (2003).
[6] A. J. Apponi, M. C. McCarthy, C. A. Gottlieb, and P. Thaddeus, J. Chem. Phys. **111**, 3911 (1999).
[7] M. C. McCarthy, A. J. Apponi, and P. Thaddeus, J. Chem. Phys. **111**, 7175 (1999).

[8] M. C. McCarthy, S. Thorwirth, C. A. Gottlieb, and P. Thaddeus, J. Am. Chem. Soc. **126**, 4096 (2004).
[9] M. J. Travers, M. C. McCarthy, C. A. Gottlieb, and P. Thaddeus, Astrophys. J. **483**, L135 (1997).
[10] S. Thorwirth, J. Gauss, M. C. McCarthy, F. Shindo, and P. Thaddeus, Chem. Comm. **5292** (2008).
[11] L. Bizzocchi, C. Degli Esposti, and P. Botschwina, J. Chem. Phys. **119**, 170 (2003).
[12] M. C. McCarthy, A. J. Apponi, V. D. Gordon, C. A. Gottlieb, P. Thaddeus, T. D. Crawford, and J. F. Stanton, J. Chem. Phys. **111**, 6750 (1999).
[13] K. Suma, Y. Sumiyoshi, and Y. Endo, Science **308**, 1885 (2005).
[14] K. Suma, Y. Sumiyoshi, and Y. Endo, J. Am. Chem. Soc. **127**, 14998 (2005).
[15] M. Koerber, O. Baum, J. Hahn, T. F. Giesen, S. Schlemmer, and J. Gauss, Inorg. Chem. **48**, 2269 (2009).
[16] A. Domenicano and I. Hargittai, editors, *Accurate Molecular Structures: Their Determination and Importance* (Oxford University Press, Oxford, 1992).
[17] C. C. Costain, Can. J. Phys. **47**, 2431 (1969).
[18] R. S. Winton and W. Gordy, Phys. Lett. A **32**, 219 (1970).
[19] W. H. Flygare, Chem. Rev. **74**, 653 (1974).
[20] A. G. G. M Tielens, *The Physics and Chemistry of the Interstellar Medium* (Cambridge University Press, Cambridge, 2005).
[21] G. Winnewisser, E. Herbst, and H. Ungerechts, in *Spectroscopy of the Earth's Atmosphere and Interstellar Medium*, edited by K. N. Rao and A. Weber (Academic Press, San Diego, 1992).
[22] J. Tennyson, *Astronomical Spectroscopy* (Imperial College Press, London, 2005).
[23] E. Herbst, Chem. Soc. Rev. **30**, 168 (2001).
[24] See, for example, http://en.wikipedia.org/wiki/List_of_molecules_in_interstellar_space
[25] P. Thaddeus, J. M. Vrtilek, and C. A. Gottlieb, Astrophys. J. **299**, L63 (1985).
[26] D. Fossé, J. Cernicharo, M. Gerin, and P. Cox, Astrophys. J. **552**, 168 (2001).
[27] R. J. McMahon, M. C. McCarthy, C. A. Gottlieb, J. B. Dudek, J. F. Stanton, and P. Thaddeus, Astrophys. J. **590**, L61 (2003).
[28] S. Brünken, M. C. McCarthy, P. Thaddeus, P. D. Godfrey, and R. D. Brown, Astron. & Astrophys. **459**, 317 (2006).
[29] M. C. McCarthy, C. A. Gottlieb, H. Gupta, and P. Thaddeus, Astrophys. J. **652**, L141 (2006).
[30] S. Brünken, H. Gupta, C. A. Gottlieb, M. C. McCarthy, and P. Thaddeus, Astrophys. J. **664**, L43 (2007).
[31] G. Cazzoli, C. Puzzarini, A. Gambi, and J. Gauss, J. Chem. Phys. **125**, 054313 (2006).
[32] F. Pawłowski, P. Jørgensen, J. Olsen, F. Hegelund, T. Helgaker, J. Gauss, K. L. Bak, and J. F. Stanton, J. Chem. Phys. **116**, 6482 (2002).
[33] H. M. Pickett, J. Mol. Spectrosc. **148**, 371 (1991).
[34] P. Jensen and P. R. Bunker, editors, *Computational Molecular Spectroscopy* (John Wiley, Chichester, 2000), Part 3.
[35] S. N. Yurchenko, W. Thiel, and P. Jensen, J. Mol. Spectrosc. **245**, 126 (2007).
[36] I. A. Mills, in *Modern Spectroscopy: Modern Research*, edited by K. N. Rao and C. W. Matthews (Academic, New York, 1972), p. 115.
[37] W. Schneider and W. Thiel, Chem. Phys. Lett. **157**, 367 (1989).
[38] J. F. Stanton and J. Gauss, Int. Rev. Phys. Chem. **19**, 61 (2000).
[39] P. R. Bunker and P. Jensen, *Molecular Symmetry and Spectroscopy* (NRC Reserach Press, Ottawa, 1998), p. 211.
[40] J. K. G. Watson, in *Vibrational Spectra and Structure*, edited by J. During (Elsevier, Amsterdam, 1997), Vol. 6, p. 1.
[41] J. K. G. Watson, J. Chem. Phys. **46**, 1935 (1967).
[42] J. K. G. Watson, J. Chem. Phys. **48**, 181 (1968).

[43] J. K. G. Watson, J. Chem. Phys. **48**, 4517 (1968).
[44] E. J. Campbell, L. W. Buxton, T. J. Balle, and W. H. Flygare, J. Chem. Phys. **74**, 813 (1981).
[45] D. Papousek and M. R. Aliev, *Molecular Vibrational-Rotational Spectra* (Elsevier, New York, 1982).
[46] I. Ozier, Phys. Rev. Lett. **27**, 1329 (1971).
[47] R. F. Curl, T. Oka, and D. S. Smith, J. Mol. Spectrosc. **46**, 518 (1973).
[48] E. H. Wishnow, G. S. Orton, I. Ozier, and H. P. Gush, J. Quant. Spectrosc. & Rad. Transfer **103**, 102 (2007).
[49] F. Y. Chu and T. Oka, J. Chem. Phys. **60**, 4612 (1974).
[50] C. Styger, I. Ozier, S.-X. Wang, and A. Bauder, J. Mol. Spectrosc. **239**, 115 (2006).
[51] E. A. C. Lucken, *Nuclear Quadrupole Coupling Constants* (Academic Press, London, 1969).
[52] W. H. Flygare, J. Chem. Phys. **41**, 793 (1964).
[53] A. Abragam, *Principles of Nuclear Magnetism* (Oxford University Press, New York, 1961), p. 97.
[54] K. Schmidt-Rohr and H. W. Spiess, *Multidimensional Solid State NMR and Polymers* (Academic Press, New York, 1994), p. 19.
[55] D. L. Bryce and R. E. Wasylishen, Acc. Chem. Res. **36**, 327 (2003).
[56] M. R. Aliev and J. K. G. Watson, J. Mol. Spectrosc. **61**, 29 (1976).
[57] M. Pernpointner, M. Seth, and P. Schwerdtfeger, J. Chem. Phys. **108**, 6722 (1998).
[58] J. Gauss, K. Ruud, and T. Helgaker, J. Chem. Phys. **105**, 2804 (1996).
[59] J. M. Hollas, *High Resolution Spectroscopy* (John Wiley, Chichester, 1998).
[60] T. J. Balle and W. H. Flygare, Rev. Sci. Instrum. **52**, 33 (1981).
[61] J. S. Muenter, in *Structure and Dynamics of weakly bound complexes*, edited by A. Weber (Reidel, Dordrecht, 1987), p. 3.
[62] W. Demtröder, in *Laser Spectroscopy. Basis Concepts and Instrumentation*, Springer Series in Chemical Physics 5, edited by F. P. Schäfer (Springer-Verlag, Heidelberg, 1982).
[63] M. W. P. Strandberg, *Microwave Spectroscopy* (Methuen, London, 1954).
[64] J. K. G. Watson, Mol. Phys. **15**, 479 (1968).
[65] J. K. G. Watson, Mol. Phys. **19**, 465 (1970).
[66] H. Meyer, Ann. Rev. **53**, 141 (2002).
[67] J. H. Van Vleck, Phys. Rev. **33**, 467 (1933).
[68] E. C. Kemble, *Fundamental Principles of Quantum Mechanics* (Dover, New York, 1958), p. 391.
[69] H. H. Nielsen, Rev. Mod. Phys. **23**, 90 (1951).
[70] J. Vázquez and J.F. Stanton, to be published.
[71] E. B. Wilson, J. C. Decius, and P. C. Cross, *Molecular Vibrations* (Dover, New York, 1980), pp. 289–291.
[72] A. L. L. East, C. S. Johnson, and W. D. Allen, J. Chem. Phys. **98**, 1299 (1993).
[73] P. Barletta, S. V. Shirin, N. F. Zobov, O. L. Polyansky, J. Tennyson, E. F. Valeev, and A. G. Császár, J. Chem. Phys. **125**, 204307 (2006).
[74] G. Wlodarczak, R. Bocquet, A. Bauer, and J. Demaison, J. Mol. Spectrosc. **129**, 371 (1988).
[75] J. Tang and S. Saito, J. Mol. Spectrosc. **169**, 92 (1995).
[76] C. Degli Esposti, L. Bizzocchi, P. Botschwina, K. M. T. Yamada, G. Winnewisser, S. Thorwirth, and P. Förster, J. Mol. Spectrosc. **230**, 185 (2005).
[77] T. Amano, T. Hirao, and J. Takano, J. Mol. Spectrosc. **234**, 170 (2005).
[78] L. Bizzocchi and C. Degli Esposti, J. Mol. Spectrosc. **241**, 67 (2007).
[79] C. W. Kern and R. L. Matcha, J. Chem. Phys. **49**, 2081 (1968).
[80] A. A. Auer, J. Gauss, and J. F. Stanton, J. Chem. Phys. **118**, 10407 (2003).
[81] K. Ruud, in *Calculation of NMR and EPR Parameters: Theory and Application*, edited by M. Kaupp, M. Bühl, and V. G. Malkin (John Wiley, Weinheim, 2004), Chap. 10.
[82] K. Ruud, P.-O. Åstrand, and P. R. Taylor, J. Chem. Phys. **112**, 2668 (2000).
[83] P.-O. Åstrand, K. Ruud, and P. R. Taylor, J. Chem. Phys. **112**, 2655 (2000).

[84] C. E. Dykstra and D. J. Malik, J. Chem. Phys. **87**, 2806 (1987).
[85] D. Sundholm, J. Gauss, and A. Schäfer, J. Chem. Phys. **105**, 11051 (1996).
[86] M. E. Harding, J. Vázquez, J. F. Stanton, G. Diezemann, and J. Gauss, J. Chem. Phys., to be submitted.
[87] M. Born and R. J. Oppenheimer, Ann. Phys. **84**, 457 (1927).
[88] R. D. Levine and R. B. Bernstein, *Molecular Reaction Dynamics and Chemical Reactivity* (Oxford University Press, New York, 1987).
[89] M. Klessinger and J. Michl, *Excited States and Photochemistry of Organic Molecules* (VCH, New York, 1995).
[90] A. Szabo and N. S. Ostlund, *Modern Quantum Chemistry* (McGraw-Hill, New York, 1989).
[91] I. N. Levine, *Quantum Chemistry* (Prentice Hall, Englewoods Cliffs, 1999).
[92] T. Helgaker, P. Jørgensen, and J. Olsen, *Molecular Electronic Structure Theory* (John Wiley, Chichester, 2000).
[93] F. Jensen, *Introduction to Computational Chemistry* (John Wiley, Chichester, 1999).
[94] C. J. Cramer, *Essentials of Computational Chemistry* (John Wiley, Chichester, 2001).
[95] T. Helgaker and P. R. Taylor, in *Modern Electronic Structure Theory*, edited by D.R. Yarkony (World Scientific, Singapore, 1995), p. 725.
[96] C. C. J. Roothaan, Rev. Mod. Phys. **23**, 69 (1951).
[97] P. Hohenberg and W. Kohn, Phys. Rev. **136**, B864 (1964).
[98] W. J. Kohn and L. Sham, Phys. Rev. **140**, A1133 (1965).
[99] R. G. Parr and W. Yang, *Density-Functional Theory of Atoms and Molecules* (Oxford University Press, New York, 1989).
[100] W. Koch and M. C. Holthausen, *A Chemist's Guide to Density-Functional Theory* (Wiley-VCH, Weinheim, 2000).
[101] C. Ochsenfeld, J. Kussmann, and D. S. Lambrecht, Rev. Comp. Chem. **23**, 1 (2007).
[102] R. J. Bartlett, Ann. Rev. Phys. Chem. **32**, 359 (1981).
[103] D. Cremer, in *Encyclopedia of Computational Chemistry*, edited by P. v. R. Schleyer, N. L. Allinger, T. Clark, J. Gasteiger, P. A. Kollman, H. F. Schaefer III, and P. R. Schreiner (John Wiley, Chichester, 1998), p. 1706.
[104] C. Møller and M. S. Plesset, Phys. Rev. **46**, 618 (1934).
[105] R. J. Bartlett, J. Phys. Chem. **93**, 1697 (1989).
[106] R. J. Bartlett and J. F. Stanton, Rev. Comp. Chem. **5**, 65 (1994).
[107] R. J. Bartlett, in *Modern Electronic Structure Theory*, edited by D. R. Yarkony (World Scientific, Singapore, 1995), p. 1047.
[108] J. Gauss, in *Encyclopedia of Computational Chemistry*, edited by P. v. R. Schleyer, N. L. Allinger, T. Clark, J. Gasteiger, P. A. Kollman, H. F. Schaefer III, and P. R. Schreiner (John Wiley, New York, 1998), p. 615.
[109] T. D. Crawford and H. F. Schaefer III, Rev. Comp. Chem. **14**, 33 (2000).
[110] R. J. Bartlett and M. Musiał, Rev. Mod. Phys. **79**, 291 (2007).
[111] C. A. White and M. Head-Gordon, J. Chem. Phys. **101**, 6593 (1994).
[112] C. Ochsenfeld, C. A. White, and M. Head-Gordon, J. Chem. Phys. **109**, 1663 (1998).
[113] B. O. Roos, Adv. Chem. Phys. **69**, 399 (1987).
[114] H. J. Werner, Adv. Chem. Phys. **69**, 1 (1987).
[115] P. G. Szalay, in *Encyclopedia of Computatonal Chemistry (online edition)*, edited by P. v. R. Schleyer, H. F. Schaefer III, P. R. Schreiner, W. L. Jorgensen, W. Thiel, and R. C. Glen (John Wiley, Chichester, 2005).
[116] J. A. Pople and R. K. Nesbet, J. Chem. Phys. **22**, 571 (1954).
[117] R. J. Bartlett and D. M. Silver, J. Chem. Phys. **62**, 3258 (1975).
[118] J. A. Pople, J. S. Binkley, and R. Seeger, Int. J. Quant. Chem. Symp. **10**, 1 (1976).
[119] R. Krishnan and J. A. Pople, Int. J. Quant. Chem. **14**, 91 (1978).
[120] R. Krishnan, M. J. Frisch, and J. A. Pople, J. Chem. Phys. **72**, 4244 (1980).

[121] J. Olsen, O. Christiansen, H. Koch, and P. Jørgensen, J. Chem. Phys. **105**, 5082 (1996).
[122] P. Saxe, H. F. Schaefer III, and N. C. Handy, Chem. Phys. Lett. **79**, 202 (1981).
[123] J. Čížek, J. Chem. Phys. **45**, 4256 (1966).
[124] J. Čížek, Adv. Chem. Phys. **14**, 35 (1966).
[125] J. Paldus and J. Čížek, Phys. Rev. A **5**, 50 (1972).
[126] J. F. Stanton, J. Gauss, J. D. Watts, and R. J. Bartlett, J. Chem. Phys. **94**, 4334 (1991).
[127] R. J. Bartlett and G. D. Purvis III, Int. J. Quantum Chem. **14**, 561 (1978).
[128] J. A. Pople, R. Krishnan, H. B. Schlegel, and J. S. Binkley, Int. J. Quantum Chem. **14**, 545 (1978).
[129] G. D. Purvis III and R. J. Bartlett, J. Chem. Phys. **76**, 1910 (1982).
[130] J. Noga and R. J. Bartlett, J. Chem. Phys. **86**, 1041 (1987).
[131] G. E. Scuseria and H. F. Schaefer III, Chem. Phys. Lett. **132**, 382 (1988).
[132] N. Oliphant and L. Adamowicz, J. Chem. Phys. **95**, 6645 (1991).
[133] S. A. Kucharski and R. J. Bartlett, J. Chem. Phys. **97**, 4282 (1992).
[134] M. Kállay and P. R. Surján, J. Chem. Phys. **115**, 2945 (2001).
[135] T. H. Dunning Jr, J. Phys. Chem. A **104**, 9062 (2000).
[136] Y. S. Lee, S. A. Kucharski, and R. J. Bartlett, J. Chem. Phys. **81**, 5906 (1984).
[137] J. Noga, R. J. Bartlett, and M. Urban, Chem. Phys. Lett. **134**, 126 (1987).
[138] H. Koch, O. Christiansen, P. Jørgensen, A. M. Sanchez de Meras, and T. Helgaker, J. Chem. Phys. **106**, 1808 (1997).
[139] S. A. Kucharski and R. J. Bartlett, Chem. Phys. Lett. **158**, 550 (1989).
[140] M. Urban, J. Noga, S. J. Cole, and R. J. Bartlett, J. Chem. Phys. **83**, 4041 (1985).
[141] K. Raghavachari, G. W. Trucks, J. A. Pople, and M. Head-Gordon, Chem. Phys. Lett. **157**, 479 (1989).
[142] R. J. Bartlett, J. D. Watts, S. A. Kucharski, and J. Noga, Chem. Phys. Lett. **165**, 513 (1990).
[143] S. A. Kucharski and R. J. Bartlett, Chem. Phys. Lett. **158**, 550 (1989).
[144] Y. Bomble, M. Kállay, J. Gauss, and J. F. Stanton, J. Chem. Phys. **123**, 054101 (2005).
[145] M. Kállay and J. Gauss, J. Chem. Phys. **123**, 214105 (2005).
[146] M. Kállay and J. Gauss, J. Chem. Phys. **129**, 144101 (2008).
[147] J. F. Stanton, Chem. Phys. Lett. **281**, 130 (1997).
[148] R. M. Olson, J. L. Bentz, R. A. Kendall, M. W. Schmidt, and M. S. Gordon, J. Chem. Theor. Comp. **3**, 1312 (2007).
[149] M. E. Harding, T. Metzroth, J. Gauss, and A. A. Auer, J. Chem. Theor. Comp. **4**, 64 (2008).
[150] T. Helgaker, P. Jørgensen, and J. Olsen, *Molecular Electronic Structure Theory* (John Wiley, Chichester, 2000), Chap. 6.
[151] J. A. Pople and W. J. Hehre, J. Comp. Phys. **27**, 161 (1978).
[152] M. Dupuis, J. Rys, and H. F. King, J. Chem. Phys. **65**, 111 (1976).
[153] L. E. McMurchie and E. R. Davidson, J. Comp. Phys. **26**, 218 (1978).
[154] S. Obara and A. Saika, J. Chem. Phys. **84**, 3963 (1986).
[155] W. J. Hehre, R. F. Stewart, and J. A. Pople, J. Chem. Phys. **51**, 2657 (1969).
[156] S. Huzinaga, J. Chem. Phys. **42**, 1283 (1965).
[157] T. H. Dunning Jr, J. Chem. Phys. **53**, 2823 (1970).
[158] T. H. Dunning Jr, J. Chem. Phys. **55**, 716 (1971).
[159] A. Schäfer, H. Horn, and R. Ahlrichs, J. Chem. Phys. **97**, 2571 (1992).
[160] A. Schäfer, C. Huber, and R. Ahlrichs, J. Chem. Phys. **100**, 5829 (1994).
[161] R. Ahlrichs and K. May, Phys. Chem. Chem. Phys. **2**, 943 (2000).
[162] F. Weigend, F. Furche, and R. Ahlrichs, J. Chem. Phys. **119**, 12753 (2003).
[163] C. M. Reeves, J. Chem. Phys. **39**, 1 (1963).
[164] C. M. Reeves, J. Chem. Phys. **39**, 11 (1963).
[165] See http://bse.pnl.gov/bse/portal.
[166] E. R. Davidson and D. Feller, Chem. Rev. **86**, 681 (1986).

[167] J. Almlöf and P. R. Taylor, Adv. Quantum Chem. **22**, 301 (1992).
[168] T. H. Dunning Jr, K. A. Peterson, and D. E. Woon, in *Encyclopedia of Computational Chemistry*, edited by P. v. R. Schleyer, N.L. Allinger, T. Clark, J. Gasteiger, P. A. Kollman, H. F. Schaefer III, and P. R. Schreiner (John Wiley, Chichester, 1998), p. 88.
[169] T. Helgaker, W. Klopper, H. Koch, and J. Noga, J. Chem. Phys. **106**, 9639 (1997).
[170] A. Halkier, P. Jørgensen, W. Klopper, H. Koch, J. Olsen, and A. K. Wilson, Chem. Phys. Lett. **286**, 243 (1998).
[171] T. H. Dunning Jr, J. Chem. Phys. **90**, 1007 (1989).
[172] A. K. Wilson, T. van Mourik, and T. H. Dunning Jr, J. Mol. Struct. (THEOCHEM) **388**, 339 (1998).
[173] D. E. Woon and T. H. Dunning Jr, J. Chem. Phys. **98**, 1358 (1993).
[174] T. van Mourik and T. H. Dunning Jr, Int. J. Quantum Chem. **76**, 205 (2000).
[175] A. K. Wilson, D. E. Woon, K. A. Peterson, and T. H. Dunning Jr, J. Chem. Phys. **110**, 76677 (1999).
[176] N. B. Balabanov and K. A. Peterson, J. Chem. Phys. **123**, 064107 (2005).
[177] D. E. Woon and T. H. Dunning Jr, J. Chem. Phys. **103**, 4572 (1995).
[178] K. A. Peterson and T. H. Dunning Jr, J. Chem. Phys. **117**, 10548 (2002).
[179] N. J. DeYonker, K. A. Peterson, and A. Wilson, J. Phys. Chem. **A 111**, 11383 (2007).
[180] R. A. Kendall, T. H. Dunning Jr, and R. J. Harrison, J. Chem. Phys. **96**, 6796 (1992).
[181] D. E. Woon and T. H. Dunning Jr, J. Chem. Phys. **100**, 2975 (1994).
[182] T. van Mourik, Mol. Phys. **96**, 529 (1999).
[183] D. Feller, J. Chem. Phys. **98**, 7059 (1993).
[184] A G. Császár, W. D. Allen, and H. F. Schaefer III, J. Chem. Phys. **108**, 9751 (1998).
[185] A. D. Boese, M. Oren, O. Atasoylu, J. M. L. Martin, M. Kállay, and J. Gauss, J. Chem. Phys. **120**, 4129 (2004).
[186] A. Tajti, P. G. Szalay, A. G. Császár, M. Kállay, J. Gauss, E. F. Valeev, B. A. Flowers, J. Vázquez, and J. F. Stanton, J. Chem. Phys. **121**, 11599 (2004).
[187] D. Feller and K. A. Peterson, J. Chem. Phys. **126**, 114105 (2007).
[188] Y. J. Bomble, J. Vázquez, M. Kállay, C. Michauk, P. G. Szalay, A. G. Császár, J. Gauss, and J. F. Stanton, J. Chem. Phys. **125**, 064108 (2006).
[189] M. E. Harding, J. Vázquez, B. Ruscic, A. K. Wilson, J. Gauss, and J. F. Stanton, J. Chem. Phys. **128**, 114111 (2008).
[190] M. Heckert, M. Kállay, D. P. Tew, W. Klopper, and J. Gauss, J. Chem. Phys. **125**, 0044108 (2006).
[191] C. Puzzarini, M. Heckert, and J. Gauss, J. Chem. Phys **128**, 194108 (2008).
[192] M. Heckert, M. Kállay, and J. Gauss, Mol. Phys. **103**, 2109 (2005).
[193] R. Krishnan, J. S. Binkley, R. Seeger, and J. A. Pople, J. Chem. Phys. **72**, 650 (1980).
[194] A. J. Sadlej, Collec. Czech. Chem. Commun. **53**, 1995 (1998).
[195] J. Almlöf and P. R. Taylor, J. Chem. Phys. **86**, 4070 (1987).
[196] J. Almlöf and P. R. Taylor, J. Chem. Phys. **92**, 551 (1990).
[197] P.-O. Widmark, P. Å. Malmqvist, and B. O. Roos, Theor, Chem. Acc. **77**, 291 (1990).
[198] P.-O. Widmark, B. J. Persson, and B. O. Roos, Theor. Chem. Acc. **79**, 419 (1991).
[199] K. Pierloot, B. Dumez, P.-O. Widmark, and B. O. Roos, Theor. Chem. Acc. **90**, 87 (1991).
[200] W. Klopper, F. R. Manby, S. Ten-No, and E. F. Valeev, Int. Rev. Phys. Chem. **25**, 427 (2006).
[201] J. Noga, S. Kedžuch, J. Šimunek, and S. Ten-no, J. Chem. Phys. **128**, 174103 (2008).
[202] T. B. Adler, G. Knizia, and H.-J. Werner, J. Chem. Phys. **127**, 221106 (2008).
[203] D. P. Tew, W. Klopper, C. Neiss, and C. Hättig, Phys. Chem. Chem. Phys. **9**, 1921 (2007).
[204] A. Köhn, G. W. Richings, and D. P. Tew, J. Chem. Phys. **129**, 201103 (2008).
[205] J. Gauss, in *Modern Methods and Algorithms of Quantum Chemistry*, edited by J. Grotendorst (John von Neumann Institute for Computing, Jülich, 2000), p. 509.

[206] H. B. Schlegel, in *Encyclopedia of Computational Chemistry*, edited by P. v. R. Schleyer, N. L. Allinger, T. Clark, J. Gasteiger, P. A. Kollman, H. F. Schaefer III, and P. R. Schreiner (John Wiley, New York, 1998), p. 1136.
[207] P. E. Gill, W. Murray, and M. H. Wright, *Practical Optimization* (Academic Press, London, 1981), Chap. 4.
[208] P. Pulay, Mol. Phys. **17**, 197 (1969).
[209] M. Kállay and J. Gauss, J. Mol. Struct. (THEOCHEM) **768**, 71 (2006).
[210] T. Helgaker and P. R. Taylor, Theor. Chim. Acta **83**, 177 (1992).
[211] S. Reine, E. Tellgren, and T. Helgaker, Phys. Chem. Chem. Phys. **9**, 4771 (2007).
[212] T. Helgaker and P. Jørgensen, Theor. Chim. Acta **75**, 111 (1989).
[213] T. Helgaker, P. Jørgensen, and N. C. Handy, Theor. Chim, Acta **76**, 227 (1989).
[214] T. Helgaker and P. Jørgensen, in *Methods in Computational Molecular Physics*, edited by S. Wilson and G. H. F. Diercksen (Plenum Press, New York, 1992).
[215] N. C. Handy and H. F. Schaefer III, J. Chem. Phys. **51**, 5031 (1984).
[216] A. Dalgarno and A. L. Stewart, Proc. Roy. Soc. A **247**, 245 (1958).
[217] P. Pulay, J. Chem. Phys. **78**, 5043 (1983).
[218] P. Jørgensen and T. Helgaker, J. Chem. Phys. **89**, 1560 (1988).
[219] J. A. Pople, R. Krishnan, H. B. Schlegel, and J. S. Binkley, Int. J. Quant. Chem. Symp. **13**, 225 (1979).
[220] J. Gerratt and I. M. Mills, J. Chem. Phys. **49**, 1719 (1968).
[221] H. Koch, H. J. Aa. Jensen, P. Jørgensen, T. Helgaker, G. E. Scuseria, and H. F. Schaefer III, J. Chem. Phys **92**, 4924 (1990).
[222] P. G. Szalay, Int. J. Quantum Chem. **55**, 151 (1993).
[223] J. Arponen, Ann. Phys. **151**, 311 (1983).
[224] L. Adamowicz, W. D. Laidig, and R. J. Bartlett, Int. J. Quantum Chem. Symp. **18**, 245 (1984).
[225] J. F. Stanton and J. Gauss, in *Modern Ideas in Coupled-Cluster Methods*, edited by R. J. Bartlett (World Scientific, Singapore, 1997), p. 49.
[226] J. Gauss and J. F. Stanton, J. Chem. Phys. **10**, 2574 (1996).
[227] E. A. Salter, H. Sekino, and R. J. Bartlett, J. Chem. Phys. **87**, 502 (1987).
[228] O. Christiansen, C. Hättig, and J. Gauss, J. Chem. Phys. **109**, 4745 (1998).
[229] O. Christiansen, C. Hättig, and P. Jørgensen, Int. J. Quantum Chem. **68**, 1 (1998).
[230] J. Gauss, J. F. Stanton, and R. J. Bartlett, J. Chem. Phys. **95**, 2623 (1991).
[231] J. Gauss and J. F. Stanton, Chem. Phys. Lett. **276**, 70 (1997).
[232] R. Krishnan, H. B. Schlegel, and J. A. Pople, J. Chem. Phys. **72**, 4654 (1980).
[233] B. R. Brooks, W. D. Laidig, P. Saxe, J. D. Goddard, Y. Yamaguchi, and H. F. Schaefer III, J. Chem. Phys. **72**, 4652 (1980).
[234] S. Kato and K. Morokuma, Chem. Phys. Lett. **65**, 19 (1979).
[235] J. D. Goddard, N. C. Handy, and H. F. Schaefer III, J. Chem. Phys. **71**, 1525 (1978).
[236] A. C. Scheiner, G. E. Scuseria, J. E. Rice, T. J. Lee, and H. F. Schaefer III, J. Chem. Phys. **87**, 5361 (1987).
[237] J. Gauss, J. F. Stanton, and R. J. Bartlett, J. Chem. Phys. **95**, 2639 (1991).
[238] J. Gauss, W. J. Lauderdale, J. F. Stanton, J. D. Watts, and R. J. Bartlett, Chem. Phys. Lett. **182**, 207 (1991).
[239] E. A. Salter, G. W. Trucks, and R. J. Bartlett, J. Chem. Phys. **90**, 1752 (1989).
[240] G. E. Scuseria and H. F. Schaefer III, Chem. Phys. Lett. **146**, 23 (1988).
[241] J. Gauss and J. F. Stanton, Phys. Chem. Chem. Phys. **2**, 2047 (2000).
[242] J. Gauss and J. F. Stanton, J. Chem. Phys. **116**, 1773 (2002).
[243] M. Kállay, J. Gauss, and P. G. Szalay, J. Chem. Phys. **119**, 2991 (2004).
[244] J. Gauss and D. Cremer, Chem. Phys. Lett. **163**, 549 (1989).
[245] G. E. Scuseria, J. Chem. Phys. **94**, 442 (1991).
[246] T. J. Lee and A. P. Rendell, J. Chem. Phys. **94**, 6229 (1991).

[247] J. D. Watts, J. Gauss, and R. J. Bartlett, Chem. Phys. Lett. **200**, 1 (1992).
[248] J. D. Watts, J. Gauss, and R. J. Bartlett, J. Chem. Phys. **98**, 8718 (1993).
[249] Y. Yamaguchi, Y. Osamura, G. Fitzgerald, and H. F. Schaefer III, J. Chem. Phys. **78**, 1607 (1983).
[250] R. N. Camp, H. F. King, J. W. McIver Jr, and D. Mullally, J. Chem. Phys. **79**, 1089 (1983).
[251] N. C. Handy, R. D. Amos, J. F. Gaw, J. E. Rice, E. Simandiras, T. J. Lee, R. J. Harrison, W. D. Laidig, G. B. Fitzgerald, and R. J. Bartlett, in *Geometrical Derivatives of Energy Surfaces and Molecular Properties*, edited by P. Jørgensen and J. Simons (Reidel, Dordrecht, 1986), p. 179.
[252] N. C. Handy, R. D. Amos, J. F. Gaw, J. E. Rice, and E. D. Simandiras, Chem. Phys. Lett. **120**, 151 (1985).
[253] R. J. Harrison, G. B. Fitzgerald, W. D. Laidig, and R. J. Bartlett, Chem. Phys. Lett. **124**, 291 (1986).
[254] J. F. Stanton, J. Gauss, and R. J. Bartlett, Chem. Phys. Lett. **195**, 194 (1992).
[255] J. Gauss, J. F. Stanton, and R. J. Bartlett, J. Chem. Phys. **97**, 7825 (1992).
[256] P. G. Szalay, J. Gauss, and J. F. Stanton, Theor. Chim. Acta **100**, 5 (1998).
[257] J. Gauss, J. Chem. Phys. **116**, 4773 (2002).
[258] M. Kállay and J. Gauss, J. Chem. Phys. **120**, 6841 (2004).
[259] J. Gauss and J. F. Stanton, J. Chem. Phys. **102**, 251 (1995).
[260] J. Gauss and J. F. Stanton, J. Chem. Phys. **103**, 3561 (1995).
[261] R. Kobayashi, H. Koch, and P. Jørgensen, Chem. Phys. Lett. **219**, 30 (1994).
[262] O. Christiansen, J. Gauss, and J. F. Stanton, Chem. Phys. Lett. **292**, 437 (1998).
[263] M. Hanauer and A. Köhn, J. Chem. Phys. **131**, 124118 (2009).
[264] J. F. Gaw, Y. Yamaguchi, and H. F. Schaefer III, J. Chem. Phys. **83**, 1741 (1985).
[265] C. Hättig, O. Christiansen, and P. Jørgensen, Chem. Phys. Lett. **269**, 428 (1997).
[266] J. Gauss, O. Christiansen, and J. F. Stanton, Chem. Phys. Lett. **296**, 117 (1998).
[267] D. P. O'Neill, M. Kállay, and J. Gauss, J. Chem. Phys. **127**, 134109 (2007).
[268] D. P. O'Neill, M. Kállay, and J. Gauss, Mol. Phys. **105**, 2447 (2007).
[269] J. F. Stanton, C. L. Lopreore, and J. Gauss, J. Chem. Phys. **108**, 7190 (1998).
[270] Coupled-Cluster techniques for Computational Chemistry, a quantum chemical program package written by J. F. Stanton, J. Gauss, M. E. Harding, P. G. Szalay with contributions from A. A. Auer, R. J. Bartlett, U. Benedikt, C. Berger, D. E. Bernholdt, Y. J. Bomble, O. Christiansen, M. Heckert, O. Heun, C. Huber, T.-C. Jagau, D. Jonsson, J. Jusélius, K. Klein, W. J. Lauderdale, D. Matthews, T. Metzroth, D. P. O'Neill, D. R. Price, E. Prochnow, K. Ruud, F. Schiffmann, S. Stopkowicz, M. E. Varner, J. Vázquez, F. Wang, J. D. Watts and the integral packages MOLECULE (J. Almlöf, P.R. Taylor), PROPS (P. R. Taylor), ABACUS (T. Helgaker, H. J.Aa. Jensen, P. Jørgensen, J. Olsen), and ECP routines by A.V. Mitin and C. van Wüllen. For the current version, see http://www.cfour.de
[271] J. Gauss, K. Ruud, and M. Kállay, J. Chem. Phys. **127**, 074101 (2007).
[272] R. S. Ram, Z. Morbi, B. Guo, K. Q. Zhang, P. F. Bernath, J. van der Auwera, J. W. C. Johns, and S. P. Davis, Astrophys. J. Suppl. **103**, 247 (1996).
[273] J. Bendtsen and F. Rasmussen, J. Raman Spectrosc. **31**, 433 (2000).
[274] H. Bürger, G. Pawelke, A. Rahner, E. H. Appelman, and I. M. Mills, J. Mol. Spectrosc. **128**, 278 (1988).
[275] A. G. Császár, G. Czakó, T. Furtenbacher, J. Tennyson, V. Szalay, S. V. Shirin, N. F. Zobov, and O. L. Polyansky, J. Chem. Phys. **122**, 214305 (2005).
[276] S. Coriani, D. Marchesan, J. Gauss, C. Hättig, P. Jørgensen, and T. Helgaker, J. Chem. Phys. **123**, 184107 (2005).
[277] M. Quack and M. Willeke, Helv. Chim. Acta **86**, 1641 (2003).

[278] R. I. Ovsyannikov, V. V. Melnikov, W. Thiel, P. Jensen, O. Baum, T. F. Giesen, and S. N. Yurchenko, J. Chem. Phys. **129**, 154314 (2008).
[279] K. M. T. Yamada, P. Jensen, S. C. Ross, O. Baum, T. F. Giesen, and S. Schlemmer, J. Mol. Structure **927**, 96 (2009).
[280] S. N. Yurchenko, A. Yachmenev, W. Thiel, O. Baum, T. F. Giesen, V. V. Melnikov, and P. Jensen, J. Mol. Spectrosc. **257**, 57 (2009).
[281] M. Behnke, J. Suhr, S. Thorwirth, F. Lewen, H. Lichau, J. Hahn, J. Gauss, K. M. T. Yamada, and G. Winnewisser, J. Mol. Spectrosc. **221**, 121 (2003).
[282] S. Brünken, M. Behnke, S. Thorwirth, K. M. T. Yamada, T. F. Giesen, F. Lewen, J. Hahn, and G. Winnewisser, J. Mol. Struct. **742**, 237 (2005).
[283] O. Baum, S. Esser, N. Gierse, S. Brünken, F. Lewen, J. Hahn, J. Gauss, S. Schlemmer, and T. F. Giesen, J. Mol. Struct. **795**, 256 (2006).
[284] M. Koerber, O. Baum, U. Hahn, J. Gauss, T. F. Giesen, and S. Schlemmer, J. Mol. Spectrosc. **257**, 34 (2009).
[285] L. Bizzocchi, C. Degli Esposti, and P. Botschwina, J. Chem. Phys. **113**, 1465 (2000).
[286] L. Bizzocchi, C. Degli Esposti, and P. Botschwina, Chem. Phys. Lett. **319**, 411 (2000).
[287] A. Huckauf, A. Guarnieri, Ä. Heyl, P. Botschwina, C. Bartel, and D. Lentz, Chem. Phys. Lett. **303**, 607 (1999).
[288] P. Botschwina, Ä. Heyl, W. Chen, M. C. McCarthy, J.-U. Grabow, M. J. Travers, and P. Thaddeus, J. Chem. Phys. **109**, 3108 (1998).
[289] C. Puzzarini, G. Cazzoli, A. Baldacci, A. Baldan, C. Michauk, and J. Gauss, J. Chem. Phys. **127**, 164302 (2007).
[290] K. Kuchitsu, in *Accurate Molecular Structures*, edited by A. Domenicano and I. Hargittai (Oxford University Press, Oxford, 1992), p. 14.
[291] P. Pulay, W. Meyer, and J. E. Boggs, J. Chem. Phys. **68**, 5077 (1978).
[292] A. L. L. East, W. D. Allen, and S. J. Klippenstein, J. Chem. Phys. **102**, 8506 (1995).
[293] W. D. Allen, A. L. L. East, and A. G. Császár, in *Structures and Conformations of Nonrigid Molecules*, edited by J. Laane, M. Dakkouri, B. van der Vecken, and H. Oberhammer (Kluwer, Dordrecht, 1993), p. 343.
[294] M. C. McCarthy, C. A. Gottlieb, P. Thaddeus, M. Horn, and P. Botschwina, J. Chem. Phys. **103**, 7820 (1995).
[295] C. Bartel, P. Botschwina, H. Bürger, A. Guarnieri, Ä. Heyl, A. Huckauf, D. Lentz, T. Merzliak, and E. B. Mkdami, Angew. Chem. **110**, 3036 (1998).
[296] L. Bizzocchi, C. Degli Esposti, and P. Botschwina, J. Mol. Spectrosc. **225**, 145 (2004).
[297] P. Botschwina and C. Puzzarini, J. Mol. Spectrosc. **208**, 292 (2001).
[298] P. Botschwina, Phys. Chem. Chem. Phys. **5**, 3337 (2003).
[299] L. Margulés, F. Lewen, G. Winnewisser, P. Botschwina, and H. S. P. Müller, Phys. Chem. Chem. Phys. **5**, 2770 (2003).
[300] J. Gauss and J. F. Stanton, J. Mol. Struct. **485–486**, 43 (1999).
[301] J. Gauss and J. F. Stanton, J. Phys. Chem. A **104**, 1319 (2000).
[302] J. Gauss and J. F. Stanton, J. Phys. Chem. A **104**, 2865 (2000).
[303] J. F. Stanton, J. Gauss, and O. Christiansen, J. Chem. Phys. **114**, 2993 (2001).
[304] J. Gauss and J. F. Stanton, Int. J. Quant. Chem. **77**, 305 (2000).
[305] A. A. Auer and J. Gauss, Phys. Chem. Chem. Phys. **3**, 3001 (2001).
[306] R. W. Larsen, F. Pawłowski, F. Hegelund, P. Jørgensen, J. Gauss, and B. Nelander, Phys. Chem. Chem. Phys. **5**, 5031 (2003).
[307] P. G. Szalay, L. S. Thøgersen, J. Olsen, M. Kállay, and J. Gauss, J. Phys. Chem. A **108**, 3030 (2004).
[308] C. Puzzarini, G. Cazzoli, A. Gambi, and J. Gauss, J. Chem. Phys. **125**, 054307 (2006).
[309] S. Thorwirth, M. E. Harding, D. Muders, and J. Gauss, J. Mol. Spectrosc. **251**, 220 (2008).

[310] M. C. McCarthy, C. A. Gottlieb, P. Thaddeus, S. Thorwirth, and J. Gauss, J. Chem. Phys., submitted for publication (2010).
[311] C. Puzzarini, G. Cazzoli, and J. Gauss, J. Mol. Spectrosc. Submitted for publication 2010.
[312] J. F. Stanton, Mol. Phys. **97**, 841 (1999).
[313] R. J. McMahon, R. J. Halter, R. L. Fimmen, R. J. Wilson, S. A. Peebles, R. L. Kuczkowski, and J. F. Stanton, J. Am. Chem. Soc. **122**, 939 (2000).
[314] R. J. Halter, R. L. Fimmen, R. J. McMahon, S. A. Peebles, R. L. Kuczkowski, and J. F. Stanton, J. Am. Chem. Soc. **123**, 12353 (2001).
[315] J. Vázquez and J. F. Stanton, J. Phys. Chem. A **106**, 4429 (2002).
[316] A. J. Matzger, K. D. Lewis, C. E. Nathan, S. A. Peebles, R. A. Peebles, R. L. Kuczkowski, J. F. Stanton, and J. J. Oh, J. Phys. Chem. A **106**, 12110 (2002).
[317] S. Thorwirth, M. C. McCarthy, C. A. Gottlieb, P. Thaddeus, H. Gupta, and J. F. Stanton, J. Chem. Phys. **123**, 054326 (2005).
[318] C. Puzzarini and G. Cazzoli, J. Mol. Spectrosc. **240**, 260 (2006).
[319] C. Puzzarini, J. Mol. Spectrosc. **242**, 70 (2007).
[320] G. Cazzoli, L. Cludi, M. Contento, and C. Puzzarini, J. Mol. Spectrosc. **251**, 229 (2008).
[321] C. Puzzarini and G. Cazzoli, J. Mol. Spectrosc. **256**, 53 (2009).
[322] J. Demaison, Mol. Phys. **105**, 3109 (2007).
[323] J. Demaison, J. Lievin, A. G. Csaszar, and C. Gutle, J. Phys. Chem. **112**, 4477 (2008).
[324] J. Demaison and H. D. Rudolph, J. Mol. Spectrosc. **248**, 66 (2008).
[325] J. Demaison, J. Mol. Spectrosc. **239**, 201 (2006).
[326] J. Demaison, H. Sormova, H. Bürger, L. Margules, F. L. Constantin, and A. Ceausu-Velcescu, J. Mol. Spectrosc. **232**, 323 (2005).
[327] J. Demaison, H. Møllendal, A. Perrin, J. Orphal, F. K. Tchana, H. D. Rudolph, and F. Willaert, J. Mol. Spectrosc. **232**, 174 (2005).
[328] J. Breidung, J. Cosleou, J. Demaison, K. Sarka, and W. Thiel, Mol. Phys. **102**, 1827 (2004).
[329] J. Demaison, J. E. Boggs, and H. D. Rudolph, J. Mol. Struct. **695**, 145 (2004).
[330] N. C. Craig, P. Groner, D. C. McKean, and M. J. Tubergen, Int. J. Quantum Chem. **95**, 837 (2003).
[331] N. C. Craig, R. A. Appleman, H. E. Barnes, E. Morales, J. A. Smith, S. Klee, M. Lock, and G. C. Mellau, J. Phys. Chem. A **102**, 6745 (1998).
[332] N. C. Craig, P. Groner, and D. C. McKean, J. Phys. Chem. A **110**, 7461 (2006).
[333] N. C. Craig, D. Feller, P. Groner, H. Y. Hsin, D. C. McKean, and D. J. Nemchick, J. Phys. Chem. A **111**, 2498 (2007).
[334] P. Groner and R. D. Warren, J. Mol. Struct. **599**, 323 (2001).
[335] P. Groner and S. G. Kukolich, J. Mol. Struct. **780–781**, 178 (2006).
[336] J. L. Alonso, A. G. Lesarri, L. A. Leal, and J. C. Lopez, J. Mol. Spectrosc. **162**, 4 (1993).
[337] C. Puzzarini, G. Cazzoli, L. Dore, and A. Gambi, Phys. Chem. Chem. Phys. **3**, 4189 (2001).
[338] G. Cazzoli, C. Puzzarini, and A. Gambi, J. Chem. Phys. **120**, 6495 (2004).
[339] H. Takeo, M. Sugie, and C. Matsumura, J. Mol. Struct. **190**, 205 (1988).
[340] K. P. Huber and G. H. Herzberg, *Constants of Diatomic Molecules* (Van Nostrand Reinhold, New York, 1979).
[341] M. Bogey, C. Demuynck, and J. L. Destombes, Mol. Phys. **66**, 955 (1989).
[342] K. A. Peterson and T. H. Dunning Jr, J. Chem. Phys. **106**, 4119 (1997).
[343] L. Dore, L. Cludi, A. Mazzavillani, G. Cazzoli, and C. Puzzarini, Phys. Chem. Chem. Phys. **9**, 2275 (1999).
[344] T. Hirano, R. Okuda, U. Nagashima, V. Špirko, and P. Jensen, J. Mol. Spectrosc. **236**, 234 (2006).
[345] T. Hirano, R. Okuda, U. Nagashima, and P. Jensen, J. Mol. Spectrosc. **250**, 33 (2008).
[346] G. Cazzoli and C. Puzzarini, J. Mol. Spectrosc. **253**, 106 (2009).
[347] L. Bizzochi, C. Degli Esposti, and P. Botschwina, J. Mol. Struct. **780–781**, 148 (2006).

[348] K. M. T. Yamada, C. Degli Esposti, P. Botschwina, P. Förster, L. Bizzochi, S. Thorwirth, and G. Winnewisser, Astron. & Astrophys. **425**, 767 (2004).
[349] L. Bizzochi, C. Degli Esposti, and P. Botschwina, Phys. Chem. Chem. Phys. **6**, 46 (2004).
[350] L. Bizzochi, C. Degli Esposti, and P. Botschwina, Phys. Chem. Chem. Phys. **5**, 4090 (2003).
[351] Z. Zelinger, T. Amano, B. Ahrens, S. Brünken, F. Lewen, H. S. P. Müller, and G. Winnewisser, J. Mol. Spectrosc. **220**, 223 (2003).
[352] Z. Kisiel, L. Pszczolkowski, G. Cazzoli, and G. Cotti, J. Mol. Spectrosc. **173**, 477 (1995).
[353] M. Jackson, L. R. Zink, M. C. McCarthy, L. Perez, and J. M. Brown, J. Mol. Spectrosc. **247**, 128 (2008).
[354] T. C. Killian, C. A. Gottlieb, and P. Thaddeus, J. Chem. Phys. **127**, 114320 (2007).
[355] F. L. Constantin, J. Demaison, L. Fégard, M. Litz, H. Bürger, and P. Pracna, J. Mol. Spectrosc. **243**, 234 (2007).
[356] R. Z. Martinez, D. Bermejo, J. Santos, and P. Cancio, J. Mol. Spectrosc. **168**, 343 (1994).
[357] J. Bendtsen, J. Raman Spectrosc. **2**, 133 (1974).
[358] W. D. Allen, Y. Yamaguchi, A. G. Császár, D. A. Clabo Jr, R. B. Remington, and H. F. Schaefer III, Chem. Phys. **145**, 427 (1990).
[359] D. A. Clabo Jr, W. D. Allen, R. B. Remington, Y. Yamaguchi, and H. F. Schaefer III, Chem. Phys. **123**, 187 (1988).
[360] V. Barone, J. Chem. Phys. **122**, 014108 (2005).
[361] K. L. Bak, J. Gauss, T. Helgaker, P. Jørgensen, and J. Olsen, Chem. Phys. Lett. **319**, 563 (2000).
[362] A. Halkier, H. Larsen, J. Olsen, P. Jørgensen, and J. Gauss, J. Chem. Phys. **110**, 734 (1999).
[363] A. Halkier, W. Klopper, T. Helgaker, and P. Jørgensen, J. Chem. Phys. **111**, 4424 (1999).
[364] D. Mauer, G. Winnewisser, K. M. T. Yamada, J. Hahn, and K. Reinartz, Z. Naturforsch. **43a**, 617 (1988).
[365] M. Liedtke, A. H. Saleck, K. M. T. Yamada, G. Winnewisser, D. Cremer, E. Kraka, A. Dolgner, J. Hahn, and S. Dobos, J. Phys. Chem. **97**, 11204 (1993).
[366] G. Cazzoli, C. Puzzarini, A. Baldacci, and A. Baldan, J. Mol. Spectrosc. **241**, 112 (2007).
[367] S. Stopkowicz and J. Gauss, J. Chem. Phys. **129**, 164119 (2008).
[368] P. Pyykkö, Z. Naturforsch. **47a**, 189 (1992).
[369] P. Pyykkö, Mol. Phys. **99**, 1617 (2001).
[370] P. Pyykkö, Mol. Phys. **106**, 1965 (2008).
[371] A. Halkier, H. Koch, O. Christiansen, P. Jørgensen, and T. Helgaker, J. Chem. Phys. **107**, 849 (1997).
[372] L. Olsen, O. Christiansen, L. Hemmingsen, S. P. A. Sauer, and K. V. Mikkelsen, J. Chem. Phys. **116**, 1424 (2002).
[373] J. Gauss and K. Ruud, Int. J. Quant. Chem. Symp. **29**, 437 (1995).
[374] M. Pernpointner, in *Relativistic Electronic Structure Theory, Part 2: Applications*, edited by P. Schwerdtfeger (Elsevier, Amsterdam, 2004), p. 289.
[375] I. Malkin, O. L. Malkina, and V. G. Malkin, Chem. Phys. Lett. **361**, 23 (2002).
[376] F. Neese, A. Wolf, T. Fleig, M. Reiher, and B. A. Hess, J. Chem. Phys. **122**, 204107 (2005).
[377] R. Mastalerz, G. Barone, R. Lindh, and M. Reiher, J. Chem. Phys. **127**, 074105 (2007).
[378] L. Visscher, T. Enevoldsen, T. Saue, and J. Oddershede, J. Chem. Phys. **109**, 9677 (1998).
[379] V. Kellö and A. J. Sadlej, J. Chem. Phys. **120**, 9424 (2004).
[380] P. Schwerdtfeger, R. Bast, M. C. L. Gerry, C. R. Jacob, M. Jansen, V. Kellö, A. V. Mudring, A. J. Sadlej, T. Saue, T. Söhnel, and F. E. Wagner, J. Chem. Phys. **122**, 124317 (2005).
[381] H. Yakobi, E. Eliav, L. Visscher, and U. Kaldor, J. Chem. Phys. **126**, 054301 (2007).
[382] C. R. Jacob, L. Visscher, C. Thierfelder, and P. Schwerdtfeger, J. Chem. Phys. **127**, 204303 (2007).
[383] C. Thierfelder, P. Schwerdtfeger, and T. Saue, Phys. Rev. A **76**, 034501 (2007).
[384] G. Cazzoli, C. Puzzarini, S. Stopkowicz, and J. Gauss, Mol. Phys. **106**, 1181 (2008).

[385] K. G. Dyall and K. Fægri, *Relativistic Quantum Chemistry* (Oxford University Press, New York, 2007).
[386] W. Kutzelnigg, in *Relativistic Electronic Structure Theory, Part 1: Fundamentals*, edited by P. Schwerdtfeger (Elsevier, Amsterdam, 2002), p. 664 ff.
[387] A. Wolf, M. Reiher, and B. A. Hess, in *Relativistic Electronic Structure Theory, Part 1: Fundamentals*, edited by P. Schwerdtfeger (Elsevier, Amsterdam, 2002), p. 622 ff.
[388] C. Klemp, M. Bruns, J. Gauss, U. Häussermann, G. Stoßer, L. van Wüllen, M. Jansen, and H. Schnöckel, J. Am. Chem. Soc. **123**, 9099 (2001).
[389] C. M. Lederer and V. S. Shirley, *Table of Isotopes* , 7th ed (John Wiley, New York, 1978).
[390] D. Taqqu, Helv. Phys. Acta **51**, 755 (1978).
[391] V. Kellö and A. J. Sadlej, Chem. Phys. Lett. **197**, 641 (1990).
[392] V. Kellö and A. J. Sadlej, Mol. Phys. **89**, 127 (1996).
[393] H. Haas and H. M. Petrilli, Phys. Rev. B **61**, 13588 (2000).
[394] E. van Lenthe and E. J. Baerends, J. Chem. Phys. **112**, 8279 (2000).
[395] J. Bieroń, P. Pyykkö, D. Sundholm, V. Kellö, and A. Sadlej, Phys. Rev. A **64**, 052507 (2001).
[396] H. Yakobi, E. Eliav, L. Visscher, and U. Kaldor, J. Chem. Phys. **126**, 054301 (2007).
[397] J. Gauss, M. E. Harding, S. Stopkowicz, and C. Puzzarini, to be published.
[398] V. Kellö and A. J. Sadlej, Phys. Rev. A **60**, 3575 (1999).
[399] F. J. Lovas and E. Tiemann, J. Phys. Chem. Ref. Data **3**, 609 (1974).
[400] N. Hansen, H. Mäder, and F. Temps, Chem. Phys. Lett. **327**, 97 (2000).
[401] N. Hansen, H. Mäder, and F. Temps, Chem. Phys. Lett. **409**, 149 (2005).
[402] N. Hansen, H. Mäder, and F. Temps, Phys. Chem. Chem. Phys. **3**, 50 (2001).
[403] G. Cazzoli, C. Puzzarini, and J. Gauss, Astrophys. J. Suppl. **159**, 181 (2005).
[404] G. Cazzoli and C. Puzzarini, J. Mol. Spectrosc. **233**, 280 (2005).
[405] H. Spahn, H. S. P. Müller, T. F. Giesen, J.-U. Grabow, M. E. Harding, J. Gauss, and S. Schlemmer, Chem. Phys. **346**, 132 (2008).
[406] F. F. S. van der Tak, H. S. P. Müller, M. E. Harding, and J. Gauss, Astron. & Astrophys. **507**, 347 (2009).
[407] G. Cazzoli, C. Puzzarini, M. E. Harding, and J. Gauss, Chem. Phys. Lett. **473**, 21 (2009).
[408] G. Cazzoli, C. Puzzarini, and J. Gauss, J. Mol. Spectrosc. **259**, 93 (2010).
[409] C. Puzzarini, G. Cazzoli, M. E. Harding, J. Vázquez, and J. Gauss, J. Chem. Phys. **131**, 234304 (2009).
[410] G. Cazzoli and C. Puzzarini, J. Mol. Spectrosc. **231**, 124 (2005).
[411] G. Cazzoli and C. Puzzarini, J. Mol. Spectrosc. **226**, 161 (2004).
[412] G. Cazzoli and C. Puzzarini, Phys. Chem. Chem. Phys. **6**, 5133 (2004).
[413] G. Cazzoli, C. Puzzarini, and A. V. Lapinov, Astrophys. J. **611**, 615 (2004).
[414] G. Cazzoli, L. Dore, C. Puzzarini, and S. Beninati, Phys. Chem. Chem. Phys. **4**, 3575 (2002).
[415] L. Bizzocchi, C. Degli Esposti, L. Dore, and C. Puzzarini, Chem. Phys. Lett. **408**, 13 (2005).
[416] C. Puzzarini, L. Dore, and G. Cazzoli, J. Mol. Spectrosc. **217**, 19 (2003).
[417] G. Cazzoli and C. Puzzarini, J. Mol. Spectrosc. **239**, 64 (2006).
[418] G. Cazzoli and C. Puzzarini, J. Mol. Spectrosc. **240**, 153 (2006).
[419] G. Cazzoli and C. Puzzarini, J. Mol. Spectrosc. **247**, 187 (2008)(E).
[420] G. Cazzoli, L. Dore, and C. Puzzarini, Astron. Astrophys. **507**, 1701 (2009).
[421] G. Klapper, L. Surin, F. Lewen, H. S. P. Müller, I. Pak, and G. Winnewisser, Astrophys. J. **582**, 262 (2003).
[422] G. Klapper, F. Lewen, S. P. Belov, and G. Winnewisser, Z. Naturforsch. A **55**, 441 (2000).
[423] G. Klapper, F. Lewen, R. Gendriesch, S. P. Belov, and G. Winnewisser, J. Mol. Spectrosc. **201**, 124 (2000).
[424] C. J. Jameson, Chem. Rev. **91**, 1375 (1991).
[425] R. E. Wasylishen and D. L. Bryce, J. Chem. Phys. **117**, 10061 (2002).
[426] M. Gee, R. E. Wasylishen, and A. Laaksonen, J. Phys. Chem. A **103**, 10805 (1999).

[427] J. Oddershede and J. Geertsen, J. Chem. Phys. **92**, 6036 (1990).
[428] F. London, J. Phys. Radium **8**, 397 (1937).
[429] H. Hameka, Mol. Phys. **1**, 203 (1958).
[430] R. Ditchfield, Mol. Phys. **27**, 789 (1974).
[431] K. Wolinski, J. F. Hinton, and P. Pulay, J. Am. Chem. Soc. **112**, 8251 (1990).
[432] J. Gauss and D. Sundholm, Mol. Phys. **91**, 449 (1997).
[433] C. Puzzarini, S. Coriani, A. Rizzo, and J. Gauss, Chem. Phys. Lett. **409**, 118 (2005).
[434] M. A. Frerking and W. D. Langer, J. Chem. Phys. **74**, 6990 (1981).
[435] R. E. Wasylishen, S. Mooibroek, and J. B. Macdonald, J. Chem. Phys. **81**, 1057 (1984).
[436] C. Puzzarini, T. Metzroth, and J. Gauss, to be published.
[437] M. Schulz-Dobrick, T. Metzroth, H. W. Spiess, J. Gauss, and I. Schnell, Chem. Phys. Chem. **5**, 1 (2005).
[438] E. W. Kaiser, J. Chem. Phys. **53**, 1686 (1970).
[439] T. Enevoldsen, J. Oddershede, and S. P. A. Sauer, Theor. Chem. Acc. **100**, 275 (1998).
[440] O. Vahtras, H. Ågren, P. Jørgensen, H. J. Aa. Jensen, S. B. Padkjaer, and T. Helgaker, J. Chem. Phys. **96**, 6120 (1992).
[441] S. A. Perera, M. Nooijen, and R. J. Bartlett, J. Chem. Phys. **104**, 3290 (1996).
[442] A. A. Auer and J. Gauss, J. Chem. Phys. **115**, 1619 (2001).
[443] D. L. Bryce, R. E. Wasylishen, J. Autschbach, and T. Ziegler, J. Am. Chem. Soc. **124**, 4894 (2004).
[444] J. T. Hougen, J. Chem. Phys. **57**, 4207 (1972).